Search for a scalar partner of the top quark in the jets plus missing transverse momentum final state at $\sqrt{s} = 13$ TeV with the ATLAS detector

The ATLAS collaboration

E-mail: atlas.publications@cern.ch

ABSTRACT: A search for pair production of a scalar partner of the top quark in events with four or more jets plus missing transverse momentum is presented. An analysis of $36.1\,\text{fb}^{-1}$ of $\sqrt{s} = 13$ TeV proton-proton collisions collected using the ATLAS detector at the LHC yields no significant excess over the expected Standard Model background. To interpret the results a simplified supersymmetric model is used where the top squark is assumed to decay via $\tilde{t}_1 \to t^{(*)}\tilde{\chi}_1^0$ and $\tilde{t}_1 \to b\tilde{\chi}_1^\pm \to bW^{(*)}\tilde{\chi}_1^0$, where $\tilde{\chi}_1^0$ ($\tilde{\chi}_1^\pm$) denotes the lightest neutralino (chargino). Exclusion limits are placed in terms of the top-squark and neutralino masses. Assuming a branching ratio of 100% to $t\tilde{\chi}_1^0$, top-squark masses in the range 450–1000 GeV are excluded for $\tilde{\chi}_1^0$ masses below 160 GeV. In the case where $m_{\tilde{t}_1} \sim m_t + m_{\tilde{\chi}_1^0}$, top-squark masses in the range 235–590 GeV are excluded.

Contents

1 Introduction

Supersymmetry (SUSY) [1–6] is an extension of the Standard Model (SM) that can resolve, for example, the gauge hierarchy problem [7–10] by introducing supersymmetric partners of the known bosons and fermions. The SUSY partner to the top quark, the top squark ($\tilde{t}$), plays an important role in cancelling potentially large top-quark loop corrections in the Higgs boson mass. The superpartners of the left- and right-handed top quarks, $\tilde{t}_{\mathrm{L}}$ and $\tilde{t}_{\mathrm{R}}$, mix to form the two mass eigenstates $\tilde{t}_1$ and $\tilde{t}_2$, where $\tilde{t}_1$ is the lighter one. Throughout this paper it is assumed that the analysis is only sensitive to $\tilde{t}_1$.

In R-parity-conserving SUSY models [11], the supersymmetric partners are produced in pairs. Top squarks are produced by strong interactions through quark-antiquark ($q\bar{q}$) annihilation or gluon-gluon fusion, and the cross section of direct top-squark pair production is largely decoupled from the specific choice of SUSY model parameters [12–15]. The decay of the top squark depends on the mixing of the superpartners of left- and right-handed top quarks, the masses of the top superpartner, and the mixing parameters of the fermionic partners of the electroweak and Higgs bosons. The mass eigenstates of the partners of electroweak gauge and Higgs bosons (binos, winos, higgsinos) are collectively known as charginos, $\tilde{\chi}_i^{\pm}$, $i = 1, 2$, and neutralinos, $\tilde{\chi}_i^0$, $i = 1, \ldots, 4$, where $\tilde{\chi}_1^0$ is assumed

to be the lightest supersymmetric particle (LSP) which is stable and a dark-matter candidate [16, 17]. For the models considered, either $\tilde{\chi}_2^0$ or $\tilde{\chi}_1^\pm$ is assumed to be the next lightest supersymmetric particle (NLSP). Three different decay scenarios are considered in this search: (a) both top squarks decay via $\tilde{t}_1 \to t^{(*)} \tilde{\chi}_1^0$, (b) at least one of the top squarks decays via $\tilde{t}_1 \to b\tilde{\chi}_1^\pm \to bW^{(*)}\tilde{\chi}_1^0$, with various hypotheses for $m_{\tilde{\chi}_1^0}$ and $m_{\tilde{\chi}_1^\pm}$, and (c) where $m_{\tilde{\chi}_2^0}$ is small enough for at least one top squark to decay via $\tilde{t}_1 \to t\tilde{\chi}_2^0 \to h/Z\tilde{\chi}_1^0$, where h is the SM-like Higgs boson with a mass of 125 GeV, as illustrated in figure 1(a)−(c), respectively. The interpretation of the results uses simplified models [18–20] where only one or two decay steps are allowed. In the case with two allowed decays, referred to later in this paper as a natural SUSY-inspired mixed grid, the mass splitting between the $\tilde{\chi}_1^\pm$ and the $\tilde{\chi}_1^0$, $\Delta m(\tilde{\chi}_1^\pm, \tilde{\chi}_1^0)$, is assumed to be 1 GeV. A grid of signal samples is generated across the plane of the top-squark and $\tilde{\chi}_1^0$ masses with a grid spacing of 50 GeV across most of the plane, assuming maximal mixing between the partners of the left- and right-handed top quarks. In both the one- and two-step decay scenarios the LSP is considered to be a pure bino state. Additionally, results are interpreted in two slices of phenomenological MSSM (pMSSM) [21, 22] models, referred to as wino-NLSP and well-tempered neutralino pMSSM models in the remainder of this paper. The pMSSM models are based on the more general MSSM [23, 24] but with the additional requirements of no new sources of CP violation and flavour-changing neutral currents, as well as first- and second-generation sfermion mass and trilinear coupling degeneracy. Finally, results are also interpreted in a simplified model which is inspired by the pMSSM and is referred to as non-asymptotic higgsino. Details of the models that are used in the various interpretations are given in section 9.

In addition to direct pair production, top squarks can be produced indirectly through gluino decays, as shown in figure 1(d). This search considers models where the mass difference between the top squark and the neutralino is small, i.e. $\Delta m(\tilde{t}_1, \tilde{\chi}_1^0) = 5$ GeV. In this scenario, the jets originating from the $\tilde{t}_1$ decays have momenta below the experimental acceptance, resulting in a signature nearly identical to that of $\tilde{t}_1 \to t\tilde{\chi}_1^0$ signal models (figure 1(a)).

This paper presents the search for top-squark pair production using a time-integrated luminosity of $36.1\,\mathrm{fb}^{-1}$ of proton-proton (pp) collisions data provided by the Large Hadron Collider (LHC) at a centre-of-mass energy of $\sqrt{s} = 13$ TeV. The data were collected by the ATLAS detector in 2015 and 2016. All-hadronic final states with at least four jets and large missing transverse momentum[1] ($\mathbf{p}_\mathrm{T}^\mathrm{miss}$, whose magnitude is referred to as $E_\mathrm{T}^\mathrm{miss}$) are considered, and the results are interpreted according to a variety of signal models as described above. Signal regions are defined to maximize the experimental sensitivity over a large region of kinematic phase space. Sensitivity to high top-squark masses ~ 1000 GeV (as in figure 1(a)) and top squarks produced through gluino decays (as in figure 1(d))

---

[1]ATLAS uses a right-handed coordinate system with its origin at the nominal interaction point (IP) in the centre of the detector and the z-axis along the beam pipe. The x-axis points from the IP to the centre of the LHC ring, and the y-axis points upwards. Cylindrical coordinates (r, ϕ) are used in the transverse plane, ϕ being the azimuthal angle around the z-axis. The pseudorapidity is defined in terms of the polar angle θ as $\eta = -\ln\tan(\theta/2)$. Angular distance is measured in units of $\Delta R \equiv \sqrt{(\Delta\eta)^2 + (\Delta\phi)^2}$. The transverse momentum is the momentum component in the transverse plane.
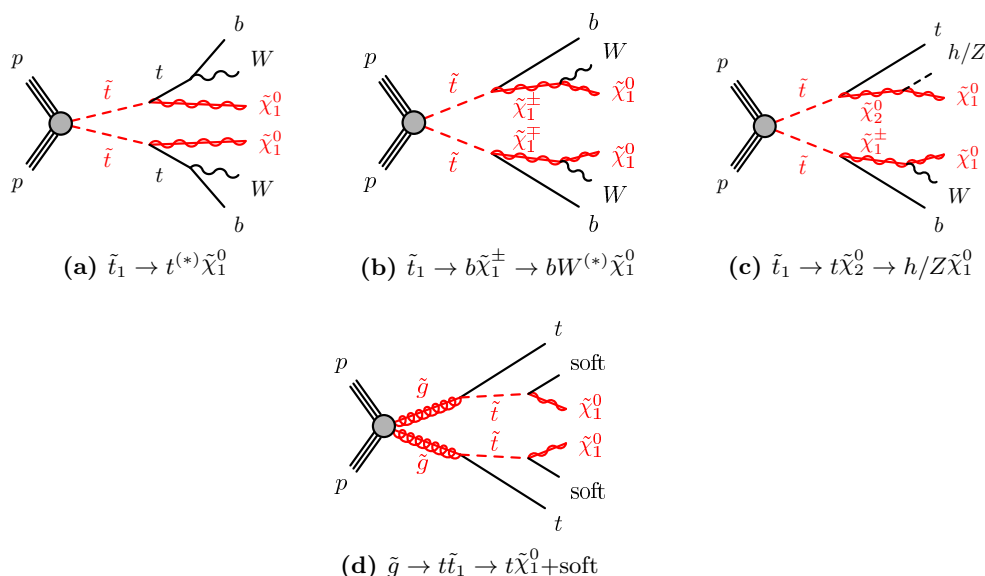
Figure 1. The decay topologies of the signal models considered with experimental signatures of four or more jets plus missing transverse momentum. Decay products that have transverse momenta below detector thresholds are designated by the term "soft".

is achieved by exploiting techniques designed to reconstruct top quarks that are Lorentz-boosted in the lab frame. The dominant SM background process for this kinematic region is $Z \to \nu\bar{\nu}$ produced in association with jets initiated by heavy-flavour quarks (heavy-flavour jets). The sensitivity to the decay into $b\tilde{\chi}_1^\pm$ is enhanced by vetoing events containing hadronically decaying top-quark candidates to reduce the $t\bar{t}$ background, leaving $Z \to \nu\bar{\nu}$ as the largest SM background. Sensitivity to the region where $m_{\tilde{t}_1} - m_{\tilde{\chi}_1^0} \sim m_t$, which typically has relatively low-p_{T} final-state jets and low $E_{\mathrm{T}}^{\mathrm{miss}}$, is achieved by exploiting events in which high-p_{T} jets from initial-state radiation (ISR) boosts the di-top-squark system in the transverse plane. For this regime, $t\bar{t}$ production gives the dominant background contribution. Similar searches based on $\sqrt{s} = 8\,\mathrm{TeV}$ and $\sqrt{s} = 13\,\mathrm{TeV}$ data collected at the LHC have been performed by both the ATLAS [25–28] and CMS [29–33] collaborations.

2 ATLAS detector

The ATLAS experiment [34] at the LHC is a multi-purpose particle detector with a cylindrical forward-backward and ϕ-symmetric geometry and an approximate 4π coverage in solid angle. It consists of an inner tracking detector surrounded by a thin superconducting solenoid providing a 2 T axial magnetic field, electromagnetic and hadron calorimeters, and a muon spectrometer. The inner tracking detector covers the pseudorapidity range $|\eta| < 2.5$. It consists of silicon pixel, silicon microstrip, and transition radiation tracking detectors. The newly installed innermost layer of pixel sensors [35, 36] was operational for the first time during the 2015 data-taking. Lead/liquid-argon (LAr) sampling calorimeters provide electromagnetic (EM) energy measurements with high granularity. A hadron

(steel/scintillator-tile) calorimeter covers the central pseudorapidity range ($|\eta| < 1.7$). The end-cap and forward regions are instrumented with LAr calorimeters for both the EM and hadronic energy measurements up to $|\eta| = 4.9$. The muon spectrometer surrounds the calorimeters and features three large air-core toroidal superconducting magnets with eight coils each, providing coverage up to $|\eta| = 2.7$. The field integral of the toroids ranges between 2.0 and 6.0 Tm across most of the detector. It includes a system of precision tracking chambers and fast detectors for triggering.

3 Trigger and data collection

The data were collected from August to November 2015 and April to October 2016 at a pp centre-of-mass energy of 13 TeV with 25 ns bunch spacing. A two-level trigger system [37] is used to select events. The first-level trigger is implemented in hardware and uses a subset of the detector information to reduce the event rate to at most 100 kHz. This is followed by a software-based trigger that reduces the accepted event rate to 1 kHz for offline storage.

In all search regions, a missing transverse momentum trigger, which is fully efficient for offline calibrated $E_T^{miss} > 250$ GeV in signal events, was used to collect data events.

Data samples enriched in the major sources of background were collected with electron or muon triggers. The electron trigger selects events based on the presence of clusters of energy in the electromagnetic calorimeter, with a shower shape consistent with that expected for an electron, and a matching track in the tracking system. The muon trigger selects events containing one or more muon candidates based on tracks identified in the muon spectrometer and inner detector. The electron and muon triggers used are more than 99% efficient for isolated electrons and muons with p_T above 28 GeV.

Triggers based on the presence of high-p_T jets were used to collect data samples for the estimation of the multijet and all-hadronic $t\bar{t}$ background. The jet p_T thresholds ranged from 20 to 400 GeV. In order to stay within the bandwidth limits of the trigger system, only a fraction of the events passing these triggers was recorded to permanent storage.

4 Simulated event samples and signal modelling

Simulated events are used to model the SUSY signal and to aid in the description of the background processes. Signal models were all generated with MG5_aMC@NLO 2.2-2.4 [38] interfaced to PYTHIA8 [39] for the parton showering (PS) and hadronization and with EvtGen 1.2.0 [40] for the b- and c-hadron decays. The matrix element (ME) calculation was performed at tree level and includes the emission of up to two additional partons for all signal samples. The parton distribution function (PDF) set used for the generation of the signal samples is NNPDF2.3LO [41] with the A14 [42] set of tuned underlying-event and shower parameters (UE tune). The ME-PS matching was performed with the CKKW-L [43] prescription, with a matching scale set to one quarter of the mass of the $\tilde{t}_1$, or $\tilde{g}$ for the gluino pair production model. All signal cross sections were calculated to next-to-leading order in the strong coupling constant, adding the resummation of soft-gluon emission at next-to-leading-logarithm accuracy (NLO+NLL) [12–14]. The nominal

cross section and the uncertainty were taken from an envelope of cross-section predictions using different PDF sets and factorization and renormalization scales, as described in ref. [15]. For pMSSM models, the sparticle mass spectra were calculated with Softsusy 3.7.3 [44, 45] while the decays of each sparticle were performed by HDECAY 3.4 [46] and SDECAY 1.5/1.5a [47].

SM background samples were generated with different MC event generators depending on the process. The background sources of Z + jets and W + jets events were generated with SHERPA 2.2.1 [48] using the NNPDF3.0NNLO [41] PDF set and the UE tune provided by SHERPA. Top-quark pair production where at least one of the top quarks decays semileptonically and single-top production were simulated with POWHEG-BOX 2 [49] and interfaced to PYTHIA6 [50] for PS and hadronization, with the CT10 [51] PDF set and using the PERUGIA2012 [52] set of tuned shower and underlying-event parameters. MG5_AMC@NLO interfaced to PYTHIA8 for PS and hadronization was used to generate the $t\bar{t}+V$ (where V is a W or Z boson) and $t\bar{t}+\gamma$ samples at NLO with the NNPDF3.0NLO PDF set. The underlying-event tune used is A14 with the NNPDF2.3LO PDF set. Diboson production was generated with SHERPA 2.2.1 using the CT10 PDF set. Finally, $V\gamma$ processes were generated with SHERPA 2.1 using the CT10 PDF set. Additional information can be found in refs. [53–57].

The detector simulation [58] was performed using either GEANT4 [59] or a fast simulation framework where the showers in the electromagnetic and hadronic calorimeters are simulated with a parameterized description [60] and the rest of the detector is simulated with GEANT4. The fast simulation was validated against full GEANT4 simulation for several selected signal samples and subsequently used for all signal samples because of the large number of signal grid points needed for interpretation. All SM background samples used the GEANT4 set-up. All MC samples were produced with a varying number of simulated minimum-bias interactions overlaid on the hard-scattering event to account for multiple pp interactions in the same or nearby bunch crossing (pile-up). These events were produced using PYTHIA8 with the A2 tune [61] and MSTW 2008 PDF set [62]. The simulated events were reweighted to match the distribution of the number of pp interactions per bunch crossing in data. Corrections were applied to the simulated events to correct for differences between data and simulation for the lepton-trigger and reconstruction efficiencies, momentum scale, energy resolution, isolation, and for the efficiency of identifying jets containing b-hadrons, together with the probability for mis-tagging jets containing only light-flavour and charm hadrons.

5 Event reconstruction

Events are required to have a primary vertex [63] reconstructed from at least two tracks with $p_\text{T} > 400\,\text{MeV}$. Among the vertices found, the vertex with the largest summed p_T^2 of the associated tracks is chosen.

Jets are reconstructed from three-dimensional topological clusters of noise-suppressed calorimeter cells [64] using the anti-k_t jet algorithm [65, 66] with a radius parameter $R = 0.4$. An area-based correction is applied to account for energy from additional pp col-

lisions based on an estimate of the pile-up activity in a given event [67]. Calibrated [68] jet candidates are required to have $p_T > 20$ GeV and $|\eta| < 2.8$. Events containing jets arising from non-collision sources or detector noise [69] are removed ("no bad jets" requirement). Additional selections based on track information are applied to jets with $p_T < 60$ GeV and $|\eta| < 2.4$ to reject jets that originate from pile-up interactions [70].

Jets containing b-hadrons and which are within the inner detector acceptance ($|\eta| < 2.5$) are identified (as b-tagged jets) with a multivariate algorithm that exploits the impact parameters of the charged-particle tracks, the presence of secondary vertices, and the reconstructed flight paths of b- and c-hadrons inside the jet [71–73]. The output of the multivariate algorithm is a single b-tagging weight which signifies the likelihood of a jet containing b-hadrons. The average identification efficiency of jets containing b-hadrons is 77% as determined in simulated $t\bar{t}$ events. A rejection factor of approximately 130 is reached for jets initiated by light quarks and gluons and 6 for jets initiated by charm quarks.

Electron candidates are reconstructed from clusters of energy deposits in the electromagnetic calorimeter that are matched to a track in the inner detector. They are required to have $|\eta| < 2.47$, $p_T > 7$ GeV and must pass a variant of the "very loose" likelihood-based selection [74, 75]. The electromagnetic shower of an electron can also form a jet such that a procedure is required to resolve this ambiguity. In the case where the separation between an electron candidate and a non-b-tagged (b-tagged) jet is $\Delta R < 0.2$,[2] the candidate is considered to be an electron (b-tagged jet). If the separation between an electron candidate and any jet satisfies $0.2 < \Delta R < 0.4$, the candidate is considered to be a jet, and the electron candidate is removed.

Muons are reconstructed by matching tracks in the inner detector to tracks in the muon spectrometer and are required to have $|\eta| < 2.7$ and $p_T > 6$ GeV. If the separation between a muon and any jet is $\Delta R < 0.4$, the muon is omitted. Events containing muons identified as originating from cosmic rays ($|d_0| > 0.2$ mm and $|z_0| > 1$ mm) or as poorly reconstructed ($\sigma(q/p)/|(q/p)| > 0.2$) are removed ("cosmic and bad muon" requirement). Here, d_0 is the transverse impact parameter of a track with respect to the primary vertex, z_0 is the distance of this point from the primary vertex projected onto the z-axis, and $\sigma(q/p)/|(q/p)|$ provides a measure of the momentum uncertainty for a particle with charge q.

The $\mathbf{p}_T^{miss}$ vector is the negative vector sum of the p_T of all selected and calibrated electrons, muons, and jets in the event. An extra term is added to account for small energy depositions in the event that are not associated with any of the selected objects. This "soft" term is calculated from inner detector tracks with $p_T > 400$ MeV matched to the primary vertex, to make it resilient to pile-up contamination, not associated with physics objects [76]. The missing transverse momentum from the tracking system (denoted by $\mathbf{p}_T^{miss,track}$, with magnitude $E_T^{miss,track}$) is computed from the vector sum of the reconstructed inner detector tracks with $p_T > 400$ MeV, $|\eta| < 2.5$, that are associated with the primary vertex in the event. The $\mathbf{p}_T^{miss,track}$ and $E_T^{miss,track}$ are used to reject events with large calorimeter-based E_T^{miss} due to pile-up contamination or jet energy mismeasurements.

---

[2]For the overlap removal, rapidity, defined as $\frac{1}{2}\ln\frac{E+p_z}{E-p_z}$, is used instead of pseudorapidity in the ΔR definition.

These events, where the $\mathbf{p}_T^{\mathrm{miss,track}}$ tends to not be aligned with the $\mathbf{p}_T^{\mathrm{miss}}$ and the E_T^{miss} tends to be much larger than the $E_T^{\mathrm{miss,track}}$, are rejected by requiring that the $\Delta\phi$ between the $\mathbf{p}_T^{\mathrm{miss}}$ and $\mathbf{p}_T^{\mathrm{miss,track}}$ is less than $\pi/3$ and that the $E_T^{\mathrm{miss,track}} > 30\,\mathrm{GeV}$.

The requirements on electrons and muons are tightened for the selection of events in background control regions (described in section 7) containing leptons. Electron and muon candidates are required to have $p_T > 20\,\mathrm{GeV}$ ($p_T > 28\,\mathrm{GeV}$) for regions using the E_T^{miss} (lepton) triggers and to satisfy p_T-dependent track- and calorimeter-based isolation criteria. The calorimeter-based isolation is determined by taking the ratio of the sum of energy deposits in a cone of $R = 0.2$ around the electron or muon candidate and the energy deposits associated with the electron and muon. The track-based isolation is estimated in a similar way but using a variable cone size with a maximum value of $R = 0.2$ for electrons and $R = 0.3$ for muons. An isolation requirement is made that is 95% efficient for electron or muon candidates with $p_T = 25\,\mathrm{GeV}$ and 99% for candidates with $p_T = 60\,\mathrm{GeV}$.

Electron candidates are required to pass a "tight" likelihood-based selection [74]. The impact parameter of the electron in the transverse plane with respect to the reconstructed event primary vertex is required to be less than five times the impact parameter uncertainty (σ_{d_0}). The impact parameter along the beam direction, $|z_0 \times \sin\theta|$, is required to be less than 0.5 mm. Further selection criteria are also imposed on reconstructed muons: muon candidates are required to pass a "medium" quality selection [77]. In addition, the requirements $|d_0| < 3\sigma_{d_0}$ and $|z_0 \times \sin\theta| < 0.5$ mm are imposed for muon candidates.

6 Signal region definitions

The main experimental signature for all signal topologies is the presence of multiple jets (two of which are b-tagged), no muons or electrons, and significant missing transverse momentum.

Five sets of signal regions (SRA-E) are defined to target each topology and kinematic regime. SRA (SRB) is sensitive to production of high-mass $\tilde{t}_1$ pairs with large (intermediate) $\Delta m(\tilde{t}_1, \tilde{\chi}_1^0)$. Both SRA and SRB employ top-mass reconstruction techniques to reject background. SRC is designed for the highly compressed region with $\Delta m(\tilde{t}_1, \tilde{\chi}_1^0) \sim m_t$. In this signal region, initial-state radiation (ISR) is used to improve sensitivity to these decays. SRD is targeted at $\tilde{t}_1 \to b\tilde{\chi}_1^\pm$ decays, where no top-quark candidates are reconstructed. SRE is optimized for scenarios with highly boosted top quarks that can occur in gluino-mediated top-squark production.

A common preselection is defined for all signal regions. At least four jets are required, of which at least one must be b-tagged. The four leading jets (ordered in p_T) must satisfy $p_T^{0-3} > 80, 80, 40, 40\,\mathrm{GeV}$ due to the tendency for signal events to have more energetic jets than background. Events containing reconstructed electrons or muons are vetoed. The E_T^{miss} trigger threshold motivates the requirement $E_T^{\mathrm{miss}} > 250\,\mathrm{GeV}$ and rejects most of the background from multijet and all-hadronic $t\bar{t}$ events. In order to reject events with mismeasured E_T^{miss} originating from multijet and hadronic $t\bar{t}$ decays, an angular separation between the azimuthal angle of the two highest-p_T jets and the $\mathbf{p}_T^{\mathrm{miss}}$ is required: $\left|\Delta\phi\left(\mathrm{jet}^{0,1}, \mathbf{p}_T^{\mathrm{miss}}\right)\right| > 0.4$. Further rejection of such events is achieved by requiring the
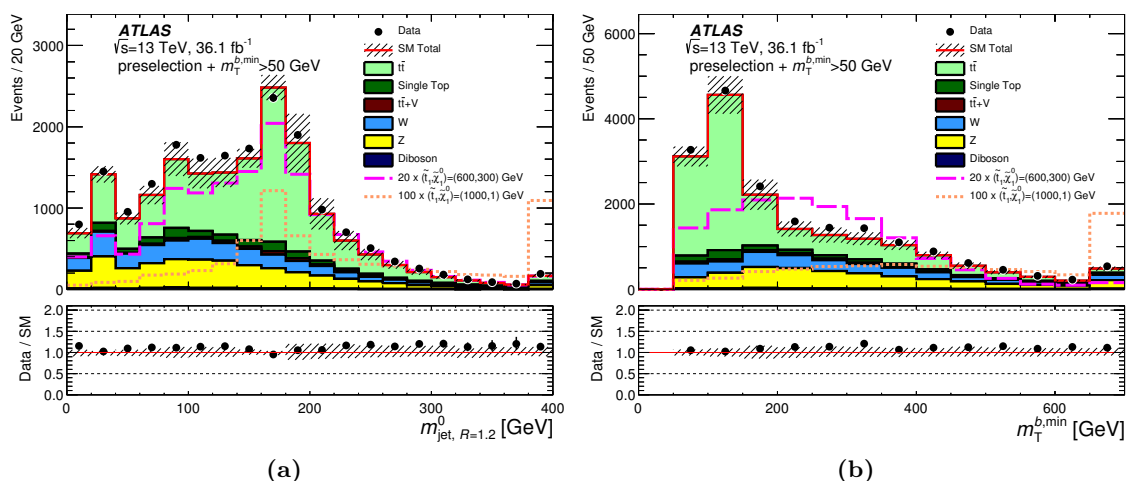
Figure 2. Distributions of the discriminating variables (a) $m_{\mathrm{jet}, R=1.2}^0$ and (b) $m_{\mathrm{T}}^{b,\mathrm{min}}$ after the common preselection and an additional $m_{\mathrm{T}}^{b,\mathrm{min}} > 50\,\mathrm{GeV}$ requirement. The stacked histograms show the SM prediction before being normalized using scale factors derived from the simultaneous fit (detailed in section 7) to all dominant backgrounds. The "Data/SM" plots show the ratio of data events to the total SM prediction. The hatched uncertainty band around the SM prediction and in the ratio plots illustrates the combination of statistical and detector-related systematic uncertainties. The rightmost bin includes overflow events.

$\mathbf{p}_{\mathrm{T}}^{\mathrm{miss,track}}$ to be aligned in ϕ with respect to the $\mathbf{p}_{\mathrm{T}}^{\mathrm{miss}}$ calculated from the calorimeter system: $E_{\mathrm{T}}^{\mathrm{miss,track}} > 30\,\mathrm{GeV}$ and $\left|\Delta\phi\left(\mathbf{p}_{\mathrm{T}}^{\mathrm{miss}}, \mathbf{p}_{\mathrm{T}}^{\mathrm{miss,track}}\right)\right| < \pi/3$.

Signal regions A and B. SRA and SRB are targeted at direct top-squark pair production where the top squarks decay via $\tilde{t}_1 \to t\tilde{\chi}_1^0$ with $\Delta m(\tilde{t}_1, \tilde{\chi}_1^0) > m_t$. SRA is optimized for $m_{\tilde{t}_1} = 1000\,\mathrm{GeV}$ and $m_{\tilde{\chi}_1^0} = 1\,\mathrm{GeV}$, while SRB is optimized for $m_{\tilde{t}_1} = 600\,\mathrm{GeV}$, $m_{\tilde{\chi}_1^0} = 300\,\mathrm{GeV}$. At least two b-tagged jets ($N_{b-\mathrm{jet}} \geq 2$) are required and an additional requirement on the $\Delta\phi$ of the three leading jets and $\mathbf{p}_{\mathrm{T}}^{\mathrm{miss}}$ of $\left|\Delta\phi\left(\mathrm{jet}^{0,1,2}, \mathbf{p}_{\mathrm{T}}^{\mathrm{miss}}\right)\right| > 0.4$ is made.

The decay products of the $t\bar{t}$ system in the all-hadronic decay mode can often be reconstructed as six distinct $R = 0.4$ jets. The transverse shape of these jets is typically circular with a radius equal to this radius parameter, but when two of the jets are less than $2R$ apart in η–ϕ space, the one-to-one correspondence of a jet with a top-quark daughter may no longer hold. Thus, the two hadronic top candidates are reconstructed by applying the anti-k_t clustering algorithm [65] to the $R = 0.4$ jets, using reclustered radius parameters of $R = 0.8$ and $R = 1.2$. Two $R = 1.2$ reclustered jets are required; the mass of the highest-p_{T} $R = 1.2$ reclustered jet is shown in figure 2(a). The events are divided into three categories based on the resulting $R = 1.2$ reclustered jet masses ordered in p_{T}, as illustrated in figure 3: the "TT" category includes events with two top candidates, i.e. with masses $m_{\mathrm{jet}, R=1.2}^0 > 120\,\mathrm{GeV}$ and $m_{\mathrm{jet}, R=1.2}^1 > 120\,\mathrm{GeV}$; the "TW" category contains events with one top candidate and a W candidate, i.e. where $m_{\mathrm{jet}, R=1.2}^0 > 120\,\mathrm{GeV}$ and $60 < m_{\mathrm{jet}, R=1.2}^1 < 120\,\mathrm{GeV}$; and the "T0" category represents events with only one top
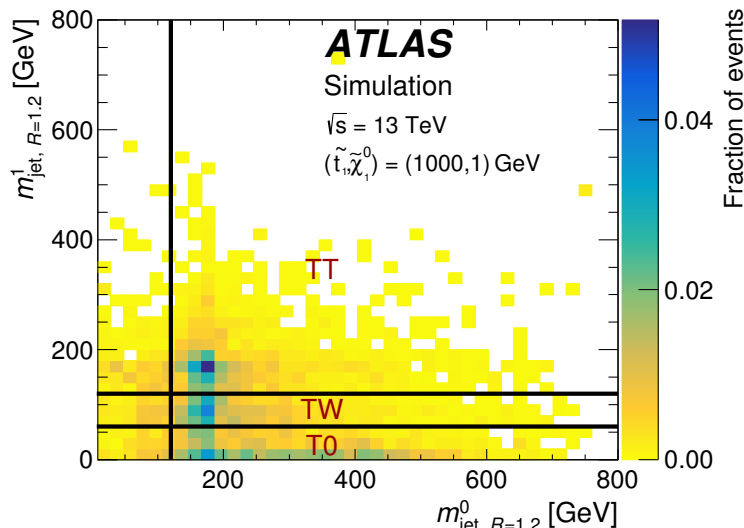
Figure 3. Illustration of signal-region categories (TT, TW, and T0) based on the $R = 1.2$ reclustered top-candidate masses for simulated direct top-squark pair production with $(m_{\tilde{t}_1}, m_{\tilde{\chi}_1^0}) = (1000, 1)$ GeV after the loose preselection requirement described in the text. The black lines represent the requirements on the reclustered jet masses.

candidate, i.e. where $m_{\text{jet},R=1.2}^0 > 120 \, \text{GeV}$ and $m_{\text{jet},R=1.2}^1 < 60 \, \text{GeV}$. Since the signal-to-background ratio is different in each of these categories, they are optimized individually for SRA and SRB.

The most powerful discriminating variable against SM $t\bar{t}$ production is the $E_{\text{T}}^{\text{miss}}$ value, which for the signal results from the undetected $\tilde{\chi}_1^0$ neutralinos. Substantial $t\bar{t}$ background rejection is provided by additional requirements that reject events in which one W boson decays via a charged lepton plus neutrino. The first requirement is that the transverse mass (m_{T}) calculated from the $E_{\text{T}}^{\text{miss}}$ and the b-tagged jet with minimum distance in ϕ to the $\mathbf{p}_{\text{T}}^{\text{miss}}$ direction is above 200 GeV:

$$m_{\text{T}}^{b,\text{min}} = \sqrt{2 \, p_{\text{T}}^b \, E_{\text{T}}^{\text{miss}} \left[1 - \cos \Delta\phi \left(\mathbf{p}_{\text{T}}^b, \mathbf{p}_{\text{T}}^{\text{miss}} \right) \right]} > 200 \, \text{GeV},$$

since its upper bound (ideally, without consideration of resolution effects) is below the top-quark mass for the $t\bar{t}$ background, as illustrated in figure 2(b). An additional requirement is made on the mass of the leading (in p_{T}) $R = 0.8$ reclustered jet to be consistent with a W candidate: $m_{\text{jet},R=0.8}^0 > 60 \, \text{GeV}$. Additionally, requirements on the stransverse mass ($m_{\text{T2}}^{\chi^2}$) [78, 79] are made which are especially powerful in the T0 category where a χ^2 method is applied to reconstruct top quarks with lower momenta where reclustering was suboptimal. The $m_{\text{T2}}^{\chi^2}$ variable is constructed from the direction and magnitude of the $\mathbf{p}_{\text{T}}^{\text{miss}}$ vector in the transverse plane as well as the direction of two top-quark candidates reconstructed using a χ^2 method. The minimization in this method is done in terms of a χ^2-like penalty function, $\chi^2 = (m_{\text{cand}} - m_{\text{true}})^2 / m_{\text{true}}$, where m_{cand} is the candidate mass and m_{true} is set to 80.4 GeV for W candidates and 173.2 GeV for top candidates. Initially, single or pairs of $R = 0.4$ jets form W candidates which are then combined with additional

Signal Region		TT	TW	T0
	$m_{\mathrm{jet},R=1.2}^0$		$> 120\,\mathrm{GeV}$	
	$m_{\mathrm{jet},R=1.2}^1$	$> 120\,\mathrm{GeV}$	$[60, 120]\,\mathrm{GeV}$	$< 60\,\mathrm{GeV}$
	$m_{\mathrm{T}}^{b,\mathrm{min}}$		$> 200\,\mathrm{GeV}$	
	$N_{b-\mathrm{jet}}$		≥ 2	
	τ-veto		yes	
	$\left| \Delta\phi\left(\mathrm{jet}^{0,1,2}, \mathbf{p}_{\mathrm{T}}^{\mathrm{miss}}\right) \right|$		> 0.4	
A	$m_{\mathrm{jet},R=0.8}^0$		$> 60\,\mathrm{GeV}$	
	$\Delta R\,(b,b)$	> 1		$-$
	$m_{\mathrm{T2}}^{\chi^2}$	$> 400\,\mathrm{GeV}$	$> 400\,\mathrm{GeV}$	$> 500\,\mathrm{GeV}$
	$E_{\mathrm{T}}^{\mathrm{miss}}$	$> 400\,\mathrm{GeV}$	$> 500\,\mathrm{GeV}$	$> 550\,\mathrm{GeV}$
B	$m_{\mathrm{T}}^{b,\mathrm{max}}$		$> 200\,\mathrm{GeV}$	
	$\Delta R\,(b,b)$		> 1.2	

Table 1. Selection criteria for SRA and SRB, in addition to the common preselection requirements described in the text. The signal regions are separated into topological categories based on reconstructed top-candidate masses.

b-tagged jets in the event to construct top candidates. The top candidates selected by the χ^2 method are only used for the momenta in $m_{\mathrm{T2}}^{\chi^2}$ while the mass hypotheses for the top quarks and the invisible particles are set to $173.2\,\mathrm{GeV}$ and $0\,\mathrm{GeV}$, respectively. Finally, a "τ-veto" requirement is applied to reject semi-hadronically decaying τ-lepton candidates likely to have originated from a $W \to \tau\nu$ decay. Here, events that contain a non-b-tagged jet within $|\eta| < 2.5$ with fewer than four associated charged-particle tracks with $p_{\mathrm{T}} > 500\,\mathrm{MeV}$, and where the $\Delta\phi$ between the jet and the $\mathbf{p}_{\mathrm{T}}^{\mathrm{miss}}$ is less than $\pi/5$, are vetoed. The systematic uncertainties for this requirement are found to be negligible [25]. In SRB, additional discrimination is provided by $m_{\mathrm{T}}^{b,\mathrm{max}}$ and $\Delta R(b,b)$. The former quantity is analogous to $m_{\mathrm{T}}^{b,\mathrm{min}}$ except that the transverse mass is computed with the b-tagged jet that has the largest $\Delta\phi$ with respect to the $\mathbf{p}_{\mathrm{T}}^{\mathrm{miss}}$ direction. The latter quantity provides additional discrimination against background where the two jets with highest b-tagging weights originate from a gluon splitting. Table 1 summarizes the selection criteria that are used in these two signal regions. The categories are statistically combined within SRA and SRB to maximize the sensitivity to signal.

Signal regions C. SRC is optimized for direct top-squark pair production where $\Delta m(\tilde{t}_1, \tilde{\chi}_1^0) \approx m_t$, a regime in which the signal topology is similar to SM $t\bar{t}$ production. In the presence of high-momentum ISR, which can be reconstructed as multiple jets forming an ISR system, the di-top-squark system is boosted in the transverse plane. The ratio of the $E_{\mathrm{T}}^{\mathrm{miss}}$ to the p_{T} of the ISR system in the centre-of-mass (CM) frame of the entire (ISR plus di-top-squark) system ($p_{\mathrm{T}}^{\mathrm{ISR}}$), defined as R_{ISR}, is proportional to the ratio of the $\tilde{\chi}_1^0$

Variable	SRC1	SRC2	SRC3	SRC4	SRC5
$N_{b-\mathrm{jet}}$	≥ 1				
$N_{b-\mathrm{jet}}^{\mathrm{S}}$	≥ 1				
$N_{\mathrm{jet}}^{\mathrm{S}}$	≥ 5				
$p_{\mathrm{T},b}^{0,\mathrm{S}}$	$> 40\,\mathrm{GeV}$				
m_{S}	$> 300\,\mathrm{GeV}$				
$\Delta\phi(\mathrm{ISR}, \mathbf{p}_{\mathrm{T}}^{\mathrm{miss}})$	> 3.0				
$p_{\mathrm{T}}^{\mathrm{ISR}}$	$> 400\,\mathrm{GeV}$				
$p_{\mathrm{T}}^{4,\mathrm{S}}$	$> 50\,\mathrm{GeV}$				
R_{ISR}	0.30–0.40	0.40–0.50	0.50–0.60	0.60–0.70	0.70–0.80

Table 2. Selection criteria for SRC, in addition to the common preselection requirements described in the text. The signal regions are separated into windows based on ranges of R_{ISR}.

and $\tilde{t}_1$ masses [80, 81]:

$$R_{\mathrm{ISR}} \equiv \frac{E_{\mathrm{T}}^{\mathrm{miss}}}{p_{\mathrm{T}}^{\mathrm{ISR}}} \sim \frac{m_{\tilde{\chi}_1^0}}{m_{\tilde{t}_1}}.$$

A "recursive jigsaw reconstruction technique", as described in ref. [82], is used to divide each event into an ISR hemisphere and a sparticle hemisphere, where the latter consists of the pair of candidate top squarks, each of which decays via a top quark and a $\tilde{\chi}_1^0$. Objects are grouped together based on their proximity in the lab frame's transverse plane by minimizing the reconstructed transverse masses of the ISR system and sparticle system simultaneously over all choices of object assignment. Kinematic variables are then defined based on this assignment of objects to either the ISR system or the sparticle system. This method is equivalent to grouping the event objects according to the axis of maximum back-to-back p_{T} in the event's CM frame where the p_{T} of all accepted objects sums vectorially to zero. In events with a high-p_{T} ISR gluon, the axis of maximum back-to-back p_{T}, also known as the thrust axis, approximates the direction of the ISR and sparticles' back-to-back recoil.

The selection criteria for this signal region are summarized in table 2. The events are divided into five windows (SRC1-5) defined by non-overlapping ranges of the reconstructed R_{ISR}, which target different top-squark and $\tilde{\chi}_1^0$ masses: e.g., SRC2 is optimized for $m_{\tilde{t}_1} = 300\,\mathrm{GeV}$ and $m_{\tilde{\chi}_1^0} = 127\,\mathrm{GeV}$, and SRC4 is optimized for $m_{\tilde{t}_1} = 500\,\mathrm{GeV}$ and $m_{\tilde{\chi}_1^0} = 327\,\mathrm{GeV}$. At least five jets must be assigned to the sparticle hemisphere of the event ($N_{\mathrm{jet}}^{\mathrm{S}}$), and at least one of those jets ($N_{b-\mathrm{jet}}^{\mathrm{S}}$) must be b-tagged. Transverse-momentum requirements on $p_{\mathrm{T}}^{\mathrm{ISR}}$, the highest-$p_{\mathrm{T}}$ b-jet in the sparticle hemisphere ($p_{\mathrm{T},b}^{0,\mathrm{S}}$), and the fourth-highest-p_{T} jet in the sparticle hemisphere ($p_{\mathrm{T}}^{4,\mathrm{S}}$) are applied. The transverse mass formed by the sparticle system and the $E_{\mathrm{T}}^{\mathrm{miss}}$, defined as m_{S}, is required to be $> 300\,\mathrm{GeV}$. The ISR system is also required to be separated in azimuth from the $\mathbf{p}_{\mathrm{T}}^{\mathrm{miss}}$ in the CM frame; this variable is defined as $\Delta\phi(\mathrm{ISR}, \mathbf{p}_{\mathrm{T}}^{\mathrm{miss}})$. Similarly to the categories defined for SRA and SRB, the individual SRCs are statistically combined to improve signal sensitivity.

Variable	SRD-low	SRD-high
$\left\lvert\Delta\phi\left(\mathrm{jet}^{0,1,2},\mathbf{p}_{\mathrm{T}}^{\mathrm{miss}}\right)\right\rvert$	> 0.4	
$N_{b-\mathrm{jet}}$	≥ 2	
$\Delta R\left(b,b\right)$	> 0.8	
$p_{\mathrm{T}}^{0,b}+p_{\mathrm{T}}^{1,b}$	$> 300\,\mathrm{GeV}$	$> 400\,\mathrm{GeV}$
τ-veto	yes	
p_{T}^1	$> 150\,\mathrm{GeV}$	
p_{T}^3	$> 100\,\mathrm{GeV}$	$> 80\,\mathrm{GeV}$
p_{T}^4	$> 60\,\mathrm{GeV}$	
$m_{\mathrm{T}}^{b,\mathrm{min}}$	$> 250\,\mathrm{GeV}$	$> 350\,\mathrm{GeV}$
$m_{\mathrm{T}}^{b,\mathrm{max}}$	$> 300\,\mathrm{GeV}$	$> 450\,\mathrm{GeV}$

Table 3. Selection criteria for SRD, in addition to the common preselection requirements described in the text.

Signal regions D. SRD is optimized for direct top-squark pair production where both top squarks decay via $\tilde{t}_1 \to b\tilde{\chi}_1^{\pm}$ where $m_{\tilde{\chi}_1^{\pm}} = 2m_{\tilde{\chi}_1^0}$. In this signal region, at least five jets are required, two of which must be b-tagged. The scalar sum of the transverse momenta of the two jets with the highest b-tagging weights ($p_{\mathrm{T}}^{0,b}+p_{\mathrm{T}}^{1,b}$) as well as the second (p_{T}^1), fourth (p_{T}^3), and fifth (p_{T}^4) jet transverse momenta are used for additional background rejection. Subregions SRD-low and SRD-high are optimized for $m_{\tilde{t}_1} = 400\,\mathrm{GeV}$ with $m_{\tilde{\chi}_1^0} = 50\,\mathrm{GeV}$, and $m_{\tilde{t}_1} = 700\,\mathrm{GeV}$ with $m_{\tilde{\chi}_1^0} = 100\,\mathrm{GeV}$, respectively. Tighter leading and sub-leading jet p_{T} requirements are made for SRD-high, as summarized in table 3.

Signal region E. SRE is designed for models which have highly boosted top quarks. Such signatures can arise from direct pair production of high-mass top partners, or from the gluino-mediated compressed $\tilde{t}_1$ scenario with large $\Delta m(\tilde{g}, \tilde{t}_1)$. In this regime, reclustered jets with $R = 0.8$ are utilized to optimize the experimental sensitivity to these highly boosted top quarks. In this signal region, at least two jets out of the four or more required jets must be b-tagged. Additional discrimination is provided by the $E_{\mathrm{T}}^{\mathrm{miss}}$ significance: $E_{\mathrm{T}}^{\mathrm{miss}}/\sqrt{H_{\mathrm{T}}}$, where H_{T} is the scalar sum of the p_{T} of all reconstructed $R = 0.4$ jets in an event. The selection criteria for SRE, optimized for $m_{\tilde{g}} = 1700\,\mathrm{GeV}$, $m_{\tilde{t}_1} = 400\,\mathrm{GeV}$, and $m_{\tilde{\chi}_1^0} = 395\,\mathrm{GeV}$, are summarized in table 4.

7 Background estimation

The main SM background process in SRA, SRB, SRD, and SRE is $Z \to \nu\bar{\nu}$ production in association with heavy-flavour jets. The second most significant background is $t\bar{t}$ production where one W boson decays via a lepton and neutrino and the lepton (particularly a hadronically decaying τ lepton) is either not identified or is reconstructed as a jet. This process gives the major background contribution in SRC and an important background

Variable	SRE
$\left\lvert \Delta\phi\left(\text{jet}^{0,1,2}, \mathbf{p}_{\text{T}}^{\text{miss}}\right)\right\rvert$	> 0.4
$N_{b-\text{jet}}$	≥ 2
$m_{\text{jet},R=0.8}^{0}$	$> 120\,\text{GeV}$
$m_{\text{jet},R=0.8}^{1}$	$> 80\,\text{GeV}$
$m_{\text{T}}^{b,\min}$	$> 200\,\text{GeV}$
$E_{\text{T}}^{\text{miss}}$	$> 550\,\text{GeV}$
H_{T}	$> 800\,\text{GeV}$
$E_{\text{T}}^{\text{miss}}/\sqrt{H_{\text{T}}}$	$> 18\sqrt{\text{GeV}}$

Table 4. Selection criteria for SRE in addition to the common preselection requirements described in the text.

in SRB, SRD and SRE as well. Other important background processes are $W \to \ell\nu$ plus heavy-flavour jets, single top quark, and the irreducible background from $t\bar{t}+Z$, where the Z boson decays into two neutrinos.

The main background contributions are estimated primarily from comparisons between data and simulation outside the signal regions. Control regions (CRs) are designed to enhance a particular background process, and are orthogonal to the SRs while probing a similar event topology. The CRs are used to normalize the simulation to data, but extrapolation from the CR to the SR is taken from simulation. Sufficient data are needed to avoid large statistical uncertainties in the background estimates, and the CR definitions are chosen to be kinematically as close as possible to all SRs, to minimize the systematic uncertainties associated with extrapolating the background yield from the CR to the SR. Where CR definitions are farther from the SR definition, validation regions are employed to cross-check the extrapolation. In addition, control-region selection criteria are chosen to minimize potential contamination from signal that could shadow contributions in the signal regions. The signal contamination is below 8% in all CRs for all signal points that have not been excluded by previous ATLAS searches. No significant difference in the background estimates was found between the case where only SM backgrounds were considered and when signal is included in the estimation. As the CRs are not 100% pure in the process of interest, the cross-contamination between CRs from other processes is estimated. The normalization factors and the cross-contamination are determined simultaneously for all regions using a fit described below.

Detailed CR definitions are given in tables 5, 6, and 7. They are used for the Z (CRZs), $t\bar{t}$ (CRTs), W (CRW), single top (CRST), and $t\bar{t}+Z$ (CRTTGamma) background estimation. The $\left\lvert \Delta\phi\left(\text{jet}^{0,1,2}, \mathbf{p}_{\text{T}}^{\text{miss}}\right)\right\rvert$ and $m_{\text{T}}(\ell, E_{\text{T}}^{\text{miss}})$ requirements are designed to reduce contamination from SM multijet processes. The number of leptons (from this point on, lepton is used to mean electron or muon) is indicated by N_{ℓ} and the transverse momentum of the lepton is indicated by p_{T}^{ℓ}. In all one-lepton CRs, once the trigger and minimum p_{T}^{ℓ} selection are applied, the lepton is treated as a non-b-tagged jet (to emulate the hadronic τ

Selection	CRZAB-TT-TW	CRZAB-T0	CRZD	CRZE
Trigger	electron or muon			
N_ℓ	2, opposite charge, same flavour			
p_T^ℓ	$> 28\,\mathrm{GeV}$			
$m_{\ell\ell}$	$[86,96]\,\mathrm{GeV}$			
N_jet	≥ 4			
$p_\mathrm{T}^0,\ p_\mathrm{T}^1,\ p_\mathrm{T}^2,\ p_\mathrm{T}^3$	$80, 80, 40, 40\,\mathrm{GeV}$			
$E_\mathrm{T}^\mathrm{miss}$	$< 50\,\mathrm{GeV}$			
$E_\mathrm{T}^{\mathrm{miss}'}$	$> 100\mathrm{GeV}$			
$N_{b-\mathrm{jet}}$	≥ 2			
$m_{\mathrm{jet},R=1.2}^0$	$> 120\,\mathrm{GeV}$		–	
$m_{\mathrm{jet},R=1.2}^1$	$> 60\,\mathrm{GeV}$	$< 60\,\mathrm{GeV}$	–	
$m_\mathrm{T}^{b,\mathrm{min}'}$	–		$> 200\,\mathrm{GeV}$	
$m_\mathrm{T}^{b,\mathrm{max}'}$	–		$> 200\,\mathrm{GeV}$	–
H_T	–			$> 500\,\mathrm{GeV}$

Table 5. Selection criteria for the $Z + \mathrm{jets}$ control regions used to estimate the $Z + \mathrm{jets}$ background contributions in the signal regions.

decays in the SRs) in the computation of all jet-related variables. In the two-lepton CRZs, a lepton-p_T requirement of at least $28\,\mathrm{GeV}$ is made to ensure the trigger selection is fully efficient. The invariant mass of the two oppositely charged leptons, denoted by $m_{\ell\ell}$, must be consistent with the leptons having originated from a Z boson. The transverse momenta of these leptons are then vectorially added to the $\mathbf{p}_\mathrm{T}^\mathrm{miss}$ to mimic the $Z \to \nu\bar{\nu}$ decays in the SRs, forming the quantity $E_\mathrm{T}^{\mathrm{miss}'}$. Quantities that depend on the $E_\mathrm{T}^\mathrm{miss}$ are recalculated in the CRZs using $E_\mathrm{T}^{\mathrm{miss}'}$ and identified by the addition of a prime (e.g. $m_\mathrm{T}^{b,\mathrm{min}'}$ and $m_\mathrm{T}^{b,\mathrm{max}'}$). Requirements such as the maximum $m_\mathrm{T}(\ell, E_\mathrm{T}^\mathrm{miss})$ and the minimum ΔR between the two highest-weight b-tagged jets and the lepton, $\Delta R\,(b,\ell)_\mathrm{min}$, are used to enforce orthogonality between CRT, CRW, and CRST. In CRST, the requirement on the ΔR between the two highest-weight b-tagged jets, $\Delta R\,(b,b)$, is used to reject $t\bar{t}$ contamination from the control region enriched in single-top events. Finally, the normalization of the $t\bar{t}+W/Z$ background in the signal region, which is completely dominated by $t\bar{t} + Z(\to \nu\nu)$, is estimated with a $t\bar{t} + \gamma$ control region in a way similar to the method described in ref. [27]. The same lepton triggers and lepton-p_T requirements are used for the $t\bar{t} + \gamma$ control region as in the CRZs. Additionally, the presence of an isolated photon with $p_\mathrm{T} > 150\,\mathrm{GeV}$ is required and it is used to model the Z decay in the signal regions because of the similarity between the diagrams for photon and Z production. Similarly to the Z control region, the photon is used in the estimation of $E_\mathrm{T}^\mathrm{miss}$-related variables.

Selection	CRTA-TT	CRTA-TW	CRTA-T0	CRTB-TT	CRTB-TW	CRTB-T0	CRTC	CRTD	CRTE
Trigger	$E_{\mathrm{T}}^{\mathrm{miss}}$								
N_ℓ	1								
p_{T}^ℓ	> 20 GeV								
N_{jet}	≥ 4 (including electron or muon)								
$p_{\mathrm{T}}^0,\, p_{\mathrm{T}}^1,\, p_{\mathrm{T}}^2,\, p_{\mathrm{T}}^3$	80, 80, 40, 40 GeV								
$N_{b-\mathrm{jet}}$	≥ 2								
$\left|\Delta\phi\left(\mathrm{jet}^{0,1}, \mathbf{p}_{\mathrm{T}}^{\mathrm{miss}}\right)\right|$	> 0.4								
$\left|\Delta\phi\left(\mathrm{jet}^{0,1,2}, \mathbf{p}_{\mathrm{T}}^{\mathrm{miss}}\right)\right|$	> 0.4						–	> 0.4	
$m_{\mathrm{T}}(\ell, E_{\mathrm{T}}^{\mathrm{miss}})$	[30, 100] GeV						< 100 GeV	[30, 100] GeV	
$m_{\mathrm{T}}^{b,\mathrm{min}}$	> 100 GeV						–	> 100 GeV	
$\Delta R(b,\ell)_{\mathrm{min}}$	< 1.5						< 2.0	< 1.5	
$m_{\mathrm{jet},R=1.2}^0$	> 120 GeV						–		
$m_{\mathrm{jet},R=1.2}^1$	> 120 GeV	[60, 120] GeV	< 60 GeV	> 120 GeV	[60, 120] GeV	< 60 GeV	–		
$m_{\mathrm{jet},R=0.8}^0$	> 60 GeV			–					> 120 GeV
$m_{\mathrm{jet},R=0.8}^1$	–								> 80 GeV
$E_{\mathrm{T}}^{\mathrm{miss}}$	> 250 GeV	> 300 GeV	> 350 GeV	> 250 GeV					
$\Delta R(b,b)$	> 1.0	–		> 1.2			–	> 0.8	–
$m_{\mathrm{T}}^{b,\mathrm{max}}$	–			> 200 GeV			–	> 100 GeV	–
p_{T}^1	–							> 150 GeV	–
p_{T}^3	–							> 80 GeV	–
$p_{\mathrm{T}}^{0,b} + p_{\mathrm{T}}^{1,b}$	–							> 300 GeV	–
$N_{\mathrm{jet}}^{\mathrm{S}}$	–						≥ 5	–	
$N_{b\text{-tag}}^{\mathrm{S}}$	–						≥ 1	–	
$p_{\mathrm{T}}^{\mathrm{ISR}}$	–						> 400 GeV	–	
$p_{\mathrm{T}}^{4,\mathrm{S}}$	–						> 40 GeV	–	
H_{T}	–								> 500 GeV

Table 6. Selection criteria for the $t\bar{t}$ control regions used to estimate the $t\bar{t}$ background contributions in the signal regions.

To estimate the Z + jets and $t\bar{t}$ background in the different kinematic regions of the signal regions, individual control regions are designed for all signal regions where possible. Only if the statistical power of control regions is low, are they merged to form one control region for multiple signal regions. In the case of CRST, CRW, and CRTTGamma, this results in the use of one common CR for all signal regions. Distributions from the Z + jets, $t\bar{t}$, W + jets, single top, and $t\bar{t}\gamma$ control regions are shown in figure 4.

Contributions from all-hadronic $t\bar{t}$ and multijet production are found to be negligible. These are estimated from data using a procedure described in ref. [83]. The procedure determines the jet response from simulated dijet events, and then uses this response function to smear the jet response in low-$E_{\mathrm{T}}^{\mathrm{miss}}$ events. The jet response is cross-checked with data where the $E_{\mathrm{T}}^{\mathrm{miss}}$ can be unambiguously attributed to the mismeasurement of one of the jets. Diboson production, which is also subdominant, is estimated directly from simulation.
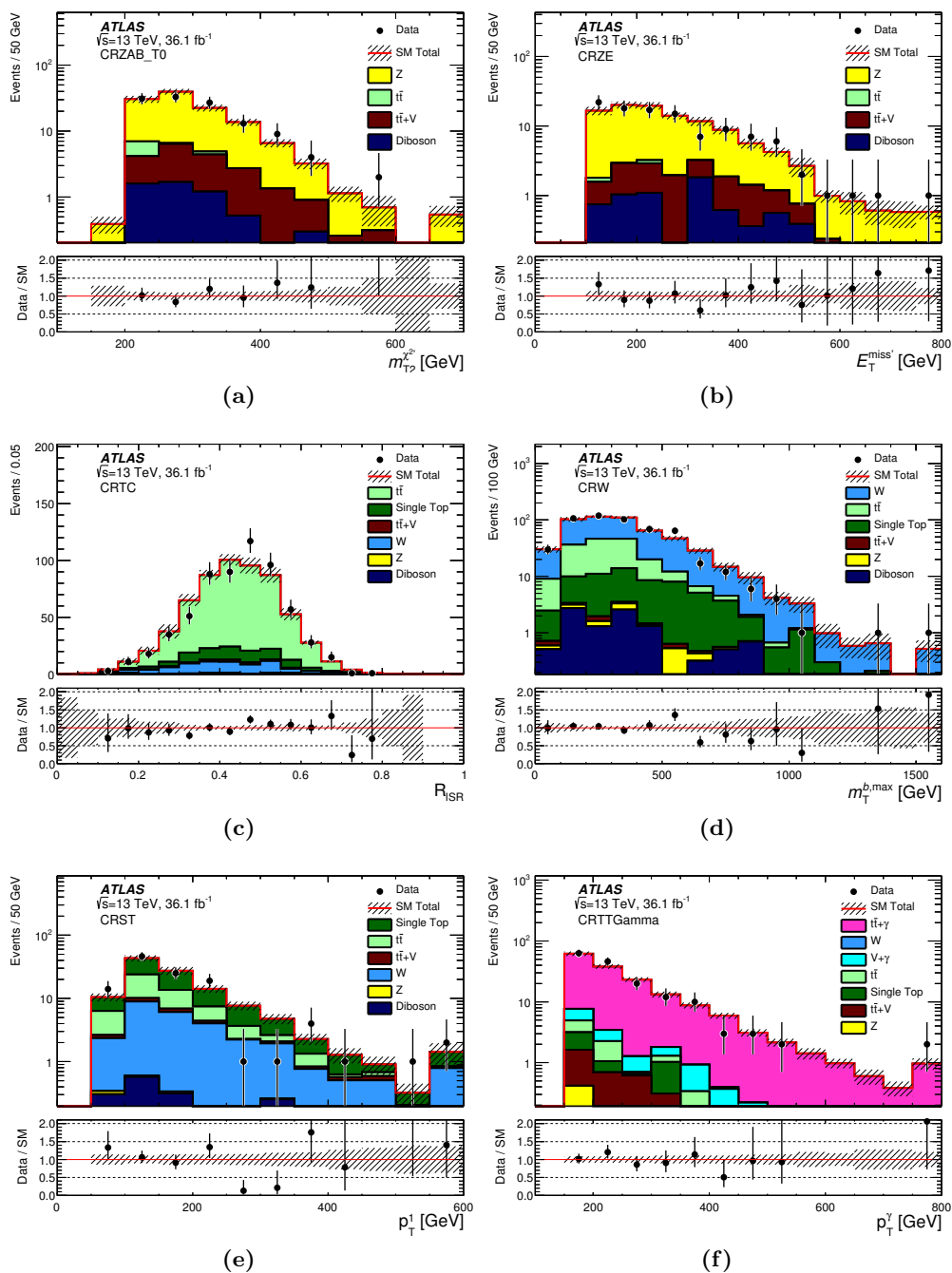
Figure 4. Distributions of (a) $m_{T2}^{\chi^{2\prime}}$ in CRZAB-T0, (b) $E_T^{miss\prime}$ in CRZE, (c) R_{ISR} in CRTC, (d) $m_T^{b,max}$ in CRW, (e) the transverse momentum of the second-leading-p_T jet in CRST, and (f) the photon p_T in CRTTGamma. The stacked histograms show the SM prediction, normalized using scale factors derived from the simultaneous fit to all backgrounds. The "Data/SM" plots show the ratio of data events to the total SM prediction. The hatched uncertainty band around the SM prediction and in the ratio plot illustrates the combination of MC statistical and detector-related systematic uncertainties. The rightmost bin includes overflow events.

Selection	CRW	CRST	CRTTGamma
Trigger	$E_{\mathrm{T}}^{\mathrm{miss}}$		electron or muon
N_ℓ	1		
p_{T}^ℓ	$> 20\,\mathrm{GeV}$		$> 28\,\mathrm{GeV}$
N_γ	$-$		1
p_{T}^γ	$-$		$> 150\,\mathrm{GeV}$
N_{jet}	≥ 4 (including electron or muon)		≥ 4
$p_{\mathrm{T}}^0,\ p_{\mathrm{T}}^1, p_{\mathrm{T}}^2, p_{\mathrm{T}}^3$	$80, 80, 40, 40\,\mathrm{GeV}$		
$N_{b-\mathrm{jet}}$	1	≥ 2	
$\left|\Delta\phi\left(\mathrm{jet}^{0,1}, \mathbf{p}_{\mathrm{T}}^{\mathrm{miss}}\right)\right|$	> 0.4		$-$
$m_{\mathrm{T}}(\ell, E_{\mathrm{T}}^{\mathrm{miss}})$	$[30, 100]\,\mathrm{GeV}$		$-$
$\Delta R\left(b, \ell\right)_{\mathrm{min}}$	> 2.0		$-$
$E_{\mathrm{T}}^{\mathrm{miss}}$	$> 250\,\mathrm{GeV}$		$-$
$\Delta R\left(b, b\right)$	$-$	> 1.5	$-$
$m_{\mathrm{jet}, R=1.2}^0$	$< 60\,\mathrm{GeV}$	$> 120\,\mathrm{GeV}$	
$m_{\mathrm{T}}^{b,\mathrm{min}}$	$-$	$> 200\,\mathrm{GeV}$	$-$

Table 7. Selection criteria for the common $W+$ jets, single-top, and $t\bar{t}+\gamma$ control-region definitions.

Simultaneous fit to determine SM background. The observed numbers of events in the various control regions are included in a binned profile likelihood fit [84] to determine the SM background estimates for Z, $t\bar{t}$, W, single top, and $t\bar{t}+Z$ in each signal region. The normalizations of these backgrounds are determined simultaneously to best match the observed data in each control region, taking contributions from all backgrounds into account. A likelihood function is built as the product of Poisson probability density functions, describing the observed and expected numbers of events in the control regions [85]. This procedure takes common systematic uncertainties (discussed in section 8) between the control and signal regions and their correlations into account as they are treated as nuisance parameters in the fit and are modelled by Gaussian probability density functions. The contributions from all other background processes (dibosons and multijets) are fixed at the values expected from the simulation, using the most accurate theoretical cross sections available, as described in section 4, while their uncertainties are used as nuisance parameters in the fit.

Zero-lepton VRs (VRZAB, VRZD, VRZE) are designed to validate the background estimate for $Z+$ jets in the signal regions. No VRZ is designed for SRC due to the negligible contribution of the Z background in this region. The definitions of the VRZs, after the common zero-lepton preselection discussed in section 6 is applied, are shown in table 8. To provide orthogonality to the signal regions, the requirement on one or more of the following variables is inverted: $\Delta R\left(b, b\right)$, $m_{\mathrm{jet}, R=1.2}^0$, $m_{\mathrm{jet}, R=0.8}^0$.

Selection	VRZAB	VRZD	VRZE
Jet p_T^0, p_T^1	$> 80, > 80\,\mathrm{GeV}$	$> 150, > 80\,\mathrm{GeV}$	$> 80, > 80\,\mathrm{GeV}$
N_{jet}	≥ 4	≥ 5	≥ 4
$N_{b-\mathrm{jet}}$	≥ 2		
τ-veto	yes		no
$m_T^{b,\mathrm{min}}$	$> 200\,\mathrm{GeV}$		
$m_{\mathrm{jet},R=1.2}^0$	$< 120\,\mathrm{GeV}$	$-$	
$\Delta R\,(b,b)$	< 1.0	< 0.8	< 1.0
$m_T^{b,\mathrm{max}}$	$-$	$> 200\,\mathrm{GeV}$	$-$
H_T	$-$		$> 500\,\mathrm{GeV}$
$E_T^{\mathrm{miss}}/\sqrt{H_T}$	$-$		$> 14\,\sqrt{\mathrm{GeV}}$
$m_{\mathrm{jet},R=0.8}^0$	$-$		$< 120\,\mathrm{GeV}$

Table 8. Selection criteria for the Z validation regions used to validate the Z background estimates in the signal regions.

To validate the $t\bar{t}$ background, zero-lepton VRs sharing the same common preselection of the signal regions and which are close to the SRA and SRB definitions are designed for each of the categories (VRTA-TT, VRTA-TW, VRTA-T0, VRTB-TT, VRTB-TW, VRTB-T0). To avoid overlap with the signal regions the $m_T^{b,\mathrm{min}}$ requirement is inverted in all validation regions. In VRTA, SRA requirements remain unchanged except for $m_{\mathrm{T2}}^{\chi^2}$ not being applied, $100 < m_T^{b,\mathrm{min}} < 200\,\mathrm{GeV}$, and the E_T^{miss} requirement being reduced by $100\,\mathrm{GeV}$. For VRTB, all requirements in the VRs are the same as in the SRs except for $m_T^{b,\mathrm{min}}$, which is $100 < m_T^{b,\mathrm{min}} < 200\,\mathrm{GeV}$ for VRTB-TT, $140 < m_T^{b,\mathrm{min}} < 200\,\mathrm{GeV}$ for VRTB-TW, and $160 < m_T^{b,\mathrm{min}} < 200\,\mathrm{GeV}$ for VRTB-T0. For SRC, the same requirements are used when defining the validation region (VRTC) except for the looser requirements of $m_\mathrm{S} > 100\,\mathrm{GeV}$, $p_T^{4,\mathrm{S}} > 40\,\mathrm{GeV}$ and $N_{\mathrm{jet}}^\mathrm{S} > 4$. The $\Delta\phi(\mathrm{ISR}, \mathbf{p}_T^{\mathrm{miss}})$ requirement is inverted and $m_\mathrm{V}/m_\mathrm{S} < 0.6$, where m_V is the transverse mass defined by the visible objects of the sparticle system and the E_T^{miss}, is applied in addition to the existing selection. The validation region to validate the background estimates in SRD (VRTD) is formed by applying the following requirements: $100 < m_T^{b,\mathrm{min}} < 200\,\mathrm{GeV}$, $p_T^{0,b} + p_T^{1,b} > 300\,\mathrm{GeV}$, $p_T^3 > 80\,\mathrm{GeV}$, and $m_T^{b,\mathrm{max}} > 300\,\mathrm{GeV}$. All other requirements are applied exactly as in SRD-low except for the requirement on p_T^4 which is dropped. Finally, the validation region defined for SRE (VRTE) applies only the same requirements on the number of b-jets, $m_{\mathrm{jet},R=0.8}^0$, and $m_{\mathrm{jet},R=0.8}^1$, and inverts the $m_T^{b,\mathrm{min}}$ requirement to $100 < m_T^{b,\mathrm{min}} < 200\,\mathrm{GeV}$. No other requirement is applied to VRTE.

A one-lepton validation region for the $W +$ jets background (VRW) is used to test the W background estimates in all SRs. In this case the validation region is designed based on the definition of CRW. Compared to CRW, the requirement that differs is $\Delta R(b_{0,1}, \ell)_{\mathrm{min}}$, which is greater than 1.8 for the validation region. Two additional requirements are included in the definition of VRW, namely $m_T^{b,\mathrm{min}} > 150\,\mathrm{GeV}$ and $m_{\mathrm{jet},R=1.2}^0 < 70\,\mathrm{GeV}$.
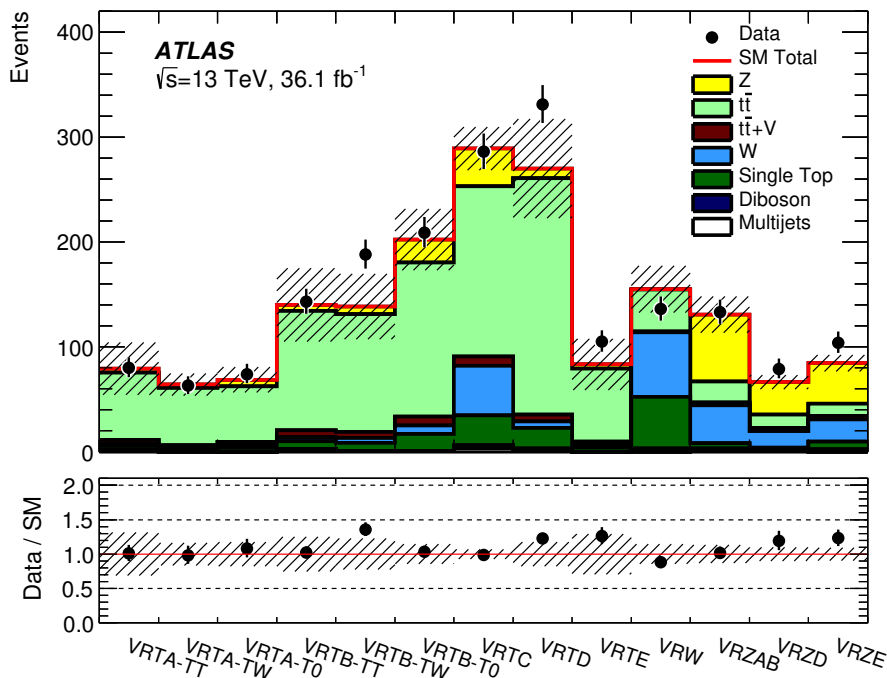
Figure 5. Yields for all validation regions after the likelihood fit. The stacked histograms show the SM prediction and the hatched uncertainty band around the SM prediction shows the total uncertainty, which consists of the MC statistical uncertainties, detector-related systematic uncertainties, and theoretical uncertainties in the extrapolation from CR to VR.

Signal contamination in all the validation regions for all considered signals that have not yet been excluded was also checked. The largest contamination found is ∼25% and occurs in the VRTs for top-squark masses below 350 GeV and in VRZD and VRZE near top-squark masses of 700 GeV. The result of the simultaneous fit procedure, which is repeated with the VRs used as test signal regions, for each VR is shown in figure 5, which displays agreement between data and MC predictions.

8 Systematic uncertainties

Experimental and theoretical systematic uncertainties in the SM predictions and signal predictions are included in the profile likelihood fit described in section 7.

Statistical uncertainties dominate the total uncertainties of the background predictions in all SRs except SRB. The dominant systematic uncertainties for SRA and SRB are shown in table 9 while the systematic uncertainties for the remaining SRs are shown in table 10. The uncertainties are shown as a relative uncertainty to the total background estimate. The main sources of detector-related systematic uncertainty in the SM background estimates are the jet energy scale (JES) and jet energy resolution (JER), b-tagging efficiency, $E_{\mathrm{T}}^{\mathrm{miss}}$ soft term, and pile-up. The effect of the JES and JER uncertainties on the background estimates in the signal regions can reach 17%. The uncertainty in the b-tagging efficiency is nowhere more than 9%. All jet- and lepton-related uncertainties are propagated to

	SRA-TT	SRA-TW	SRA-T0	SRB-TT	SRB-TW	SRB-T0
Total syst. unc.	24	23	15	19	14	15
$t\bar{t}$ theory	10	6	3	10	11	12
$t\bar{t}$+V theory	2	<1	<1	1	<1	<1
Z theory	1	3	2	<1	1	<1
Single top theory	6	3	5	3	4	5
Diboson theory	<1	2	<1	<1	<1	<1
$\mu_{t\bar{t}}$	<1	<1	<1	2	2	1
$\mu_{t\bar{t}+Z}$	6	3	2	4	3	2
μ_Z	6	10	7	5	6	4
μ_W	1	1	1	2	1	2
$\mu_{\text{single top}}$	5	3	5	4	4	5
JER	10	12	4	3	4	3
JES	4	7	1	7	4	<1
b-tagging	1	3	2	5	4	4
$E_{\mathrm{T}}^{\mathrm{miss}}$ soft term	2	2	<1	1	<1	<1
Multijet estimate	1	<1	<1	2	2	<1
Pileup	10	5	5	8	1	3

Table 9. Dominant systematic uncertainties (greater than 1% for at least one SR) for SRA and SRB in percent relative to the total background estimates. The uncertainties due to the normalization from a control region for a given signal region and background are indicated by $\mu_{t\bar{t}+Z}$, $\mu_{t\bar{t}}$, μ_Z, μ_W, and $\mu_{\text{single top}}$. The theory uncertainties are the total uncertainties for a given background. Additionally, the uncertainty due to the number of MC events in the background samples is shown as "MC statistical".

the calculation of the $E_{\mathrm{T}}^{\mathrm{miss}}$, and additional uncertainties in the energy and resolution of the soft term are also included [76]. The uncertainty in the soft term of the $E_{\mathrm{T}}^{\mathrm{miss}}$ is most significant in SRC5 at 15%. An uncertainty due to the pile-up modelling is also considered, with a contribution up to 14%. Lepton reconstruction and identification uncertainties are also considered but have a small impact.

The uncertainty in the combined 2015+2016 integrated luminosity is 3.2%. It is derived, following a methodology similar to that detailed in ref. [86], from a preliminary calibration of the luminosity scale using x–y beam-separation scans performed in August 2015 and May 2016.

Theoretical uncertainties in the modelling of the SM background are estimated. For the W/Z + jets background processes, the modelling uncertainties are estimated using SHERPA samples by varying the renormalization and factorization scales, and the merging and resummation scales (each varied up and down by a factor of two). PDF uncertainties were found to have a negligible impact. The resulting impact on the total background yields from the Z + jets theoretical uncertainties is up to 3% while the uncertainties from the W + jets sample variations are less than 3%.

	SRC1	SRC2	SRC3	SRC4	SRC5	SRD-low	SRD-high	SRE
Total syst. unc.	31	18	18	16	80	25	18	22
$t\bar{t}$ theory	27	11	14	11	71	12	10	11
$t\bar{t}$+V theory	<1	<1	<1	<1	<1	<1	<1	1
Z theory	<1	<1	<1	<1	<1	<1	<1	2
W theory	<1	<1	1	3	2	<1	<1	1
Single top theory	3	2	2	3	<1	5	6	12
$\mu_{t\bar{t}}$	4	6	6	5	5	1	1	<1
$\mu_{t\bar{t}+Z}$	<1	<1	<1	<1	<1	2	2	4
μ_Z	<1	<1	<1	<1	<1	4	5	5
μ_W	<1	<1	1	3	3	3	1	2
$\mu_{\text{single top}}$	3	2	2	3	<1	5	6	6
JER	4	10	6	5	10	3	6	4
JES	4	5	2	2	17	8	4	5
b-tagging	2	2	<1	2	4	9	7	<1
$E_{\mathrm{T}}^{\text{miss}}$ soft term	1	3	2	3	15	4	3	2
Multijet estimate	12	3	<1	<1	<1	2	2	<1
Pileup	<1	1	<1	2	14	9	<1	2

Table 10. Dominant systematic uncertainties (greater than 1% for at least one SR) for SRC, SRD, and SRE in percent relative to the total background estimates. The uncertainty due to the normalization from a control region for a given signal region and background are indicated by $\mu_{t\bar{t}+Z}$, $\mu_{t\bar{t}}$, μ_Z, μ_W, and $\mu_{\text{single top}}$. The theory uncertainties are the total uncertainties for a given background. Additionally, the uncertainty due to the number of MC events in the background samples is shown as "MC statistical".

For the $t\bar{t}$ background, uncertainties are estimated from the comparison of different matrix-element calculations, the choice of parton-showering model and the emission of additional partons in the initial and final states (comparing POWHEG-BOX+PYTHIA vs HERWIG++ and SHERPA). More details are given in ref. [55]. The largest impact of the $t\bar{t}$ theory systematic uncertainties on the total background yields arises for SRC and it varies from 11% to 71% by tightening the R_{ISR} requirement. For the $t\bar{t}$+W/Z background, the theoretical uncertainty is estimated through variations, in both $t\bar{t}$+W/Z and $t\bar{t}\gamma$ MC simulation, including the choice of renormalization and factorization scales (each varied up and down by a factor of two), the choice of PDF, as well as a comparison between MC@NLO and OpenLoops+SHERPA generators, resulting in a maximum uncertainty of 2% in SRA-TT. The single-top background is dominated by the Wt subprocess. Uncertainties are estimated for the choice of parton-showering model (PYTHIA vs HERWIG++) and for the emission of additional partons in the initial- and final-state radiation. A 30% uncertainty is assigned to the single-top background estimate to account for the effect of interference between single-top-quark and $t\bar{t}$ production. This uncertainty is estimated by comparing yields in the signal and control regions for a sample that includes resonant and non-resonant WW+bb production with the sum of the yields of resonant $t\bar{t}$ and single-top+b production. The final single-top uncertainty relative to the total background estimate is

up to 12%. The detector systematic uncertainties are also applied to the signal samples used for interpretation. Theoretical uncertainties in the signal cross section as described in section 4 are treated separately and limits on top-squark and neutralino masses are given for the $\pm 1\sigma$ values as well as the central cross section.

Signal systematic uncertainties due to detector and acceptance effects are taken into account. The main sources of these uncertainties are the JER, ranging from 3% to 6%, the JES, ranging from 2% to 5.7%, pile-up, ranging from 0.5% to 5.5% and from b-tagging efficiency, ranging from 3% to 5.5%. Uncertainties in the acceptance due to theoretical variations are taken into consideration. Those originate from variations of the QCD coupling constant α_{s}, the variations of the renormalization and factorization scales, the CKKW matching scale at which the parton-shower description and the matrix-element description are separate and the parton-shower tune variations (each varied up and down by a factor of two). These uncertainties range across the SRs between 10% and 25% for the $\tilde{t}_1 \to t^{(*)}\tilde{\chi}_1^0$ grid, the mixed grid, the non-asymptotic higgsino grid, and the $\tilde{g} \to t\tilde{t}_1 \to t\tilde{\chi}_1^0 +$soft grid. For the wino-NLSP model, they range from 15% to 20%, and for the well-tempered neutralino pMSSM model they range from 10% to 35%. Finally, the uncertainty in the estimated number of signal events which arises from the cross-section uncertainties for the various processes is taken into account by calculating two additional limits considering a $\pm 1\sigma$ change in cross section. The cross-section uncertainty is $\sim$15–20% for direct top-squark production and $\sim$15–30% for gluino production [12–15] depending on the top-squark and gluino masses.

9   Results and interpretation

The observed event yields are compared to the expected total number of background events in tables 11, 12, 13, and figure 6. The total background estimate is determined from a simultaneous fit to all control regions, based on a procedure described in section 7 but including the corresponding signal regions as well as control regions. Figure 7 shows the distribution of $E_{\mathrm{T}}^{\mathrm{miss}}$, $m_{\mathrm{T2}}^{\chi^2}$, $m_{\mathrm{T}}^{b,\mathrm{max}}$, m_{T}, R_{ISR}, and H_{T} for the various signal regions, with R_{ISR} being shown combining SRC1-5. In these distributions, the background predictions are scaled to the values determined from the simultaneous fit.

No significant excess above the SM prediction is observed in any of the signal regions. The smallest p-values, which express the probability that the background fluctuates to the data or above, are 27%, 27%, and 29% for SRB-T0, SRD-high, and SRA-TT, respectively. The largest deficit in the data can be found in SRC4 where one event is observed while 7.7 background events were expected. The 95% confidence level (CL) upper limits on the number of beyond-the-SM (BSM) events in each signal region are derived using the CL_{s} prescription [87, 88] and calculated from asymptotic formulae [84]. Model-independent limits on the visible BSM cross sections, defined as $\sigma_{\mathrm{vis}} = S_{\mathrm{obs}}^{95}/\int\mathcal{L}\,dt$, where S_{obs}^{95} is the 95% CL upper limit on the number of signal events, are reported in table 14.

The detector acceptance multiplied by the efficiency $(A \cdot \epsilon)$ is calculated for several signal regions and their benchmark points. The $A \cdot \epsilon$ values for signal regions aimed at high-energy final states, SRA and SRE, are 9% and 6% for their respective signal bench-

	SRA-TT	SRA-TW	SRA-T0	SRB-TT	SRB-TW	SRB-T0
Observed	11	9	18	38	53	206
Fitted background events						
Total SM	8.6 ± 2.1	9.3 ± 2.2	18.7 ± 2.7	39.3 ± 7.6	52.4 ± 7.4	179 ± 26
$t\bar{t}$	$0.71 ^{+0.91}_{-0.71}$	$0.51 ^{+0.55}_{-0.51}$	1.31 ± 0.64	7.3 ± 4.3	12.4 ± 5.9	43 ± 22
W + jets	0.82 ± 0.15	0.89 ± 0.56	2.00 ± 0.83	7.8 ± 2.8	4.8 ± 1.2	25.8 ± 8.8
Z + jets	2.5 ± 1.3	4.9 ± 1.9	9.8 ± 1.6	9.0 ± 2.8	16.8 ± 4.1	60.7 ± 9.6
$t\bar{t}+W/Z$	3.16 ± 0.66	1.84 ± 0.39	2.60 ± 0.53	9.3 ± 1.7	10.8 ± 1.6	20.5 ± 3.2
Single top	1.20 ± 0.81	0.70 ± 0.42	2.9 ± 1.5	4.2 ± 2.2	5.9 ± 2.8	26 ± 13
Dibosons	$--$	0.35 ± 0.26	$--$	0.13 ± 0.07	0.60 ± 0.43	1.04 ± 0.73
Multijets	0.21 ± 0.10	0.14 ± 0.09	0.12 ± 0.07	1.54 ± 0.64	1.01 ± 0.88	1.8 ± 1.5
Expected events before fit						
Total SM	7.1	7.9	16.3	32.4	46.1	162
$t\bar{t}$	0.60	0.45	1.45	6.1	12.8	47
W + jets	0.65	0.70	1.58	6.1	3.83	20.4
Z + jets	2.15	4.2	8.63	7.7	14.4	53.6
$t\bar{t}+W/Z$	2.46	1.43	2.02	7.3	8.4	15.9
Single top	1.03	0.60	2.5	3.6	5.1	22.4
Dibosons	$--$	0.35	$--$	0.13	0.60	1.03
Multijets	0.21	0.14	0.12	1.54	1.01	1.8

Table 11. Observed and expected yields, before and after the fit, for SRA and SRB. The uncertainties include MC statistical uncertainties, detector-related systematic uncertainties, and theoretical uncertainties in the extrapolation from CR to SR.

mark points of $m_{\tilde{t}_1} = 1000\,\text{GeV}$, $m_{\tilde{\chi}_1^0} = 1\,\text{GeV}$, and $m_{\tilde{g}} = 1700\,\text{GeV}$, $m_{\tilde{t}_1} = 400\,\text{GeV}$, $m_{\tilde{\chi}_1^0} = 395\,\text{GeV}$. SRB, SRD-low, and SRD-high have $A \cdot \epsilon$ of 1.4%, 0.05%, and 0.5% for $m_{\tilde{t}_1} = 600\,\text{GeV}, m_{\tilde{\chi}_1^0} = 300\,\text{GeV}$; $m_{\tilde{t}_1} = 400\,\text{GeV}, m_{\tilde{\chi}_1^\pm} = 100\,\text{GeV}, m_{\tilde{\chi}_1^0} = 50\,\text{GeV}$; and $m_{\tilde{t}_1} = 700\,\text{GeV}, m_{\tilde{\chi}_1^\pm} = 200\,\text{GeV}, m_{\tilde{\chi}_1^0} = 100\,\text{GeV}$ where the branching ratio, $B(\tilde{t}_1 \to b \tilde{\chi}_1^\pm) = 100\%$ is assumed for the SRD samples, respectively. Finally, SRC1-5 (combining the R_{ISR} windows) has an $A \cdot \epsilon$ of 0.08% for $m_{\tilde{t}_1} = 400\,\text{GeV}, m_{\tilde{\chi}_1^0} = 227\,\text{GeV}$.

The profile-likelihood-ratio test statistic is used to set limits on direct pair production of top squarks. The signal strength parameter is allowed to float in the fit [85], and any signal contamination in the CRs is taken into account. Again, limits are derived using the CL_s prescription and calculated from asymptotic formulae. Orthogonal signal subregions, such as SRA-TT, SRA-TW, and SRA-T0, are statistically combined by multiplying their likelihood functions. A similar procedure is performed for the signal subregions in SRB and SRC. For the overlapping signal regions defined for SRD (SRD-low and SRD-high), the signal region with the smallest expected CL_s value is chosen for each signal model. Once the signal subregions are combined or chosen, the signal region with the smallest expected CL_s is chosen for each signal model in the $\tilde{t}_1$–$\tilde{\chi}_1^0$ signal grid. The nominal event yield in each SR is set to the mean background expectation to determine the expected limits; contours that correspond to $\pm 1\sigma$ uncertainties in the background estimates (σ_{exp}) are also

	SRC1	SRC2	SRC3	SRC4	SRC5
Observed	20	22	22	1	0
Fitted background events					
Total SM	20.6 ± 6.5	27.6 ± 4.9	18.9 ± 3.4	7.7 ± 1.2	0.91 ± 0.73
$t\bar{t}$	12.9 ± 5.9	22.1 ± 4.3	14.6 ± 3.2	4.91 ± 0.97	$0.63 \,^{+\,0.70}_{-\,0.63}$
W + jets	0.80 ± 0.37	1.93 ± 0.49	1.91 ± 0.62	1.93 ± 0.46	0.21 ± 0.12
Z + jets	$--$	$--$	$--$	$--$	$--$
$t\bar{t}+W/Z$	0.29 ± 0.16	0.59 ± 0.38	0.56 ± 0.31	0.08 ± 0.08	0.06 ± 0.02
Single top	1.7 ± 1.3	$1.2 \,^{+\,1.4}_{-\,1.2}$	1.22 ± 0.69	0.72 ± 0.37	$--$
Dibosons	0.39 ± 0.33	$0.21 \,^{+\,0.23}_{-\,0.21}$	0.28 ± 0.18	$--$	$--$
Multijets	4.6 ± 2.4	1.58 ± 0.77	0.32 ± 0.17	0.04 ± 0.02	$--$
Expected events before fit					
Total SM	25.4	36.0	24.2	9.2	1.1
$t\bar{t}$	18.2	31.2	20.6	7.0	0.89
W + jets	0.64	1.53	1.51	1.53	0.17
Z + jets	$--$	$--$	$--$	$--$	$--$
$t\bar{t}+W/Z$	0.22	0.46	0.44	0.07	0.05
Single top	1.44	1.0	1.04	0.62	$--$
Dibosons	0.39	0.21	0.28	$--$	$--$
Multijets	4.6	1.58	0.32	0.04	$--$

Table 12. Observed and expected yields, before and after the fit. The uncertainties include MC statistical uncertainties, detector-related systematic uncertainties, and theoretical uncertainties in the extrapolation from CR to SR.

evaluated. The observed event yields determine the observed limits for each SR; these are evaluated for the nominal signal cross sections as well as for $\pm 1\sigma$ theory uncertainties in those cross sections, denoted by $\sigma_{\text{theory}}^{\text{SUSY}}$.

Figure 8 shows the observed (solid red line) and expected (solid blue line) exclusion contours at 95% CL in the $\tilde{t}_1$–$\tilde{\chi}_1^0$ mass plane for 36.1 fb^{-1}. The data excludes top-squark masses between 450 and 1000 GeV for $\tilde{\chi}_1^0$ masses below 160 GeV, extending Run-1 limits from the combination of zero- and one-lepton channels by 260 GeV. Additional constraints are set in the case where $m_{\tilde{t}_1} \approx m_t + m_{\tilde{\chi}_1^0}$, for which top-squark masses in the range 235−590 GeV are excluded. The limits in this region of the exclusion are new compared to the 8 TeV results and come from the inclusion of SRC, which takes advantage of an ISR system to discriminate between signal and the dominant $t\bar{t}$ background.

For signal models also considering top-squark decays into $b\tilde{\chi}_1^\pm$ or into additional massive neutralinos, four interpretations are considered:

	SRD-low	SRD-high	SRE
Observed	27	11	3
Fitted background events			
Total SM	25.1 ± 6.2	8.5 ± 1.5	3.64 ± 0.79
$t\bar{t}$	3.3 ± 3.3	0.98 ± 0.88	$0.21 \, ^{+\,0.39}_{-\,0.21}$
W + jets	6.1 ± 2.9	1.06 ± 0.34	0.52 ± 0.27
Z + jets	6.9 ± 1.5	3.21 ± 0.62	1.36 ± 0.25
$t\bar{t}+W/Z$	3.94 ± 0.85	1.37 ± 0.32	0.89 ± 0.19
Single top	3.8 ± 2.1	1.51 ± 0.74	0.66 ± 0.49
Dibosons	$--$	$--$	$--$
Multijets	1.12 ± 0.37	0.40 ± 0.15	$--$
Expected events before fit			
Total SM	22.4	7.7	3.02
$t\bar{t}$	3.4	1.04	0.21
W + jets	4.8	0.84	0.42
Z + jets	6.7	3.10	1.15
$t\bar{t}+W/Z$	3.06	1.07	0.69
Single top	3.3	1.30	0.56
Dibosons	$--$	$--$	$--$
Multijets	1.12	0.40	$--$

Table 13. Observed and expected yields, before and after the fit, for SRD and SRE. The uncertainties include MC statistical uncertainties, detector-related systematic unceatinties, and theoretical uncertainties in the extrapolation from CR to SR.

Natural SUSY-inspired mixed grid: a simplified model [89] where $m_{\tilde{\chi}_1^\pm} = m_{\tilde{\chi}_1^0} + 1\,\mathrm{GeV}$ with only two decay modes, $\tilde{t}_1 \to b\tilde{\chi}_1^\pm$ and $\tilde{t}_1 \to t\tilde{\chi}_1^0$, and only on-shell top-quark decays are considered. The same maximal mixing between the partners of the left- and right-handed top quarks and nature of the $\tilde{\chi}_1^0$ (pure bino) as for the $B(\tilde{t}_1 \to t\tilde{\chi}_1^0)$=100% case is assumed. The branching ratio to $\tilde{t}_1 \to t\tilde{\chi}_1^0$ is set to 0%, 25%, 50%, and 75% and yield the limits shown in figure 9.

Non-asymptotic higgsino: a pMSSM-inspired simplified model with a higgsino LSP, $m_{\tilde{\chi}_1^\pm} = m_{\tilde{\chi}_1^0} + 5\,\mathrm{GeV}$, and $m_{\tilde{\chi}_2^0} = m_{\tilde{\chi}_1^0} + 10\,\mathrm{GeV}$, assumes three sets of branching ratios for the considered decays of $\tilde{t}_1 \to t\tilde{\chi}_2^0$, $\tilde{t}_1 \to t\tilde{\chi}_1^0$, $\tilde{t}_1 \to b\tilde{\chi}_1^\pm$ [89]. A set of branching ratios with $B(\tilde{t}_1 \to t\tilde{\chi}_2^0, \tilde{t}_1 \to t\tilde{\chi}_1^0, \tilde{t}_1 \to b\tilde{\chi}_1^\pm) = 33\%$, 33%, 33% is considered, which is equivalent to a pMSSM model with the lightest top squark mostly consisting of the superpartner of left-handed top quark and $\tan\beta = 60$ (ratio of vacuum expectation values of the two Higgs doublets). Additionally, $B(\tilde{t}_1 \to t\tilde{\chi}_2^0, \tilde{t}_1 \to t\tilde{\chi}_1^0, \tilde{t}_1 \to b\tilde{\chi}_1^\pm) = 45\%$, 10%, 45% and $B(\tilde{t}_1 \to t\tilde{\chi}_2^0, \tilde{t}_1 \to t\tilde{\chi}_1^0, \tilde{t}_1 \to b\tilde{\chi}_1^\pm) = 25\%$, 50%, 25% are assumed, which correspond to scenarios with $m_{\tilde{q}L3} < m_{\tilde{t}R}$ (regardless of the choice
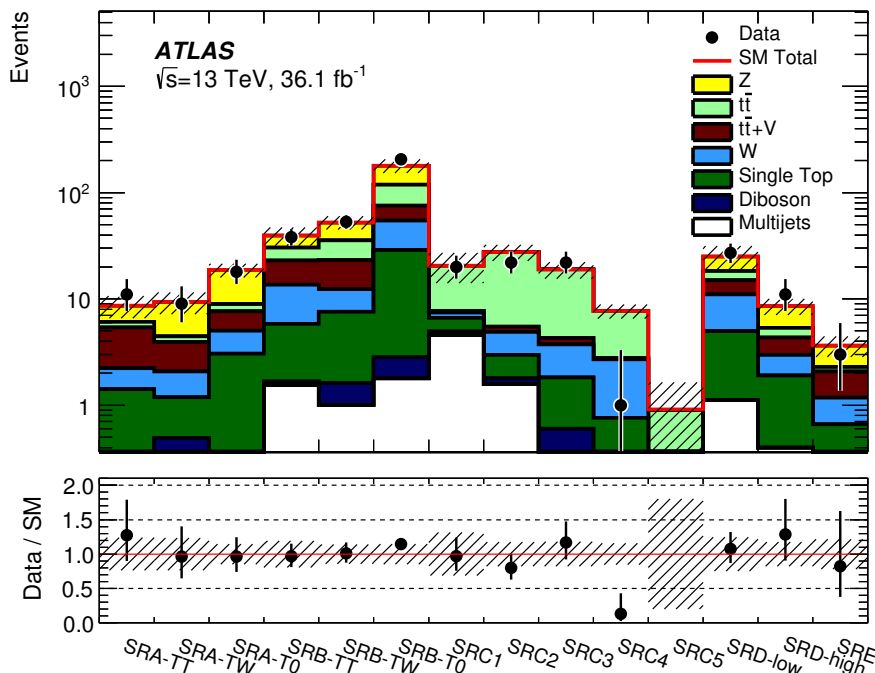
Figure 6. Yields for all signal regions after the likelihood fit. The stacked histograms show the SM prediction and the hatched uncertainty band around the SM predicttion shows total uncertainty, which consists of the MC statistical uncertainties, detector-related systematic uncertainties, and theoretical uncertainties in the extrapolation from CR to SR.

of $\tan\beta$) and $m_{\tilde{t}R} < m_{\tilde{q}L3}$ with $\tan\beta = 20$, respectively. Here $m_{\tilde{q}L3}$ represents the left-handed third-generation mass parameter and $m_{\tilde{t}R}$ is the mass parameter of the superpartner to the right-handed top-quark. Limits in the $m_{\tilde{t}_1}$ and $m_{\tilde{\chi}_1^0}$ plane are shown in figure 10.

Wino-NLSP pMSSM: a pMSSM model where the LSP is bino-like and has mass M_1 and where the NLSP is wino-like with mass M_2, while $M_2 = 2M_1$ and $m_{\tilde{t}_1} > M_1$ [89]. Limits are set for both positive and negative μ (the higgsino mass parameter) as a function of the $\tilde{t}_1$ and $\tilde{\chi}_1^0$ masses which can be translated to different M_1 and $m_{\tilde{q}L3}$, and are shown in figure 11. Only bottom and top-squark production are considered in this interpretation. Allowed decays in the top-squark production scenario are $\tilde{t}_1 \to t\tilde{\chi}_2^0 \to h/Z\tilde{\chi}_1^0$, at a maximum branching ratio of 33%, and $\tilde{t}_1 \to b\tilde{\chi}_1^\pm$. Whether the $\tilde{\chi}_2^0$ dominantly decays into a h or Z is determined by the sign of μ. Along the diagonal region, the $\tilde{t}_1 \to t\tilde{\chi}_1^0$ decay with 100% branching ratio is also considered. The equivalent decays in bottom-squark production are $\tilde{b} \to t\tilde{\chi}_1^\pm$ and $\tilde{b} \to b\tilde{\chi}_2^0$. The remaining pMSSM parameters have the following values: $M_3 = 2.2$ TeV (gluino mass parameter), $M_S = \sqrt{m_{\tilde{t}_1} m_{\tilde{t}_2}} = 1.2$ TeV (geometric mean of top-squark masses), $X_t/M_S = \sqrt{6}$ (mixing parameter between the superpartners of left- and right-handed states, where $X_t = A_t - \mu/\tan\beta$ and A_t is the trilinear coupling parameter in the top-quark sector), and $\tan\beta = 20$. All other pMSSM masses are set to >3 TeV.
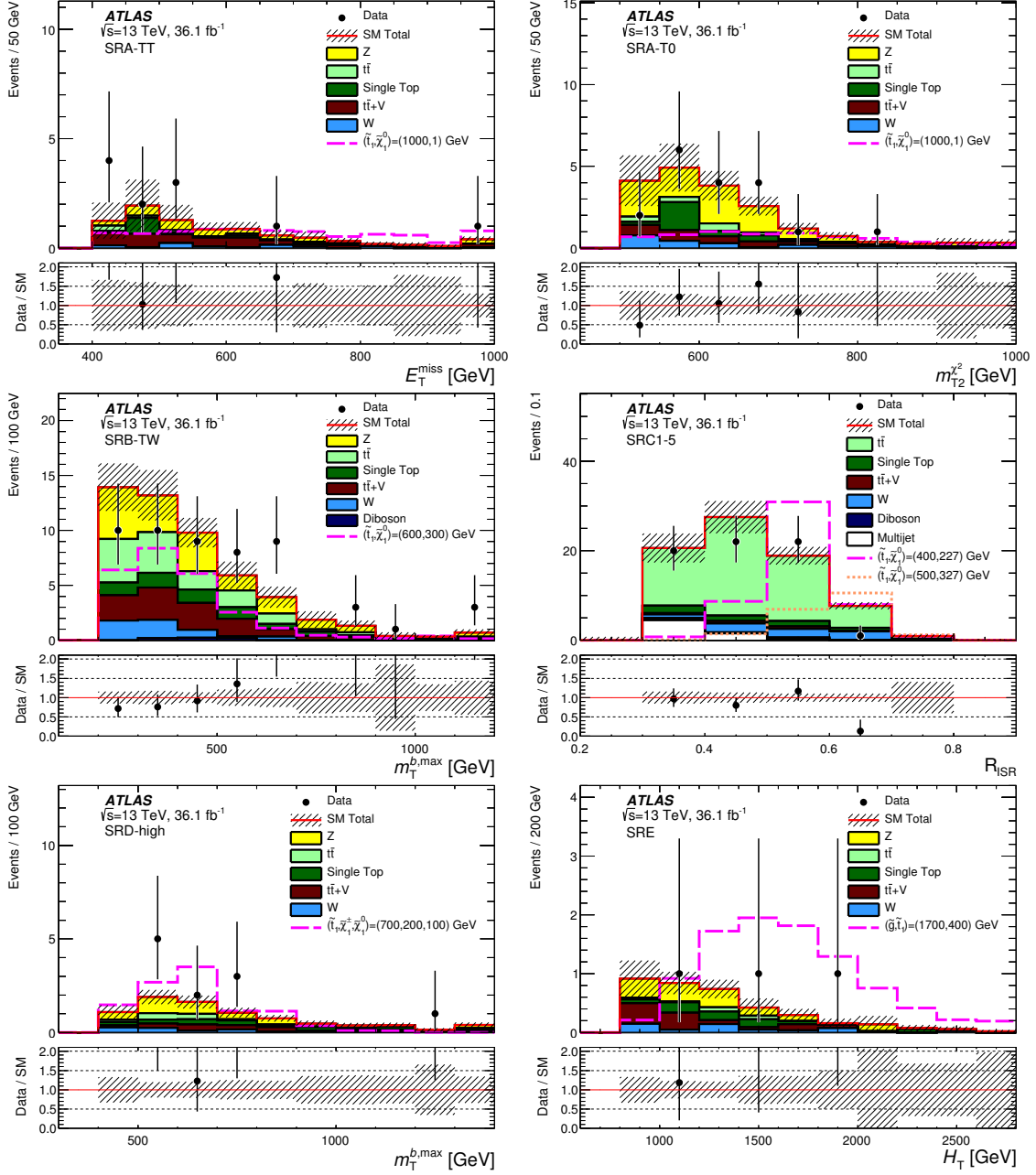
Figure 7. Distributions of E_T^{miss} for SRA-TT, $m_{T2}^{\chi^2}$ for SRA-T0, $m_T^{b,max}$ for SRB-TW, R_{ISR} for SRC1-5, $m_T^{b,max}$ for SRD-high and H_T for SRE after the likelihood fit. The stacked histograms show the SM prediction and the hatched uncertainty band around the SM prediction shows the MC statistical and detector-related systematic uncertainties. For each variable, the distribution for a representative signal point is shown.

Well-tempered neutralino pMSSM: a pMSSM model in which three light neutralinos and a light chargino, which are mixtures of bino and higgsino states, are considered with masses within 50 GeV of the lightest state [90, 91]. The model is designed to satisfy the SM Higgs boson mass and the dark-matter relic density $(0.10 < \Omega h^2 < 0.12,$

Signal channel	$\langle\sigma A\epsilon\rangle^{95}_{\mathrm{obs}}$ [fb]	S^{95}_{obs}	S^{95}_{exp}	$\mathrm{CL_B}$	$p\,(z)$
SRA-TT	0.30	11.0	$8.7^{+3.0}_{-1.4}$	0.78	0.23 (0.74)
SRA-TW	0.27	9.6	$9.6^{+2.8}_{-2.1}$	0.50	0.50 (0.00)
SRA-T0	0.31	11.2	$11.5^{+3.8}_{-2.0}$	0.46	0.50 (0.00)
SRB-TT	0.54	19.6	$20.0^{+6.5}_{-4.9}$	0.46	0.50 (0.00)
SRB-TW	0.60	21.7	$21.0^{+7.3}_{-4.3}$	0.54	0.50 (0.00)
SRB-T0	2.19	80	58^{+23}_{-17}	0.83	0.13 (1.15)
SRC1	0.42	15.1	$15.8^{+4.8}_{-3.5}$	0.48	0.50 (0.00)
SRC2	0.31	11.2	$13.9^{+5.9}_{-3.6}$	0.24	0.50 (0.00)
SRC3	0.42	15.3	$12.3^{+4.7}_{-3.4}$	0.73	0.27 (0.62)
SRC4	0.10	3.5	$6.7^{+2.8}_{-1.8}$	0.00	0.50 (0.00)
SRC5	0.09	3.2	$3.0^{+1.1}_{-0.1}$	0.23	0.23 (0.74)
SRD-low	0.50	17.9	$16.4^{+6.3}_{-4.0}$	0.62	0.36 (0.35)
SRD-high	0.30	10.9	$8.0^{+3.4}_{-1.3}$	0.79	0.21 (0.79)
SRE	0.17	6.1	$6.4^{+1.4}_{-2.4}$	0.42	0.50 (0.00)

Table 14. Left to right: 95% CL upper limits on the average visible cross section ($\langle\sigma A\epsilon\rangle^{95}_{\mathrm{obs}}$) where the average comes from possibly multiple production channels and on the number of signal events (S^{95}_{obs}). The third column (S^{95}_{exp}) shows the 95% CL upper limit on the number of signal events, given the expected number (and $\pm 1\sigma$ excursions of the expected number) of background events. The two last columns indicate the $\mathrm{CL_B}$ value, i.e. the confidence level observed for the background-only hypothesis, and the discovery p-value (p) and the corresponding significance (z).

where Ω is energy density parameter and h is the Planck constant [92]) with pMSSM parameters: $M_1 = -(\mu + \delta)$ where $\delta = 20$–$50\,\mathrm{GeV}$, $M_2 = 2.0\,\mathrm{TeV}$, $M_3 = 1.8\,\mathrm{TeV}$, $M_S = 0.8$–$1.2\,\mathrm{TeV}$, $X_t/M_S \sim \sqrt{6}$, and $\tan\beta = 20$. For this model, limits are shown in figure 12. Only bottom- and top-squark production are considered in this interpretation. The signal grid points were produced in two planes, μ vs $m_{\tilde{t}\mathrm{R}}$ and μ vs $m_{\tilde{q}\mathrm{L3}}$, and then projected to the corresponding $\tilde{t}_1$ and $\tilde{\chi}^0_1$ masses. All other pMSSM masses are set to $>3\,\mathrm{TeV}$.

The SRE results are interpreted for indirect top-squark production through gluino decays in terms of the $\tilde{t}_1$ vs $\tilde{g}$ mass plane with $\Delta m(\tilde{t}_1, \tilde{\chi}^0_1) = 5\,\mathrm{GeV}$. Gluino masses up to $m_{\tilde{g}} = 1800\,\mathrm{GeV}$ with $m_{\tilde{t}_1} < 800\,\mathrm{GeV}$ are excluded as shown in figure 13.

10 Conclusions

Results from a search for top squark pair production based on an integrated luminosity of $36.1\,\mathrm{fb}^{-1}$ of $\sqrt{s} = 13\,\mathrm{TeV}$ pp collision data recorded by the ATLAS experiment at the LHC in 2015 and 2016 are presented. Top squarks are searched for in final states with
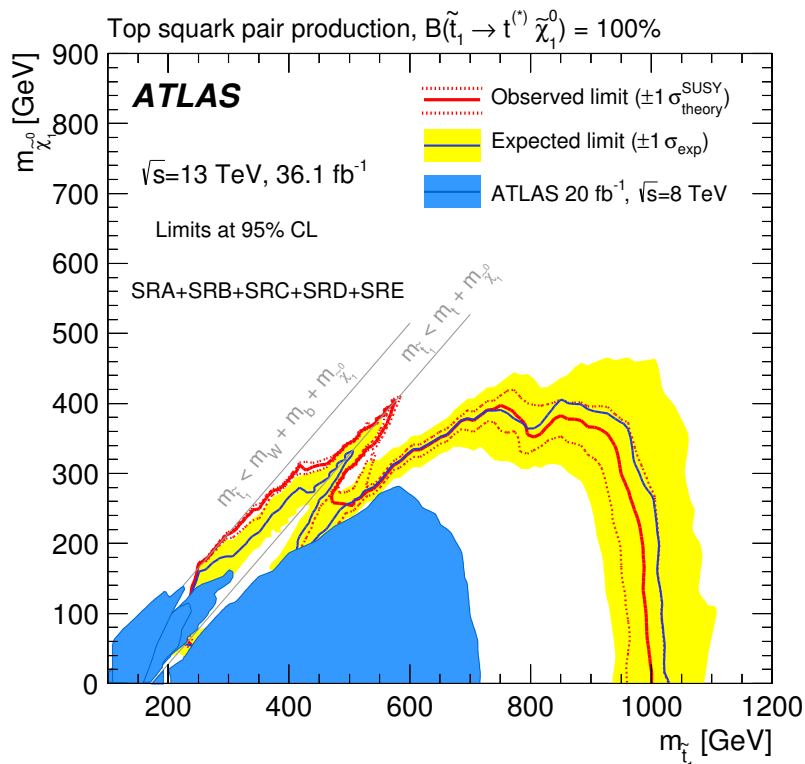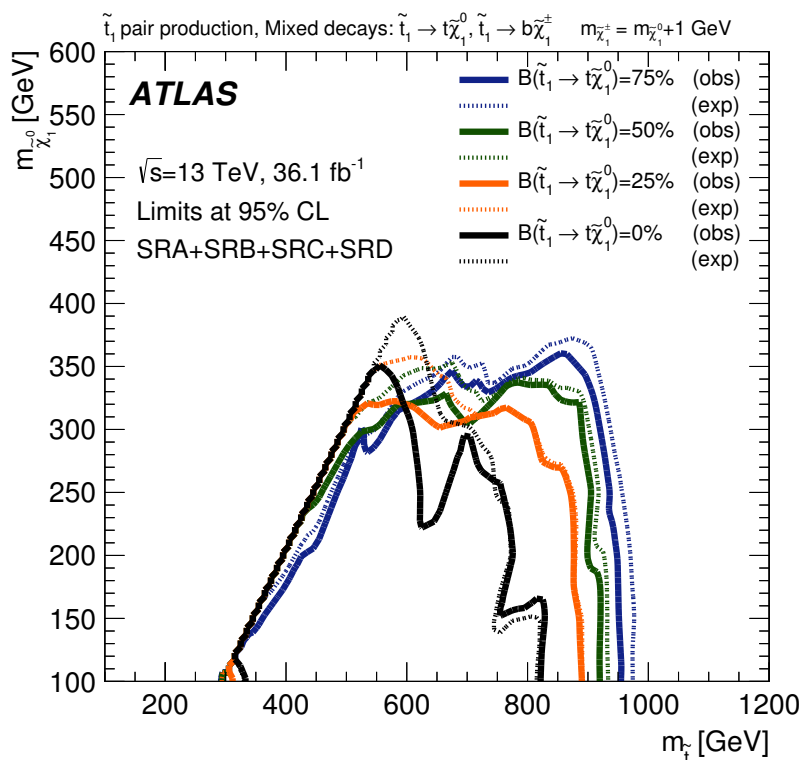
Figure 8. Observed (red solid line) and expected (blue solid line) exclusion contours at 95% CL as a function of $\tilde{t}_1$ and $\tilde{\chi}_1^0$ masses in the scenario where both top squarks decay via $\tilde{t}_1 \to t^{(*)}\tilde{\chi}_1^0$. Masses that are within the contours are excluded. Uncertainty bands corresponding to the $\pm 1\sigma$ variation of the expected limit (yellow band) and the sensitivity of the observed limit to $\pm 1\sigma$ variations of the signal theoretical uncertainties (red dotted lines) are also indicated. Observed limits from all third-generation Run-1 searches [26] at $\sqrt{s} = 8$ TeV overlaid for comparison in blue.

high-p_{T} jets and large missing transverse momentum. In this paper, direct top squark production is studied assuming top squarks decay via $\tilde{t}_1 \to t^{(*)}\tilde{\chi}_1^0$ with large or small mass differences between the top squark and the neutralino $\Delta m(\tilde{t}_1, \tilde{\chi}_1^0)$ and via $\tilde{t}_1 \to b\tilde{\chi}_1^\pm$, where $m_{\tilde{\chi}_1^\pm} = m_{\tilde{\chi}_1^0} + 1$ GeV. Additionally, gluino-mediated $\tilde{t}_1$ production is studied, in which gluinos decay via $\tilde{g} \to t\tilde{t}_1$, with a small $\Delta m(\tilde{t}_1, \tilde{\chi}_1^0)$.

No significant excess above the expected SM background is observed. Exclusion limits at 95% confidence level in the plane of the top-squark and LSP masses are derived, resulting in the exclusion of top-squark masses in the range $450-1000$ GeV for $\tilde{\chi}_1^0$ masses below 160 GeV. For the case where $m_{\tilde{t}_1} \sim m_t + m_{\tilde{\chi}_1^0}$, top-squark masses in the range $235-590$ GeV are excluded. In addition, model-independent limits and p-values for each signal region are reported. Limits that take into account an additional decay of $\tilde{t}_1 \to b\tilde{\chi}_1^\pm$ are also set with an exclusion of top-squark masses between 450 and 850 GeV for $m_{\tilde{\chi}_1^0} < 240$ GeV and $B(\tilde{t}_1 \to t\tilde{\chi}_1^0) = 50\%$ for $m_{\tilde{\chi}_1^\pm} = m_{\tilde{\chi}_1^0} + 1$ GeV. Limits are also derived in two pMSSM models, where one model assumes a wino-like NLSP and the other model is constrained by the dark-matter relic density. In addition to limits in pMSSM slices, limits are set in terms of one

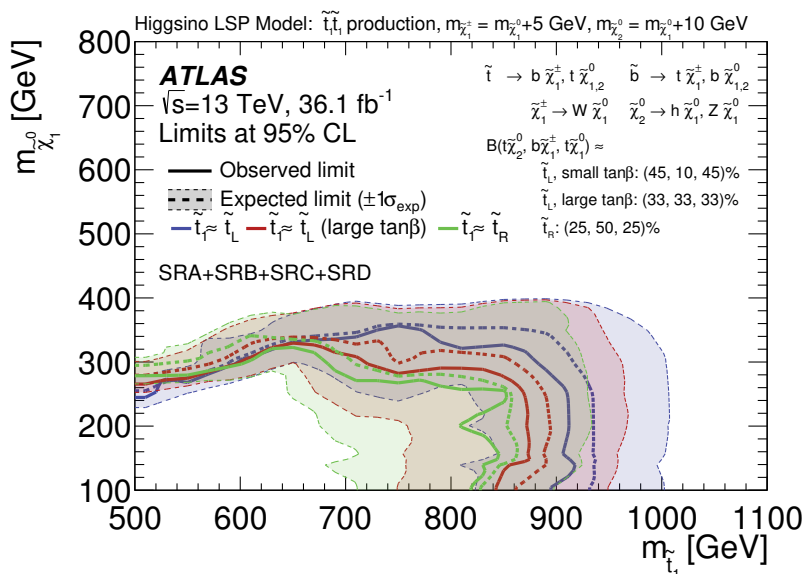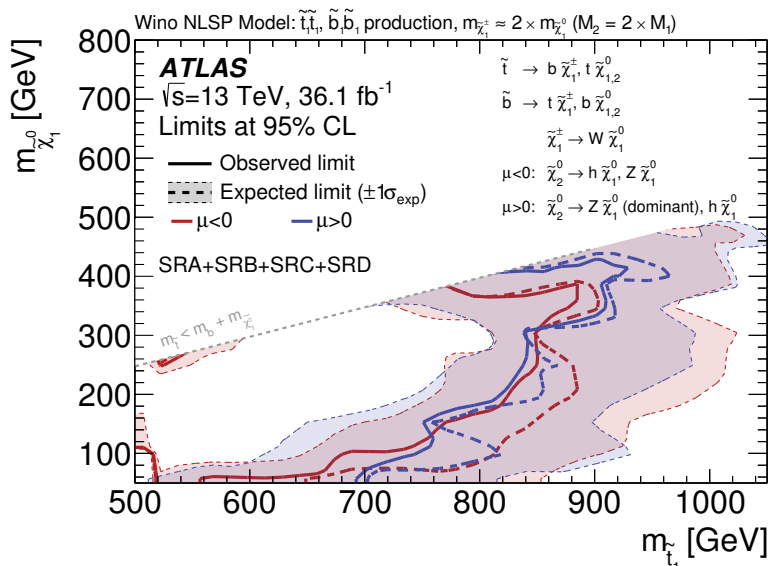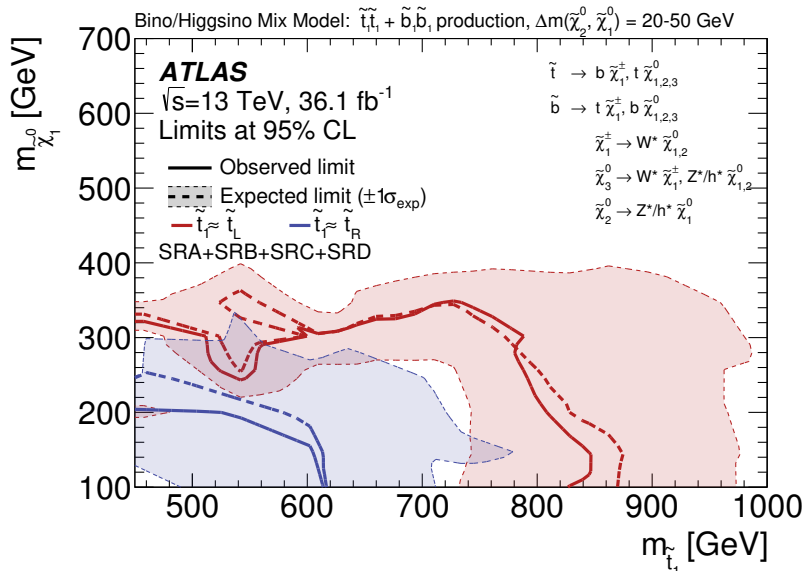**Figure 9.** Observed (solid line) and expected (dashed line) exclusion contours at 95% CL as a function of $\tilde{t}_1$ and $\tilde{\chi}_1^0$ masses and branching ratio to $\tilde{t}_1 \to t\tilde{\chi}_1^0$ in the natural SUSY-inspired mixed grid scenario where $m_{\tilde{\chi}_1^\pm} = m_{\tilde{\chi}_1^0} + 1\,\text{GeV}$.

pMSSM-inspired simplified model where $m_{\tilde{\chi}_1^\pm} = m_{\tilde{\chi}_1^0} + 5\,\text{GeV}$ and $m_{\tilde{\chi}_2^0} = m_{\tilde{\chi}_1^0} + 10\,\text{GeV}$. Finally, exclusion contours are reported for gluino production where $m_{\tilde{t}_1} = m_{\tilde{\chi}_1^0} + 5\,\text{GeV}$, resulting in gluino masses being constrained to be above $1800\,\text{GeV}$ for $\tilde{t}_1$ masses below $800\,\text{GeV}$.

Acknowledgments

Figure 10. Observed (solid line) and expected (dashed line) exclusion contours at 95% CL as a function of $m_{\tilde{t}_1}$ and $m_{\tilde{\chi}_1^0}$ for the pMSSM-inspired non-asymptotic higgsino simplified model for a small $\tan\beta$ with $B(\tilde{t}_1 \to t\tilde{\chi}_2^0,\ \tilde{t}_1 \to t\tilde{\chi}_1^0,\ \tilde{t}_1 \to b\tilde{\chi}_1^\pm) = 45\%,\ 10\%,\ 45\%$ (blue), a large $\tan\beta$ with $B(\tilde{t}_1 \to t\tilde{\chi}_2^0,\ \tilde{t}_1 \to t\tilde{\chi}_1^0,\ \tilde{t}_1 \to b\tilde{\chi}_1^\pm) = 33\%,\ 33\%,\ 33\%$ (red), and a small $\tilde{t}_R$ with $B(\tilde{t}_1 \to t\tilde{\chi}_2^0,\ \tilde{t}_1 \to t\tilde{\chi}_1^0,\ \tilde{t}_1 \to b\tilde{\chi}_1^\pm) = 25\%,\ 50\%,\ 25\%$ (green) assumption. Uncertainty bands correspond to the $\pm 1\sigma$ variation of the expected limit.

Figure 11. Observed (solid line) and expected (dashed line) exclusion contours at 95% CL as a function of $\tilde{t}_1$ and $\tilde{\chi}_1^0$ masses for the Wino NLSP pMSSM model for both positive (blue) and negative (red) values of μ. Uncertainty bands correspond to the $\pm 1\sigma$ variation of the expected limit.

Figure 12. Observed (solid line) and expected (dashed line) exclusion contours at 95% CL as a function of $\tilde{t}_1$ and $\tilde{\chi}_1^0$ masses for the $\tilde{t}_L$ scan (red) as well as for the $\tilde{t}_R$ scan (blue) in the well-tempered pMSSM model. Uncertainty bands correspond to the $\pm 1\sigma$ variation of the expected limit.
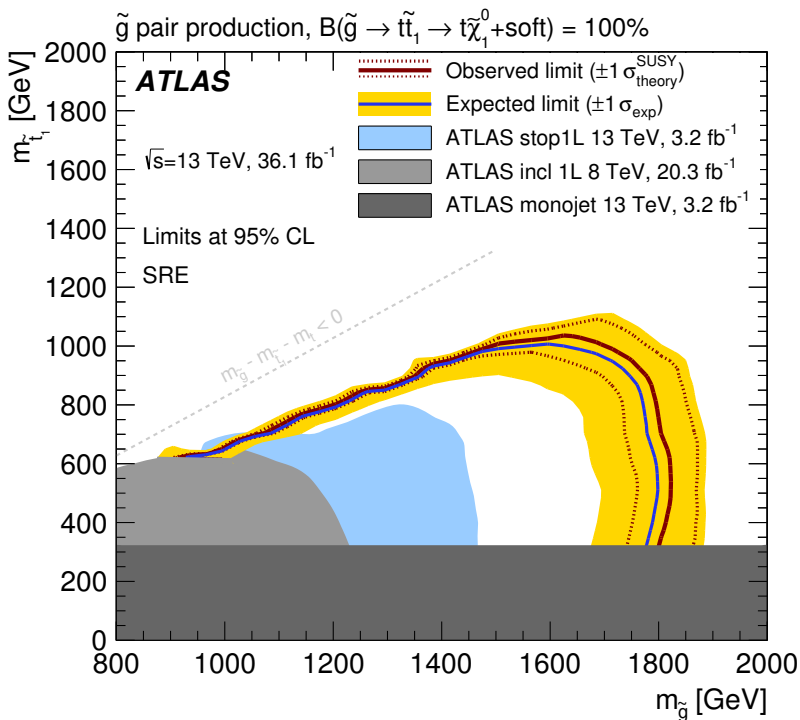

Figure 13. Observed (red solid line) and expected (blue solid line) exclusion contours at 95% CL as a function of $\tilde{g}$ and $\tilde{t}_1$ masses in the scenario where both gluinos decay via $\tilde{g} \to t\tilde{t}_1 \to t\tilde{\chi}_1^0$+soft and $\Delta m(\tilde{t}_1, \tilde{\chi}_1^0) = 5\,\mathrm{GeV}$. Uncertainty bands corresponding to the $\pm 1\sigma$ variation of the expected limit (yellow band) and the sensitivity of the observed limit to $\pm 1\sigma$ variations of the signal theoretical uncertainties (red dotted lines) are also indicated. Observed limits from previous searches with the ATLAS detector at $\sqrt{s} = 8$ and $\sqrt{s} = 13\,\mathrm{TeV}$ are overlaid in grey and blue [27, 93, 94].

References

[1] Yu.A. Golfand and E.P. Likhtman, *Extension of the Algebra of Poincaré Group Generators and Violation of p Invariance*, *JETP Lett.* **13** (1971) 323 [INSPIRE].

[2] D.V. Volkov and V.P. Akulov, *Is the Neutrino a Goldstone Particle?*, *Phys. Lett.* **B 46** (1973) 109 [INSPIRE].

[3] J. Wess and B. Zumino, *Supergauge Transformations in Four-Dimensions*, *Nucl. Phys.* **B 70** (1974) 39 [INSPIRE].

[4] J. Wess and B. Zumino, *Supergauge Invariant Extension of Quantum Electrodynamics*, *Nucl. Phys.* **B 78** (1974) 1 [INSPIRE].

[5] S. Ferrara and B. Zumino, *Supergauge Invariant Yang-Mills Theories*, *Nucl. Phys.* **B 79** (1974) 413 [INSPIRE].

[6] A. Salam and J.A. Strathdee, *Supersymmetry and Nonabelian Gauges*, *Phys. Lett.* **B 51** (1974) 353 [INSPIRE].

[7] S. Dimopoulos and H. Georgi, *Softly Broken Supersymmetry and* SU(5), *Nucl. Phys.* **B 193** (1981) 150 [INSPIRE].

[8] N. Sakai, *Naturalness in Supersymmetric Guts*, *Z. Phys.* **C 11** (1981) 153 [INSPIRE].

[9] S. Dimopoulos, S. Raby and F. Wilczek, *Supersymmetry and the Scale of Unification*, *Phys. Rev.* **D 24** (1981) 1681 [INSPIRE].

[10] L.E. Ibáñez and G.G. Ross, *Low-Energy Predictions in Supersymmetric Grand Unified Theories*, *Phys. Lett.* **B 105** (1981) 439 [INSPIRE].

[11] G.R. Farrar and P. Fayet, *Phenomenology of the Production, Decay and Detection of New Hadronic States Associated with Supersymmetry*, *Phys. Lett.* **B 76** (1978) 575 [ɪɴSPIRE].

[12] W. Beenakker, M. Krämer, T. Plehn, M. Spira and P.M. Zerwas, *Stop production at hadron colliders*, *Nucl. Phys.* **B 515** (1998) 3 [hep-ph/9710451] [ɪɴSPIRE].

[13] W. Beenakker, S. Brensing, M. Krämer, A. Kulesza, E. Laenen and I. Niessen, *Supersymmetric top and bottom squark production at hadron colliders*, *JHEP* **08** (2010) 098 [arXiv:1006.4771] [ɪɴSPIRE].

[14] W. Beenakker et al., *Squark and Gluino Hadroproduction*, *Int. J. Mod. Phys.* **A 26** (2011) 2637 [arXiv:1105.1110] [ɪɴSPIRE].

[15] C. Borschensky et al., *Squark and gluino production cross sections in pp collisions at $\sqrt{s} = 13, 14, 33$ and $100\,TeV$*, *Eur. Phys. J.* **C 74** (2014) 3174 [arXiv:1407.5066] [ɪɴSPIRE].

[16] H. Goldberg, *Constraint on the Photino Mass from Cosmology*, *Phys. Rev. Lett.* **50** (1983) 1419 [*Erratum ibid.* **103** (2009) 099905] [ɪɴSPIRE].

[17] J.R. Ellis, J.S. Hagelin, D.V. Nanopoulos, K.A. Olive and M. Srednicki, *Supersymmetric Relics from the Big Bang*, *Nucl. Phys.* **B 238** (1984) 453 [ɪɴSPIRE].

[18] J. Alwall, M.-P. Le, M. Lisanti and J.G. Wacker, *Searching for Directly Decaying Gluinos at the Tevatron*, *Phys. Lett.* **B 666** (2008) 34 [arXiv:0803.0019] [ɪɴSPIRE].

[19] J. Alwall, P. Schuster and N. Toro, *Simplified Models for a First Characterization of New Physics at the LHC*, *Phys. Rev.* **D 79** (2009) 075020 [arXiv:0810.3921] [ɪɴSPIRE].

[20] D. Alves, *Simplified Models for LHC New Physics Searches*, *J. Phys.* **G 39** (2012) 105005 [arXiv:1105.2838] [ɪɴSPIRE].

[21] MSSM WORKING GROUP collaboration, A. Djouadi et al., *The minimal supersymmetric standard model: Group summary report*, hep-ph/9901246 [ɪɴSPIRE].

[22] C.F. Berger, J.S. Gainer, J.L. Hewett and T.G. Rizzo, *Supersymmetry Without Prejudice*, *JHEP* **02** (2009) 023 [arXiv:0812.0980] [ɪɴSPIRE].

[23] P. Fayet, *Supersymmetry and Weak, Electromagnetic and Strong Interactions*, *Phys. Lett.* **B 64** (1976) 159 [ɪɴSPIRE].

[24] P. Fayet, *Spontaneously Broken Supersymmetric Theories of Weak, Electromagnetic and Strong Interactions*, *Phys. Lett.* **B 69** (1977) 489 [ɪɴSPIRE].

[25] ATLAS collaboration, *Search for direct pair production of the top squark in all-hadronic final states in proton-proton collisions at $\sqrt{s} = 8\,TeV$ with the ATLAS detector*, *JHEP* **09** (2014) 015 [arXiv:1406.1122] [ɪɴSPIRE].

[26] ATLAS collaboration, *ATLAS Run 1 searches for direct pair production of third-generation squarks at the Large Hadron Collider*, *Eur. Phys. J.* **C 75** (2015) 510 [arXiv:1506.08616] [ɪɴSPIRE].

[27] ATLAS collaboration, *Search for top squarks in final states with one isolated lepton, jets and missing transverse momentum in $\sqrt{s} = 13\,TeV$ pp collisions with the ATLAS detector*, *Phys. Rev.* **D 94** (2016) 052009 [arXiv:1606.03903] [ɪɴSPIRE].

[28] ATLAS collaboration, *Search for direct top-squark pair production in final states with two leptons in pp collisions at $\sqrt{s} = 8TeV$ with the ATLAS detector*, *JHEP* **06** (2014) 124 [arXiv:1403.4853] [ɪɴSPIRE].

[29] CMS collaboration, *Search for Supersymmetry Using Razor Variables in Events with b-Tagged Jets in pp Collisions at* $\sqrt{s} = 8\,TeV$, *Phys. Rev.* **D 91** (2015) 052018 [arXiv:1502.00300] [INSPIRE].

[30] CMS collaboration, *Search for top squark pair production in compressed-mass-spectrum scenarios in proton-proton collisions at* $\sqrt{s} = 8\,TeV$ *using the* α_T *variable*, *Phys. Lett.* **B 767** (2017) 403 [arXiv:1605.08993] [INSPIRE].

[31] CMS collaboration, *Searches for pair production of third-generation squarks in* $\sqrt{s} = 13\,TeV$ *pp collisions*, *Eur. Phys. J.* **C 77** (2017) 327 [arXiv:1612.03877] [INSPIRE].

[32] CMS collaboration, *Search for supersymmetry in the all-hadronic final state using top quark tagging in pp collisions at* $\sqrt{s} = 13\,TeV$, *Phys. Rev.* **D 96** (2017) 012004 [arXiv:1701.01954] [INSPIRE].

[33] CMS collaboration, *Search for new physics with the* M_{T2} *variable in all-jets final states produced in pp collisions at* $\sqrt{s} = 13\,TeV$, *JHEP* **10** (2016) 006 [arXiv:1603.04053] [INSPIRE].

[34] ATLAS collaboration, *The ATLAS Experiment at the CERN Large Hadron Collider*, 2008 *JINST* **3** S08003 [INSPIRE].

[35] ATLAS collaboration, *ATLAS Insertable B-Layer Technical Design Report*, ATLAS-TDR-19 (2010).

[36] ATLAS collaboration, *ATLAS Insertable B-Layer Technical Design Report Addendum*, ATLAS-TDR-19-ADD-1 (2012).

[37] ATLAS collaboration, *Performance of the ATLAS Trigger System in 2015*, *Eur. Phys. J.* **C 77** (2017) 317 [arXiv:1611.09661] [INSPIRE].

[38] J. Alwall et al., *The automated computation of tree-level and next-to-leading order differential cross sections and their matching to parton shower simulations*, *JHEP* **07** (2014) 079 [arXiv:1405.0301] [INSPIRE].

[39] T. Sjöstrand, S. Mrenna and P.Z. Skands, *A Brief Introduction to PYTHIA 8.1*, *Comput. Phys. Commun.* **178** (2008) 852 [arXiv:0710.3820] [INSPIRE].

[40] D.J. Lange, *The EvtGen particle decay simulation package*, *Nucl. Instrum. Meth.* **A 462** (2001) 152 [INSPIRE].

[41] R.D. Ball et al., *Parton distributions with LHC data*, *Nucl. Phys.* **B 867** (2013) 244 [arXiv:1207.1303] [INSPIRE].

[42] ATLAS collaboration, *ATLAS Run 1 PYTHIA8 tunes*, ATL-PHYS-PUB-2014-021 (2014).

[43] L. Lönnblad and S. Prestel, *Merging Multi-leg NLO Matrix Elements with Parton Showers*, *JHEP* **03** (2013) 166 [arXiv:1211.7278] [INSPIRE].

[44] B.C. Allanach, *SOFTSUSY: a program for calculating supersymmetric spectra*, *Comput. Phys. Commun.* **143** (2002) 305 [hep-ph/0104145] [INSPIRE].

[45] B.C. Allanach, P. Athron, L.C. Tunstall, A. Voigt and A.G. Williams, *Next-to-Minimal SOFTSUSY*, *Comput. Phys. Commun.* **185** (2014) 2322 [arXiv:1311.7659] [INSPIRE].

[46] A. Djouadi, J. Kalinowski and M. Spira, *HDECAY: A program for Higgs boson decays in the standard model and its supersymmetric extension*, *Comput. Phys. Commun.* **108** (1998) 56 [hep-ph/9704448] [INSPIRE].

[47] A. Djouadi, M.M. Muhlleitner and M. Spira, *Decays of supersymmetric particles: The Program SUSY-HIT (SUspect-SdecaY-HDECAY-InTerface)*, *Acta Phys. Polon.* **B 38** (2007) 635 [hep-ph/0609292] [INSPIRE].

[48] T. Gleisberg et al., *Event generation with SHERPA 1.1*, *JHEP* **02** (2009) 007 [arXiv:0811.4622] [INSPIRE].

[49] S. Alioli, P. Nason, C. Oleari and E. Re, *A general framework for implementing NLO calculations in shower Monte Carlo programs: the POWHEG BOX*, *JHEP* **06** (2010) 043 [arXiv:1002.2581] [INSPIRE].

[50] T. Sjöstrand, S. Mrenna and P.Z. Skands, *PYTHIA 6.4 Physics and Manual*, *JHEP* **05** (2006) 026 [hep-ph/0603175] [INSPIRE].

[51] H.-L. Lai et al., *New parton distributions for collider physics*, *Phys. Rev.* **D 82** (2010) 074024 [arXiv:1007.2241] [INSPIRE].

[52] P.Z. Skands, *Tuning Monte Carlo Generators: The Perugia Tunes*, *Phys. Rev.* **D 82** (2010) 074018 [arXiv:1005.3457] [INSPIRE].

[53] ATLAS collaboration, *Monte Carlo Generators for the Production of a W or Z/γ* Boson in Association with Jets at ATLAS in Run 2*, ATL-PHYS-PUB-2016-003 (2016).

[54] ATLAS collaboration, *Multi-Boson Simulation for 13 TeV ATLAS Analyses*, ATL-PHYS-PUB-2016-002 (2016).

[55] ATLAS collaboration, *Simulation of top quark production for the ATLAS experiment at $\sqrt{s} = 13$ TeV*, ATL-PHYS-PUB-2016-004 (2016).

[56] ATLAS collaboration, *Modelling of the $t\bar{t}H$ and $t\bar{t}V$ (V = W, Z) processes for $\sqrt{s} = 13$ TeV ATLAS analyses*, ATL-PHYS-PUB-2016-005 (2016).

[57] ATLAS collaboration, *Validation of Monte Carlo event generators in the ATLAS Collaboration for LHC Run 2*, ATL-PHYS-PUB-2016-001 (2016).

[58] ATLAS collaboration, *The ATLAS Simulation Infrastructure*, *Eur. Phys. J.* **C 70** (2010) 823 [arXiv:1005.4568] [INSPIRE].

[59] GEANT4 collaboration, S. Agostinelli et al., *GEANT4: A simulation toolkit*, *Nucl. Instrum. Meth.* **A 506** (2003) 250 [INSPIRE].

[60] ATLAS collaboration, *The simulation principle and performance of the ATLAS fast calorimeter simulation FastCaloSim*, ATL-PHYS-PUB-2010-013 (2010).

[61] ATLAS collaboration, *Summary of ATLAS PYTHIA 8 tunes*, ATL-PHYS-PUB-2012-003 (2012).

[62] A.D. Martin, W.J. Stirling, R.S. Thorne and G. Watt, *Parton distributions for the LHC*, *Eur. Phys. J.* **C 63** (2009) 189 [arXiv:0901.0002] [INSPIRE].

[63] ATLAS collaboration, *Vertex Reconstruction Performance of the ATLAS Detector at $\sqrt{s} = 13$ TeV*, ATL-PHYS-PUB-2015-026 (2015).

[64] ATLAS collaboration, *Calorimeter Clustering Algorithms: Description and Performance*, ATL-LARG-PUB-2008-002 (2008).

[65] M. Cacciari, G.P. Salam and G. Soyez, *The anti-k_t jet clustering algorithm*, *JHEP* **04** (2008) 063 [arXiv:0802.1189] [INSPIRE].

[66] M. Cacciari, G.P. Salam and G. Soyez, *FastJet User Manual*, *Eur. Phys. J.* **C 72** (2012) 1896 [arXiv:1111.6097] [INSPIRE].

[67] M. Cacciari and G.P. Salam, *Pileup subtraction using jet areas*, *Phys. Lett.* **B 659** (2008) 119 [arXiv:0707.1378] [INSPIRE].

[68] ATLAS collaboration, *Jet Calibration and Systematic Uncertainties for Jets Reconstructed in the ATLAS Detector at $\sqrt{s} = 13\,TeV$*, ATL-PHYS-PUB-2015-015 (2015).

[69] ATLAS collaboration, *Selection of jets produced in 13TeV proton-proton collisions with the ATLAS detector*, ATLAS-CONF-2015-029 (2015).

[70] ATLAS collaboration, *Tagging and suppression of pileup jets with the ATLAS detector*, ATLAS-CONF-2014-018 (2014).

[71] ATLAS collaboration, *Commissioning of the ATLAS b-tagging algorithms using $t\bar{t}$ events in early Run-2 data*, ATL-PHYS-PUB-2015-039 (2015).

[72] ATLAS collaboration, *Optimisation of the ATLAS b-tagging performance for the 2016 LHC Run*, ATL-PHYS-PUB-2016-012 (2016).

[73] ATLAS collaboration, *b-tagging in dense environments*, ATL-PHYS-PUB-2014-014 (2014).

[74] ATLAS collaboration, *Electron efficiency measurements with the ATLAS detector using 2012 LHC proton-proton collision data*, *Eur. Phys. J.* **C 77** (2017) 195 [arXiv:1612.01456] [INSPIRE].

[75] ATLAS collaboration, *Electron identification measurements in ATLAS using $\sqrt{s} = 13\,TeV$ data with 50 ns bunch spacing*, ATL-PHYS-PUB-2015-041 (2015).

[76] ATLAS collaboration, *Performance of algorithms that reconstruct missing transverse momentum in $\sqrt{s} = 8\,TeV$ proton-proton collisions in the ATLAS detector*, *Eur. Phys. J.* **C 77** (2017) 241 [arXiv:1609.09324] [INSPIRE].

[77] ATLAS collaboration, *Muon reconstruction performance of the ATLAS detector in proton-proton collision data at $\sqrt{s} = 13\,TeV$*, *Eur. Phys. J.* **C 76** (2016) 292 [arXiv:1603.05598] [INSPIRE].

[78] C.G. Lester and D.J. Summers, *Measuring masses of semiinvisibly decaying particles pair produced at hadron colliders*, *Phys. Lett.* **B 463** (1999) 99 [hep-ph/9906349] [INSPIRE].

[79] A. Barr, C. Lester and P. Stephens, *A variable for measuring masses at hadron colliders when missing energy is expected; m_{T2}: the truth behind the glamour*, *J. Phys.* **G 29** (2003) 2343 [hep-ph/0304226] [INSPIRE].

[80] H. An and L.-T. Wang, *Opening up the compressed region of top squark searches at 13 TeV LHC*, *Phys. Rev. Lett.* **115** (2015) 181602 [arXiv:1506.00653] [INSPIRE].

[81] S. Macaluso, M. Park, D. Shih and B. Tweedie, *Revealing Compressed Stops Using High-Momentum Recoils*, *JHEP* **03** (2016) 151 [arXiv:1506.07885] [INSPIRE].

[82] P. Jackson, C. Rogan and M. Santoni, *Sparticles in motion: Analyzing compressed SUSY scenarios with a new method of event reconstruction*, *Phys. Rev.* **D 95** (2017) 035031 [arXiv:1607.08307] [INSPIRE].

[83] ATLAS collaboration, *Search for squarks and gluinos with the ATLAS detector in final states with jets and missing transverse momentum using $4.7\,fb^{-1}$ of $\sqrt{s} = 7\,TeV$ proton-proton collision data*, *Phys. Rev.* **D 87** (2013) 012008 [arXiv:1208.0949] [INSPIRE].

[84] G. Cowan, K. Cranmer, E. Gross and O. Vitells, *Asymptotic formulae for likelihood-based tests of new physics*, *Eur. Phys. J.* **C 71** (2011) 1554 [*Erratum ibid.* **C 73** (2013) 2501] [arXiv:1007.1727] [INSPIRE].

[85] M. Baak, G.J. Besjes, D. Côte, A. Koutsman, J. Lorenz and D. Short, *HistFitter software framework for statistical data analysis*, *Eur. Phys. J.* **C 75** (2015) 153 [arXiv:1410.1280] [INSPIRE].

[86] ATLAS collaboration, *Luminosity determination in pp collisions at $\sqrt{s} = 8\,TeV$ using the ATLAS detector at the LHC*, *Eur. Phys. J.* **C 76** (2016) 653 [arXiv:1608.03953] [INSPIRE].

[87] T. Junk, *Confidence level computation for combining searches with small statistics*, *Nucl. Instrum. Meth.* **A 434** (1999) 435 [hep-ex/9902006] [INSPIRE].

[88] A.L. Read, *Presentation of search results: The CL_s technique*, *J. Phys.* **G 28** (2002) 2693 [INSPIRE].

[89] M. Papucci, J.T. Ruderman and A. Weiler, *Natural SUSY Endures*, *JHEP* **09** (2012) 035 [arXiv:1110.6926] [INSPIRE].

[90] ATLAS collaboration, *Dark matter interpretations of ATLAS searches for the electroweak production of supersymmetric particles in $\sqrt{s} = 8\,TeV$ proton-proton collisions*, *JHEP* **09** (2016) 175 [arXiv:1608.00872] [INSPIRE].

[91] N. Arkani-Hamed, A. Delgado and G.F. Giudice, *The Well-tempered neutralino*, *Nucl. Phys.* **B 741** (2006) 108 [hep-ph/0601041] [INSPIRE].

[92] PLANCK collaboration, P.A.R. Ade et al., *Planck 2013 results. XVI. Cosmological parameters*, *Astron. Astrophys.* **571** (2014) A16 [arXiv:1303.5076] [INSPIRE].

[93] ATLAS collaboration, *Search for squarks and gluinos in events with isolated leptons, jets and missing transverse momentum at $\sqrt{s} = 8\,TeV$ with the ATLAS detector*, *JHEP* **04** (2015) 116 [arXiv:1501.03555] [INSPIRE].

[94] ATLAS collaboration, *Search for new phenomena in final states with an energetic jet and large missing transverse momentum in pp collisions at $\sqrt{s} = 13\,TeV$ using the ATLAS detector*, *Phys. Rev.* **D 94** (2016) 032005 [arXiv:1604.07773] [INSPIRE].

[95] ATLAS collaboration, *ATLAS Computing Acknowledgements 2016–2017*, ATL-GEN-PUB-2016-002 (2016).

The ATLAS collaboration

M. Aaboud[137d], G. Aad[88], B. Abbott[115], O. Abdinov[12,*], B. Abeloos[119], S.H. Abidi[161],
O.S. AbouZeid[139], N.L. Abraham[151], H. Abramowicz[155], H. Abreu[154], R. Abreu[118],
Y. Abulaiti[148a,148b], B.S. Acharya[167a,167b,a], S. Adachi[157], L. Adamczyk[41a], J. Adelman[110],
M. Adersberger[102], T. Adye[133], A.A. Affolder[139], T. Agatonovic-Jovin[14], C. Agheorghiesei[28c],
J.A. Aguilar-Saavedra[128a,128f], S.P. Ahlen[24], F. Ahmadov[68,b], G. Aielli[135a,135b], S. Akatsuka[71],
H. Akerstedt[148a,148b], T.P.A. Åkesson[84], E. Akilli[52], A.V. Akimov[98], G.L. Alberghi[22a,22b],
J. Albert[172], P. Albicocco[50], M.J. Alconada Verzini[74], S.C. Alderweireldt[108], M. Aleksa[32],
I.N. Aleksandrov[68], C. Alexa[28b], G. Alexander[155], T. Alexopoulos[10], M. Alhroob[115], B. Ali[130],
M. Aliev[76a,76b], G. Alimonti[94a], J. Alison[33], S.P. Alkire[38], B.M.M. Allbrooke[151], B.W. Allen[118],
P.P. Allport[19], A. Aloisio[106a,106b], A. Alonso[39], F. Alonso[74], C. Alpigiani[140], A.A. Alshehri[56],
M.I. Alstaty[88], B. Alvarez Gonzalez[32], D. Álvarez Piqueras[170], M.G. Alviggi[106a,106b],
B.T. Amadio[16], Y. Amaral Coutinho[26a], C. Amelung[25], D. Amidei[92],
S.P. Amor Dos Santos[128a,128c], A. Amorim[128a,128b], S. Amoroso[32], G. Amundsen[25],
C. Anastopoulos[141], L.S. Ancu[52], N. Andari[19], T. Andeen[11], C.F. Anders[60b], J.K. Anders[77],
K.J. Anderson[33], A. Andreazza[94a,94b], V. Andrei[60a], S. Angelidakis[9], I. Angelozzi[109],
A. Angerami[38], A.V. Anisenkov[111,c], N. Anjos[13], A. Annovi[126a,126b], C. Antel[60a], M. Antonelli[50],
A. Antonov[100,*], D.J. Antrim[166], F. Anulli[134a], M. Aoki[69], L. Aperio Bella[32], G. Arabidze[93],
Y. Arai[69], J.P. Araque[128a], V. Araujo Ferraz[26a], A.T.H. Arce[48], R.E. Ardell[80], F.A. Arduh[74],
J-F. Arguin[97], S. Argyropoulos[66], M. Arik[20a], A.J. Armbruster[32], L.J. Armitage[79], O. Arnaez[161],
H. Arnold[51], M. Arratia[30], O. Arslan[23], A. Artamonov[99], G. Artoni[122], S. Artz[86], S. Asai[157],
N. Asbah[45], A. Ashkenazi[155], L. Asquith[151], K. Assamagan[27], R. Astalos[146a], M. Atkinson[169],
N.B. Atlay[143], K. Augsten[130], G. Avolio[32], B. Axen[16], M.K. Ayoub[119], G. Azuelos[97,d],
A.E. Baas[60a], M.J. Baca[19], H. Bachacou[138], K. Bachas[76a,76b], M. Backes[122], M. Backhaus[32],
P. Bagnaia[134a,134b], M. Bahmani[42], H. Bahrasemani[144], J.T. Baines[133], M. Bajic[39],
O.K. Baker[179], E.M. Baldin[111,c], P. Balek[175], F. Balli[138], W.K. Balunas[124], E. Banas[42],
A. Bandyopadhyay[23], Sw. Banerjee[176,e], A.A.E. Bannoura[178], L. Barak[32], E.L. Barberio[91],
D. Barberis[53a,53b], M. Barbero[88], T. Barillari[103], M-S Barisits[32], J.T. Barkeloo[118],
T. Barklow[145], N. Barlow[30], S.L. Barnes[36c], B.M. Barnett[133], R.M. Barnett[16],
Z. Barnovska-Blenessy[36a], A. Baroncelli[136a], G. Barone[25], A.J. Barr[122], L. Barranco Navarro[170],
F. Barreiro[85], J. Barreiro Guimarães da Costa[35a], R. Bartoldus[145], A.E. Barton[75], P. Bartos[146a],
A. Basalaev[125], A. Bassalat[119,f], R.L. Bates[56], S.J. Batista[161], J.R. Batley[30], M. Battaglia[139],
M. Bauce[134a,134b], F. Bauer[138], H.S. Bawa[145,g], J.B. Beacham[113], M.D. Beattie[75], T. Beau[83],
P.H. Beauchemin[165], P. Bechtle[23], H.P. Beck[18,h], H.C. Beck[57], K. Becker[122], M. Becker[86],
M. Beckingham[173], C. Becot[112], A.J. Beddall[20e], A. Beddall[20b], V.A. Bednyakov[68],
M. Bedognetti[109], C.P. Bee[150], T.A. Beermann[32], M. Begalli[26a], M. Begel[27], J.K. Behr[45],
A.S. Bell[81], G. Bella[155], L. Bellagamba[22a], A. Bellerive[31], M. Bellomo[154], K. Belotskiy[100],
O. Beltramello[32], N.L. Belyaev[100], O. Benary[155,*], D. Benchekroun[137a], M. Bender[102],
K. Bendtz[148a,148b], N. Benekos[10], Y. Benhammou[155], E. Benhar Noccioli[179], J. Benitez[66],
D.P. Benjamin[48], M. Benoit[52], J.R. Bensinger[25], S. Bentvelsen[109], L. Beresford[122], M. Beretta[50],
D. Berge[109], E. Bergeaas Kuutmann[168], N. Berger[5], J. Beringer[16], S. Berlendis[58],
N.R. Bernard[89], G. Bernardi[83], C. Bernius[145], F.U. Bernlochner[23], T. Berry[80], P. Berta[131],
C. Bertella[35a], G. Bertoli[148a,148b], F. Bertolucci[126a,126b], I.A. Bertram[75], C. Bertsche[45],
D. Bertsche[115], G.J. Besjes[39], O. Bessidskaia Bylund[148a,148b], M. Bessner[45], N. Besson[138],
C. Betancourt[51], A. Bethani[87], S. Bethke[103], A.J. Bevan[79], J. Beyer[103], R.M. Bianchi[127],
O. Biebel[102], D. Biedermann[17], R. Bielski[87], K. Bierwagen[86], N.V. Biesuz[126a,126b],
M. Biglietti[136a], T.R.V. Billoud[97], H. Bilokon[50], M. Bindi[57], A. Bingul[20b], C. Bini[134a,134b],

S. Biondi[22a,22b], T. Bisanz[57], C. Bittrich[47], D.M. Bjergaard[48], C.W. Black[152], J.E. Black[145], K.M. Black[24], R.E. Blair[6], T. Blazek[146a], I. Bloch[45], C. Blocker[25], A. Blue[56], W. Blum[86,*], U. Blumenschein[79], S. Blunier[34a], G.J. Bobbink[109], V.S. Bobrovnikov[111,c], S.S. Bocchetta[84], A. Bocci[48], C. Bock[102], M. Boehler[51], D. Boerner[178], D. Bogavac[102], A.G. Bogdanchikov[111], C. Bohm[148a], V. Boisvert[80], P. Bokan[168,i], T. Bold[41a], A.S. Boldyrev[101], A.E. Bolz[60b], M. Bomben[83], M. Bona[79], M. Boonekamp[138], A. Borisov[132], G. Borissov[75], J. Bortfeldt[32], D. Bortoletto[122], V. Bortolotto[62a], D. Boscherini[22a], M. Bosman[13], J.D. Bossio Sola[29], J. Boudreau[127], J. Bouffard[2], E.V. Bouhova-Thacker[75], D. Boumediene[37], C. Bourdarios[119], S.K. Boutle[56], A. Boveia[113], J. Boyd[32], I.R. Boyko[68], J. Bracinik[19], A. Brandt[8], G. Brandt[57], O. Brandt[60a], U. Bratzler[158], B. Brau[89], J.E. Brau[118], W.D. Breaden Madden[56], K. Brendlinger[45], A.J. Brennan[91], L. Brenner[109], R. Brenner[168], S. Bressler[175], D.L. Briglin[19], T.M. Bristow[49], D. Britton[56], D. Britzger[45], F.M. Brochu[30], I. Brock[23], R. Brock[93], G. Brooijmans[38], T. Brooks[80], W.K. Brooks[34b], J. Brosamer[16], E. Brost[110], J.H Broughton[19], P.A. Bruckman de Renstrom[42], D. Bruncko[146b], A. Bruni[22a], G. Bruni[22a], L.S. Bruni[109], BH Brunt[30], M. Bruschi[22a], N. Bruscino[23], P. Bryant[33], L. Bryngemark[45], T. Buanes[15], Q. Buat[144], P. Buchholz[143], A.G. Buckley[56], I.A. Budagov[68], F. Buehrer[51], M.K. Bugge[121], O. Bulekov[100], D. Bullock[8], T.J. Burch[110], S. Burdin[77], C.D. Burgard[51], A.M. Burger[5], B. Burghgrave[110], K. Burka[42], S. Burke[133], I. Burmeister[46], J.T.P. Burr[122], E. Busato[37], D. Büscher[51], V. Büscher[86], P. Bussey[56], J.M. Butler[24], C.M. Buttar[56], J.M. Butterworth[81], P. Butti[32], W. Buttinger[27], A. Buzatu[35c], A.R. Buzykaev[111,c], S. Cabrera Urbán[170], D. Caforio[130], V.M. Cairo[40a,40b], O. Cakir[4a], N. Calace[52], P. Calafiura[16], A. Calandri[88], G. Calderini[83], P. Calfayan[64], G. Callea[40a,40b], L.P. Caloba[26a], S. Calvente Lopez[85], D. Calvet[37], S. Calvet[37], T.P. Calvet[88], R. Camacho Toro[33], S. Camarda[32], P. Camarri[135a,135b], D. Cameron[121], R. Caminal Armadans[169], C. Camincher[58], S. Campana[32], M. Campanelli[81], A. Camplani[94a,94b], A. Campoverde[143], V. Canale[106a,106b], M. Cano Bret[36c], J. Cantero[116], T. Cao[155], M.D.M. Capeans Garrido[32], I. Caprini[28b], M. Caprini[28b], M. Capua[40a,40b], R.M. Carbone[38], R. Cardarelli[135a], F. Cardillo[51], I. Carli[131], T. Carli[32], G. Carlino[106a], B.T. Carlson[127], L. Carminati[94a,94b], R.M.D. Carney[148a,148b], S. Caron[108], E. Carquin[34b], S. Carrá[94a,94b], G.D. Carrillo-Montoya[32], J. Carvalho[128a,128c], D. Casadei[19], M.P. Casado[13,j], M. Casolino[13], D.W. Casper[166], R. Castelijn[109], V. Castillo Gimenez[170], N.F. Castro[128a,k], A. Catinaccio[32], J.R. Catmore[121], A. Cattai[32], J. Caudron[23], V. Cavaliere[169], E. Cavallaro[13], D. Cavalli[94a], M. Cavalli-Sforza[13], V. Cavasinni[126a,126b], E. Celebi[20d], F. Ceradini[136a,136b], L. Cerda Alberich[170], A.S. Cerqueira[26b], A. Cerri[151], L. Cerrito[135a,135b], F. Cerutti[16], A. Cervelli[18], S.A. Cetin[20d], A. Chafaq[137a], D. Chakraborty[110], S.K. Chan[59], W.S. Chan[109], Y.L. Chan[62a], P. Chang[169], J.D. Chapman[30], D.G. Charlton[19], C.C. Chau[161], C.A. Chavez Barajas[151], S. Che[113], S. Cheatham[167a,167c], A. Chegwidden[93], S. Chekanov[6], S.V. Chekulaev[163a], G.A. Chelkov[68,l], M.A. Chelstowska[32], C. Chen[67], H. Chen[27], J. Chen[36a], S. Chen[35b], S. Chen[157], X. Chen[35c,m], Y. Chen[70], H.C. Cheng[92], H.J. Cheng[35a], A. Cheplakov[68], E. Cheremushkina[132], R. Cherkaoui El Moursli[137e], E. Cheu[7], K. Cheung[63], L. Chevalier[138], V. Chiarella[50], G. Chiarelli[126a,126b], G. Chiodini[76a], A.S. Chisholm[32], A. Chitan[28b], Y.H. Chiu[172], M.V. Chizhov[68], K. Choi[64], A.R. Chomont[37], S. Chouridou[156], V. Christodoulou[81], D. Chromek-Burckhart[32], M.C. Chu[62a], J. Chudoba[129], A.J. Chuinard[90], J.J. Chwastowski[42], L. Chytka[117], A.K. Ciftci[4a], D. Cinca[46], V. Cindro[78], I.A. Cioara[23], C. Ciocca[22a,22b], A. Ciocio[16], F. Cirotto[106a,106b], Z.H. Citron[175], M. Citterio[94a], M. Ciubancan[28b], A. Clark[52], B.L. Clark[59], M.R. Clark[38], P.J. Clark[49], R.N. Clarke[16], C. Clement[148a,148b], Y. Coadou[88], M. Cobal[167a,167c], A. Coccaro[52], J. Cochran[67], L. Colasurdo[108], B. Cole[38], A.P. Colijn[109], J. Collot[58], T. Colombo[166], P. Conde Muiño[128a,128b], E. Coniavitis[51], S.H. Connell[147b], I.A. Connelly[87], S. Constantinescu[28b], G. Conti[32], F. Conventi[106a,n], M. Cooke[16],

A.M. Cooper-Sarkar[122], F. Cormier[171], K.J.R. Cormier[161], M. Corradi[134a,134b], F. Corriveau[90,o],
A. Cortes-Gonzalez[32], G. Cortiana[103], G. Costa[94a], M.J. Costa[170], D. Costanzo[141], G. Cottin[30],
G. Cowan[80], B.E. Cox[87], K. Cranmer[112], S.J. Crawley[56], R.A. Creager[124], G. Cree[31],
S. Crépé-Renaudin[58], F. Crescioli[83], W.A. Cribbs[148a,148b], M. Cristinziani[23], V. Croft[108],
G. Crosetti[40a,40b], A. Cueto[85], T. Cuhadar Donszelmann[141], A.R. Cukierman[145],
J. Cummings[179], M. Curatolo[50], J. Cúth[86], P. Czodrowski[32], G. D'amen[22a,22b], S. D'Auria[56],
L. D'eramo[83], M. D'Onofrio[77], M.J. Da Cunha Sargedas De Sousa[128a,128b], C. Da Via[87],
W. Dabrowski[41a], T. Dado[146a], T. Dai[92], O. Dale[15], F. Dallaire[97], C. Dallapiccola[89], M. Dam[39],
J.R. Dandoy[124], M.F. Daneri[29], N.P. Dang[176], A.C. Daniells[19], N.S. Dann[87], M. Danninger[171],
M. Dano Hoffmann[138], V. Dao[150], G. Darbo[53a], S. Darmora[8], J. Dassoulas[3], A. Dattagupta[118],
T. Daubney[45], W. Davey[23], C. David[45], T. Davidek[131], D.R. Davis[48], P. Davison[81], E. Dawe[91],
I. Dawson[141], K. De[8], R. de Asmundis[106a], A. De Benedetti[115], S. De Castro[22a,22b],
S. De Cecco[83], N. De Groot[108], P. de Jong[109], H. De la Torre[93], F. De Lorenzi[67], A. De Maria[57],
D. De Pedis[134a], A. De Salvo[134a], U. De Sanctis[135a,135b], A. De Santo[151],
K. De Vasconcelos Corga[88], J.B. De Vivie De Regie[119], W.J. Dearnaley[75], R. Debbe[27],
C. Debenedetti[139], D.V. Dedovich[68], N. Dehghanian[3], I. Deigaard[109], M. Del Gaudio[40a,40b],
J. Del Peso[85], D. Delgove[119], F. Deliot[138], C.M. Delitzsch[52], A. Dell'Acqua[32], L. Dell'Asta[24],
M. Dell'Orso[126a,126b], M. Della Pietra[106a,106b], D. della Volpe[52], M. Delmastro[5], C. Delporte[119],
P.A. Delsart[58], D.A. DeMarco[161], S. Demers[179], M. Demichev[68], A. Demilly[83], S.P. Denisov[132],
D. Denysiuk[138], D. Derendarz[42], J.E. Derkaoui[137d], F. Derue[83], P. Dervan[77], K. Desch[23],
C. Deterre[45], K. Dette[46], M.R. Devesa[29], P.O. Deviveiros[32], A. Dewhurst[133], S. Dhaliwal[25],
F.A. Di Bello[52], A. Di Ciaccio[135a,135b], L. Di Ciaccio[5], W.K. Di Clemente[124],
C. Di Donato[106a,106b], A. Di Girolamo[32], B. Di Girolamo[32], B. Di Micco[136a,136b], R. Di Nardo[32],
K.F. Di Petrillo[59], A. Di Simone[51], R. Di Sipio[161], D. Di Valentino[31], C. Diaconu[88],
M. Diamond[161], F.A. Dias[39], M.A. Diaz[34a], E.B. Diehl[92], J. Dietrich[17], S. Díez Cornell[45],
A. Dimitrievska[14], J. Dingfelder[23], P. Dita[28b], S. Dita[28b], F. Dittus[32], F. Djama[88],
T. Djobava[54b], J.I. Djuvsland[60a], M.A.B. do Vale[26c], D. Dobos[32], M. Dobre[28b], C. Doglioni[84],
J. Dolejsi[131], Z. Dolezal[131], M. Donadelli[26d], S. Donati[126a,126b], P. Dondero[123a,123b], J. Donini[37],
J. Dopke[133], A. Doria[106a], M.T. Dova[74], A.T. Doyle[56], E. Drechsler[57], M. Dris[10], Y. Du[36b],
J. Duarte-Campderros[155], A. Dubreuil[52], E. Duchovni[175], G. Duckeck[102], A. Ducourthial[83],
O.A. Ducu[97,p], D. Duda[109], A. Dudarev[32], A.Chr. Dudder[86], E.M. Duffield[16], L. Duflot[119],
M. Dührssen[32], M. Dumancic[175], A.E. Dumitriu[28b], A.K. Duncan[56], M. Dunford[60a],
H. Duran Yildiz[4a], M. Düren[55], A. Durglishvili[54b], D. Duschinger[47], B. Dutta[45], D. Duvnjak[1],
M. Dyndal[45], B.S. Dziedzic[42], C. Eckardt[45], K.M. Ecker[103], R.C. Edgar[92], T. Eifert[32],
G. Eigen[15], K. Einsweiler[16], T. Ekelof[168], M. El Kacimi[137c], R. El Kosseifi[88], V. Ellajosyula[88],
M. Ellert[168], S. Elles[5], F. Ellinghaus[178], A.A. Elliot[172], N. Ellis[32], J. Elmsheuser[27], M. Elsing[32],
D. Emeliyanov[133], Y. Enari[157], O.C. Endner[86], J.S. Ennis[173], J. Erdmann[46], A. Ereditato[18],
M. Ernst[27], S. Errede[169], M. Escalier[119], C. Escobar[170], B. Esposito[50], O. Estrada Pastor[170],
A.I. Etienvre[138], E. Etzion[155], H. Evans[64], A. Ezhilov[125], M. Ezzi[137e], F. Fabbri[22a,22b],
L. Fabbri[22a,22b], V. Fabiani[108], G. Facini[81], R.M. Fakhrutdinov[132], S. Falciano[134a], R.J. Falla[81],
J. Faltova[32], Y. Fang[35a], M. Fanti[94a,94b], A. Farbin[8], A. Farilla[136a], C. Farina[127],
E.M. Farina[123a,123b], T. Farooque[93], S. Farrell[16], S.M. Farrington[173], P. Farthouat[32],
F. Fassi[137e], P. Fassnacht[32], D. Fassouliotis[9], M. Faucci Giannelli[80], A. Favareto[53a,53b],
W.J. Fawcett[122], L. Fayard[119], O.L. Fedin[125,q], W. Fedorko[171], S. Feigl[121], L. Feligioni[88],
C. Feng[36b], E.J. Feng[32], H. Feng[92], M.J. Fenton[56], A.B. Fenyuk[132], L. Feremenga[8],
P. Fernandez Martinez[170], S. Fernandez Perez[13], J. Ferrando[45], A. Ferrari[168], P. Ferrari[109],
R. Ferrari[123a], D.E. Ferreira de Lima[60b], A. Ferrer[170], D. Ferrere[52], C. Ferretti[92], F. Fiedler[86],
A. Filipčič[78], M. Filipuzzi[45], F. Filthaut[108], M. Fincke-Keeler[172], K.D. Finelli[152],

M.C.N. Fiolhais[128a,128c,r], L. Fiorini[170], A. Fischer[2], C. Fischer[13], J. Fischer[178], W.C. Fisher[93],
N. Flaschel[45], I. Fleck[143], P. Fleischmann[92], R.R.M. Fletcher[124], T. Flick[178], B.M. Flierl[102],
L.R. Flores Castillo[62a], M.J. Flowerdew[103], G.T. Forcolin[87], A. Formica[138], F.A. Förster[13],
A. Forti[87], A.G. Foster[19], D. Fournier[119], H. Fox[75], S. Fracchia[141], P. Francavilla[83],
M. Franchini[22a,22b], S. Franchino[60a], D. Francis[32], L. Franconi[121], M. Franklin[59], M. Frate[166],
M. Fraternali[123a,123b], D. Freeborn[81], S.M. Fressard-Batraneanu[32], B. Freund[97], D. Froidevaux[32],
J.A. Frost[122], C. Fukunaga[158], T. Fusayasu[104], J. Fuster[170], C. Gabaldon[58], O. Gabizon[154],
A. Gabrielli[22a,22b], A. Gabrielli[16], G.P. Gach[41a], S. Gadatsch[32], S. Gadomski[80],
G. Gagliardi[53a,53b], L.G. Gagnon[97], C. Galea[108], B. Galhardo[128a,128c], E.J. Gallas[122],
B.J. Gallop[133], P. Gallus[130], G. Galster[39], K.K. Gan[113], S. Ganguly[37], Y. Gao[77], Y.S. Gao[145,g],
F.M. Garay Walls[49], C. García[170], J.E. García Navarro[170], J.A. García Pascual[35a],
M. Garcia-Sciveres[16], R.W. Gardner[33], N. Garelli[145], V. Garonne[121], A. Gascon Bravo[45],
K. Gasnikova[45], C. Gatti[50], A. Gaudiello[53a,53b], G. Gaudio[123a], I.L. Gavrilenko[98], C. Gay[171],
G. Gaycken[23], E.N. Gazis[10], C.N.P. Gee[133], J. Geisen[57], M. Geisen[86], M.P. Geisler[60a],
K. Gellerstedt[148a,148b], C. Gemme[53a], M.H. Genest[58], C. Geng[92], S. Gentile[134a,134b],
C. Gentsos[156], S. George[80], D. Gerbaudo[13], A. Gershon[155], G. Geßner[46], S. Ghasemi[143],
M. Ghneimat[23], B. Giacobbe[22a], S. Giagu[134a,134b], N. Giangiacomi[22a,22b], P. Giannetti[126a,126b],
S.M. Gibson[80], M. Gignac[171], M. Gilchriese[16], D. Gillberg[31], G. Gilles[178], D.M. Gingrich[3,d],
N. Giokaris[9,*], M.P. Giordani[167a,167c], F.M. Giorgi[22a], P.F. Giraud[138], P. Giromini[59],
D. Giugni[94a], F. Giuli[122], C. Giuliani[103], M. Giulini[60b], B.K. Gjelsten[121], S. Gkaitatzis[156],
I. Gkialas[9,s], E.L. Gkougkousis[139], P. Gkountoumis[10], L.K. Gladilin[101], C. Glasman[85],
J. Glatzer[13], P.C.F. Glaysher[45], A. Glazov[45], M. Goblirsch-Kolb[25], J. Godlewski[42],
S. Goldfarb[91], T. Golling[52], D. Golubkov[132], A. Gomes[128a,128b,128d], R. Gonçalo[128a],
R. Goncalves Gama[26a], J. Goncalves Pinto Firmino Da Costa[138], G. Gonella[51], L. Gonella[19],
A. Gongadze[68], S. González de la Hoz[170], S. Gonzalez-Sevilla[52], L. Goossens[32],
P.A. Gorbounov[99], H.A. Gordon[27], I. Gorelov[107], B. Gorini[32], E. Gorini[76a,76b], A. Gorišek[78],
A.T. Goshaw[48], C. Gössling[46], M.I. Gostkin[68], C.A. Gottardo[23], C.R. Goudet[119],
D. Goujdami[137c], A.G. Goussiou[140], N. Govender[147b,t], E. Gozani[154], L. Graber[57],
I. Grabowska-Bold[41a], P.O.J. Gradin[168], J. Gramling[166], E. Gramstad[121], S. Grancagnolo[17],
V. Gratchev[125], P.M. Gravila[28f], C. Gray[56], H.M. Gray[16], Z.D. Greenwood[82,u], C. Grefe[23],
K. Gregersen[81], I.M. Gregor[45], P. Grenier[145], K. Grevtsov[5], J. Griffiths[8], A.A. Grillo[139],
K. Grimm[75], S. Grinstein[13,v], Ph. Gris[37], J.-F. Grivaz[119], S. Groh[86], E. Gross[175],
J. Grosse-Knetter[57], G.C. Grossi[82], Z.J. Grout[81], A. Grummer[107], L. Guan[92], W. Guan[176],
J. Guenther[65], F. Guescini[163a], D. Guest[166], O. Gueta[155], B. Gui[113], E. Guido[53a,53b],
T. Guillemin[5], S. Guindon[2], U. Gul[56], C. Gumpert[32], J. Guo[36c], W. Guo[92], Y. Guo[36a,w],
R. Gupta[43], S. Gupta[122], G. Gustavino[134a,134b], P. Gutierrez[115], N.G. Gutierrez Ortiz[81],
C. Gutschow[81], C. Guyot[138], M.P. Guzik[41a], C. Gwenlan[122], C.B. Gwilliam[77], A. Haas[112],
C. Haber[16], H.K. Hadavand[8], N. Haddad[137e], A. Hadef[88], S. Hageböck[23], M. Hagihara[164],
H. Hakobyan[180,*], M. Haleem[45], J. Haley[116], G. Halladjian[93], G.D. Hallewell[88], K. Hamacher[178],
P. Hamal[117], K. Hamano[172], A. Hamilton[147a], G.N. Hamity[141], P.G. Hamnett[45], L. Han[36a],
S. Han[35a], K. Hanagaki[69,x], K. Hanawa[157], M. Hance[139], B. Haney[124], P. Hanke[60a],
J.B. Hansen[39], J.D. Hansen[39], M.C. Hansen[23], P.H. Hansen[39], K. Hara[164], A.S. Hard[176],
T. Harenberg[178], F. Hariri[119], S. Harkusha[95], R.D. Harrington[49], P.F. Harrison[173],
N.M. Hartmann[102], M. Hasegawa[70], Y. Hasegawa[142], A. Hasib[49], S. Hassani[138], S. Haug[18],
R. Hauser[93], L. Hauswald[47], L.B. Havener[38], M. Havranek[130], C.M. Hawkes[19], R.J. Hawkings[32],
D. Hayakawa[159], D. Hayden[93], C.P. Hays[122], J.M. Hays[79], H.S. Hayward[77], S.J. Haywood[133],
S.J. Head[19], T. Heck[86], V. Hedberg[84], L. Heelan[8], S. Heer[23], K.K. Heidegger[51], S. Heim[45],
T. Heim[16], B. Heinemann[45,y], J.J. Heinrich[102], L. Heinrich[112], C. Heinz[55], J. Hejbal[129],

L. Helary[32], A. Held[171], S. Hellman[148a,148b], C. Helsens[32], R.C.W. Henderson[75], Y. Heng[176],
S. Henkelmann[171], A.M. Henriques Correia[32], S. Henrot-Versille[119], G.H. Herbert[17], H. Herde[25],
V. Herget[177], Y. Hernández Jiménez[147c], H. Herr[86], G. Herten[51], R. Hertenberger[102],
L. Hervas[32], T.C. Herwig[124], G.G. Hesketh[81], N.P. Hessey[163a], J.W. Hetherly[43], S. Higashino[69],
E. Higón-Rodriguez[170], K. Hildebrand[33], E. Hill[172], J.C. Hill[30], K.H. Hiller[45], S.J. Hillier[19],
M. Hils[47], I. Hinchliffe[16], M. Hirose[51], D. Hirschbuehl[178], B. Hiti[78], O. Hladik[129], X. Hoad[49],
J. Hobbs[150], N. Hod[163a], M.C. Hodgkinson[141], P. Hodgson[141], A. Hoecker[32],
M.R. Hoeferkamp[107], F. Hoenig[102], D. Hohn[23], T.R. Holmes[33], M. Homann[46], S. Honda[164],
T. Honda[69], T.M. Hong[127], B.H. Hooberman[169], W.H. Hopkins[118], Y. Horii[105], A.J. Horton[144],
J-Y. Hostachy[58], S. Hou[153], A. Hoummada[137a], J. Howarth[87], J. Hoya[74], M. Hrabovsky[117],
J. Hrdinka[32], I. Hristova[17], J. Hrivnac[119], T. Hryn'ova[5], A. Hrynevich[96], P.J. Hsu[63],
S.-C. Hsu[140], Q. Hu[36a], S. Hu[36c], Y. Huang[35a], Z. Hubacek[130], F. Hubaut[88], F. Huegging[23],
T.B. Huffman[122], E.W. Hughes[38], G. Hughes[75], M. Huhtinen[32], P. Huo[150], N. Huseynov[68,b],
J. Huston[93], J. Huth[59], G. Iacobucci[52], G. Iakovidis[27], I. Ibragimov[143], L. Iconomidou-Fayard[119],
Z. Idrissi[137e], P. Iengo[32], O. Igonkina[109,z], T. Iizawa[174], Y. Ikegami[69], M. Ikeno[69],
Y. Ilchenko[11,aa], D. Iliadis[156], N. Ilic[145], G. Introzzi[123a,123b], P. Ioannou[9,*], M. Iodice[136a],
K. Iordanidou[38], V. Ippolito[59], M.F. Isacson[168], N. Ishijima[120], M. Ishino[157], M. Ishitsuka[159],
C. Issever[122], S. Istin[20a], F. Ito[164], J.M. Iturbe Ponce[62a], R. Iuppa[162a,162b], H. Iwasaki[69],
J.M. Izen[44], V. Izzo[106a], S. Jabbar[3], P. Jackson[1], R.M. Jacobs[23], V. Jain[2], K.B. Jakobi[86],
K. Jakobs[51], S. Jakobsen[65], T. Jakoubek[129], D.O. Jamin[116], D.K. Jana[82], R. Jansky[52],
J. Janssen[23], M. Janus[57], P.A. Janus[41a], G. Jarlskog[84], N. Javadov[68,b], T. Javůrek[51],
M. Javurkova[51], F. Jeanneau[138], L. Jeanty[16], J. Jejelava[54a,ab], A. Jelinskas[173], P. Jenni[51,ac],
C. Jeske[173], S. Jézéquel[5], H. Ji[176], J. Jia[150], H. Jiang[67], Y. Jiang[36a], Z. Jiang[145], S. Jiggins[81],
J. Jimenez Pena[170], S. Jin[35a], A. Jinaru[28b], O. Jinnouchi[159], H. Jivan[147c], P. Johansson[141],
K.A. Johns[7], C.A. Johnson[64], W.J. Johnson[140], K. Jon-And[148a,148b], R.W.L. Jones[75],
S.D. Jones[151], S. Jones[7], T.J. Jones[77], J. Jongmanns[60a], P.M. Jorge[128a,128b], J. Jovicevic[163a],
X. Ju[176], A. Juste Rozas[13,v], M.K. Köhler[175], A. Kaczmarska[42], M. Kado[119], H. Kagan[113],
M. Kagan[145], S.J. Kahn[88], T. Kaji[174], E. Kajomovitz[48], C.W. Kalderon[84], A. Kaluza[86],
S. Kama[43], A. Kamenshchikov[132], N. Kanaya[157], L. Kanjir[78], V.A. Kantserov[100], J. Kanzaki[69],
B. Kaplan[112], L.S. Kaplan[176], D. Kar[147c], K. Karakostas[10], N. Karastathis[10], M.J. Kareem[57],
E. Karentzos[10], S.N. Karpov[68], Z.M. Karpova[68], K. Karthik[112], V. Kartvelishvili[75],
A.N. Karyukhin[132], K. Kasahara[164], L. Kashif[176], R.D. Kass[113], A. Kastanas[149], Y. Kataoka[157],
C. Kato[157], A. Katre[52], J. Katzy[45], K. Kawade[70], K. Kawagoe[73], T. Kawamoto[157],
G. Kawamura[57], E.F. Kay[77], V.F. Kazanin[111,c], R. Keeler[172], R. Kehoe[43], J.S. Keller[31],
J.J. Kempster[80], J Kendrick[19], H. Keoshkerian[161], O. Kepka[129], B.P. Kerševan[78], S. Kersten[178],
R.A. Keyes[90], M. Khader[169], F. Khalil-zada[12], A. Khanov[116], A.G. Kharlamov[111,c],
T. Kharlamova[111,c], A. Khodinov[160], T.J. Khoo[52], V. Khovanskiy[99,*], E. Khramov[68],
J. Khubua[54b,ad], S. Kido[70], C.R. Kilby[80], H.Y. Kim[8], S.H. Kim[164], Y.K. Kim[33], N. Kimura[156],
O.M. Kind[17], B.T. King[77], D. Kirchmeier[47], J. Kirk[133], A.E. Kiryunin[103], T. Kishimoto[157],
D. Kisielewska[41a], V. Kitali[45], K. Kiuchi[164], O. Kivernyk[5], E. Kladiva[146b],
T. Klapdor-Kleingrothaus[51], M.H. Klein[92], M. Klein[77], U. Klein[77], K. Kleinknecht[86],
P. Klimek[110], A. Klimentov[27], R. Klingenberg[46], T. Klingl[23], T. Klioutchnikova[32],
E.-E. Kluge[60a], P. Kluit[109], S. Kluth[103], E. Kneringer[65], E.B.F.G. Knoops[88], A. Knue[103],
A. Kobayashi[157], D. Kobayashi[159], T. Kobayashi[157], M. Kobel[47], M. Kocian[145], P. Kodys[131],
T. Koffas[31], E. Koffeman[109], N.M. Köhler[103], T. Koi[145], M. Kolb[60b], I. Koletsou[5],
A.A. Komar[98,*], Y. Komori[157], T. Kondo[69], N. Kondrashova[36c], K. Köneke[51], A.C. König[108],
T. Kono[69,ae], R. Konoplich[112,af], N. Konstantinidis[81], R. Kopeliansky[64], S. Koperny[41a],
A.K. Kopp[51], K. Korcyl[42], K. Kordas[156], A. Korn[81], A.A. Korol[111,c], I. Korolkov[13],

E.V. Korolkova[141], O. Kortner[103], S. Kortner[103], T. Kosek[131], V.V. Kostyukhin[23], A. Kotwal[48],
A. Koulouris[10], A. Kourkoumeli-Charalampidi[123a,123b], C. Kourkoumelis[9], E. Kourlitis[141],
V. Kouskoura[27], A.B. Kowalewska[42], R. Kowalewski[172], T.Z. Kowalski[41a], C. Kozakai[157],
W. Kozanecki[138], A.S. Kozhin[132], V.A. Kramarenko[101], G. Kramberger[78], D. Krasnopevtsev[100],
M.W. Krasny[83], A. Krasznahorkay[32], D. Krauss[103], J.A. Kremer[41a], J. Kretzschmar[77],
K. Kreutzfeldt[55], P. Krieger[161], K. Krizka[33], K. Kroeninger[46], H. Kroha[103], J. Kroll[129],
J. Kroll[124], J. Kroseberg[23], J. Krstic[14], U. Kruchonak[68], H. Krüger[23], N. Krumnack[67],
M.C. Kruse[48], T. Kubota[91], H. Kucuk[81], S. Kuday[4b], J.T. Kuechler[178], S. Kuehn[32], A. Kugel[60a],
F. Kuger[177], T. Kuhl[45], V. Kukhtin[68], R. Kukla[88], Y. Kulchitsky[95], S. Kuleshov[34b],
Y.P. Kulinich[169], M. Kuna[134a,134b], T. Kunigo[71], A. Kupco[129], T. Kupfer[46], O. Kuprash[155],
H. Kurashige[70], L.L. Kurchaninov[163a], Y.A. Kurochkin[95], M.G. Kurth[35a], V. Kus[129],
E.S. Kuwertz[172], M. Kuze[159], J. Kvita[117], T. Kwan[172], D. Kyriazopoulos[141], A. La Rosa[103],
J.L. La Rosa Navarro[26d], L. La Rotonda[40a,40b], F. La Ruffa[40a,40b], C. Lacasta[170],
F. Lacava[134a,134b], J. Lacey[45], H. Lacker[17], D. Lacour[83], E. Ladygin[68], R. Lafaye[5], B. Laforge[83],
T. Lagouri[179], S. Lai[57], S. Lammers[64], W. Lampl[7], E. Lançon[27], U. Landgraf[51], M.P.J. Landon[79],
M.C. Lanfermann[52], V.S. Lang[60a], J.C. Lange[13], R.J. Langenberg[32], A.J. Lankford[166],
F. Lanni[27], K. Lantzsch[23], A. Lanza[123a], A. Lapertosa[53a,53b], S. Laplace[83], J.F. Laporte[138],
T. Lari[94a], F. Lasagni Manghi[22a,22b], M. Lassnig[32], P. Laurelli[50], W. Lavrijsen[16], A.T. Law[139],
P. Laycock[77], T. Lazovich[59], M. Lazzaroni[94a,94b], B. Le[91], O. Le Dortz[83], E. Le Guirriec[88],
E.P. Le Quilleuc[138], M. LeBlanc[172], T. LeCompte[6], F. Ledroit-Guillon[58], C.A. Lee[27],
G.R. Lee[133,ag], S.C. Lee[153], L. Lee[59], B. Lefebvre[90], G. Lefebvre[83], M. Lefebvre[172], F. Legger[102],
C. Leggett[16], G. Lehmann Miotto[32], X. Lei[7], W.A. Leight[45], M.A.L. Leite[26d], R. Leitner[131],
D. Lellouch[175], B. Lemmer[57], K.J.C. Leney[81], T. Lenz[23], B. Lenzi[32], R. Leone[7],
S. Leone[126a,126b], C. Leonidopoulos[49], G. Lerner[151], C. Leroy[97], A.A.J. Lesage[138], C.G. Lester[30],
M. Levchenko[125], J. Levêque[5], D. Levin[92], L.J. Levinson[175], M. Levy[19], D. Lewis[79], B. Li[36a,w],
Changqiao Li[36a], H. Li[150], L. Li[36c], Q. Li[35a], S. Li[48], X. Li[36c], Y. Li[143], Z. Liang[35a],
B. Liberti[135a], A. Liblong[161], K. Lie[62c], J. Liebal[23], W. Liebig[15], A. Limosani[152], S.C. Lin[182],
T.H. Lin[86], R.A. Linck[64], B.E. Lindquist[150], A.E. Lionti[52], E. Lipeles[124], A. Lipniacka[15],
M. Lisovyi[60b], T.M. Liss[169,ah], A. Lister[171], A.M. Litke[139], B. Liu[153,ai], H. Liu[92], H. Liu[27],
J.K.K. Liu[122], J. Liu[36b], J.B. Liu[36a], K. Liu[88], L. Liu[169], M. Liu[36a], Y.L. Liu[36a], Y. Liu[36a],
M. Livan[123a,123b], A. Lleres[58], J. Llorente Merino[35a], S.L. Lloyd[79], C.Y. Lo[62b], F. Lo Sterzo[153],
E.M. Lobodzinska[45], P. Loch[7], F.K. Loebinger[87], A. Loesle[51], K.M. Loew[25], A. Loginov[179,*],
T. Lohse[17], K. Lohwasser[141], M. Lokajicek[129], B.A. Long[24], J.D. Long[169], R.E. Long[75],
L. Longo[76a,76b], K.A. Looper[113], J.A. Lopez[34b], D. Lopez Mateos[59], I. Lopez Paz[13],
A. Lopez Solis[83], J. Lorenz[102], N. Lorenzo Martinez[5], M. Losada[21], P.J. Lösel[102], X. Lou[35a],
A. Lounis[119], J. Love[6], P.A. Love[75], H. Lu[62a], N. Lu[92], Y.J. Lu[63], H.J. Lubatti[140],
C. Luci[134a,134b], A. Lucotte[58], C. Luedtke[51], F. Luehring[64], W. Lukas[65], L. Luminari[134a],
O. Lundberg[148a,148b], B. Lund-Jensen[149], M.S. Lutz[89], P.M. Luzi[83], D. Lynn[27], R. Lysak[129],
E. Lytken[84], F. Lyu[35a], V. Lyubushkin[68], H. Ma[27], L.L. Ma[36b], Y. Ma[36b], G. Maccarrone[50],
A. Macchiolo[103], C.M. Macdonald[141], B. Maček[78], J. Machado Miguens[124,128b], D. Madaffari[170],
R. Madar[37], W.F. Mader[47], A. Madsen[45], J. Maeda[70], S. Maeland[15], T. Maeno[27],
A.S. Maevskiy[101], V. Magerl[51], J. Mahlstedt[109], C. Maiani[119], C. Maidantchik[26a], A.A. Maier[103],
T. Maier[102], A. Maio[128a,128b,128d], O. Majersky[146a], S. Majewski[118], Y. Makida[69],
N. Makovec[119], B. Malaescu[83], Pa. Malecki[42], V.P. Maleev[125], F. Malek[58], U. Mallik[66],
D. Malon[6], C. Malone[30], S. Maltezos[10], S. Malyukov[32], J. Mamuzic[170], G. Mancini[50],
I. Mandić[78], J. Maneira[128a,128b], L. Manhaes de Andrade Filho[26b], J. Manjarres Ramos[47],
K.H. Mankinen[84], A. Mann[102], A. Manousos[32], B. Mansoulie[138], J.D. Mansour[35a], R. Mantifel[90],
M. Mantoani[57], S. Manzoni[94a,94b], L. Mapelli[32], G. Marceca[29], L. March[52], L. Marchese[122],

G. Marchiori[83], M. Marcisovsky[129], M. Marjanovic[37], D.E. Marley[92], F. Marroquim[26a],
S.P. Marsden[87], Z. Marshall[16], M.U.F Martensson[168], S. Marti-Garcia[170], C.B. Martin[113],
T.A. Martin[173], V.J. Martin[49], B. Martin dit Latour[15], M. Martinez[13,v],
V.I. Martinez Outschoorn[169], S. Martin-Haugh[133], V.S. Martoiu[28b], A.C. Martyniuk[81],
A. Marzin[32], L. Masetti[86], T. Mashimo[157], R. Mashinistov[98], J. Masik[87], A.L. Maslennikov[111,c],
L. Massa[135a,135b], P. Mastrandrea[5], A. Mastroberardino[40a,40b], T. Masubuchi[157], P. Mättig[178],
J. Maurer[28b], S.J. Maxfield[77], D.A. Maximov[111,c], R. Mazini[153], I. Maznas[156],
S.M. Mazza[94a,94b], N.C. Mc Fadden[107], G. Mc Goldrick[161], S.P. Mc Kee[92], A. McCarn[92],
R.L. McCarthy[150], T.G. McCarthy[103], L.I. McClymont[81], E.F. McDonald[91], J.A. Mcfayden[81],
G. Mchedlidze[57], S.J. McMahon[133], P.C. McNamara[91], R.A. McPherson[172,o], S. Meehan[140],
T.J. Megy[51], S. Mehlhase[102], A. Mehta[77], T. Meideck[58], K. Meier[60a], B. Meirose[44],
D. Melini[170,aj], B.R. Mellado Garcia[147c], J.D. Mellenthin[57], M. Melo[146a], F. Meloni[18],
A. Melzer[23], S.B. Menary[87], L. Meng[77], X.T. Meng[92], A. Mengarelli[22a,22b], S. Menke[103],
E. Meoni[40a,40b], S. Mergelmeyer[17], P. Mermod[52], L. Merola[106a,106b], C. Meroni[94a],
F.S. Merritt[33], A. Messina[134a,134b], J. Metcalfe[6], A.S. Mete[166], C. Meyer[124], J-P. Meyer[138],
J. Meyer[109], H. Meyer Zu Theenhausen[60a], F. Miano[151], R.P. Middleton[133], S. Miglioranzi[53a,53b],
L. Mijović[49], G. Mikenberg[175], M. Mikestikova[129], M. Mikuž[78], M. Milesi[91], A. Milic[161],
D.W. Miller[33], C. Mills[49], A. Milov[175], D.A. Milstead[148a,148b], A.A. Minaenko[132], Y. Minami[157],
I.A. Minashvili[54b], A.I. Mincer[112], B. Mindur[41a], M. Mineev[68], Y. Minegishi[157], Y. Ming[176],
L.M. Mir[13], K.P. Mistry[124], T. Mitani[174], J. Mitrevski[102], V.A. Mitsou[170], A. Miucci[18],
P.S. Miyagawa[141], A. Mizukami[69], J.U. Mjörnmark[84], T. Mkrtchyan[180], M. Mlynarikova[131],
T. Moa[148a,148b], K. Mochizuki[97], P. Mogg[51], S. Mohapatra[38], S. Molander[148a,148b],
R. Moles-Valls[23], R. Monden[71], M.C. Mondragon[93], K. Mönig[45], J. Monk[39], E. Monnier[88],
A. Montalbano[150], J. Montejo Berlingen[32], F. Monticelli[74], S. Monzani[94a,94b], R.W. Moore[3],
N. Morange[119], D. Moreno[21], M. Moreno Llácer[32], P. Morettini[53a], S. Morgenstern[32], D. Mori[144],
T. Mori[157], M. Morii[59], M. Morinaga[157], V. Morisbak[121], A.K. Morley[32], G. Mornacchi[32],
J.D. Morris[79], L. Morvaj[150], P. Moschovakos[10], M. Mosidze[54b], H.J. Moss[141], J. Moss[145,ak],
K. Motohashi[159], R. Mount[145], E. Mountricha[27], E.J.W. Moyse[89], S. Muanza[88], F. Mueller[103],
J. Mueller[127], R.S.P. Mueller[102], D. Muenstermann[75], P. Mullen[56], G.A. Mullier[18],
F.J. Munoz Sanchez[87], W.J. Murray[173,133], H. Musheghyan[32], M. Muškinja[78],
A.G. Myagkov[132,al], M. Myska[130], B.P. Nachman[16], O. Nackenhorst[52], K. Nagai[122],
R. Nagai[69,ae], K. Nagano[69], Y. Nagasaka[61], K. Nagata[164], M. Nagel[51], E. Nagy[88], A.M. Nairz[32],
Y. Nakahama[105], K. Nakamura[69], T. Nakamura[157], I. Nakano[114], R.F. Naranjo Garcia[45],
R. Narayan[11], D.I. Narrias Villar[60a], I. Naryshkin[125], T. Naumann[45], G. Navarro[21], R. Nayyar[7],
H.A. Neal[92], P.Yu. Nechaeva[98], T.J. Neep[138], A. Negri[123a,123b], M. Negrini[22a], S. Nektarijevic[108],
C. Nellist[119], A. Nelson[166], M.E. Nelson[122], S. Nemecek[129], P. Nemethy[112], M. Nessi[32,am],
M.S. Neubauer[169], M. Neumann[178], P.R. Newman[19], T.Y. Ng[62c], T. Nguyen Manh[97],
R.B. Nickerson[122], R. Nicolaidou[138], J. Nielsen[139], V. Nikolaenko[132,al], I. Nikolic-Audit[83],
K. Nikolopoulos[19], J.K. Nilsen[121], P. Nilsson[27], Y. Ninomiya[157], A. Nisati[134a], N. Nishu[35c],
R. Nisius[103], I. Nitsche[46], T. Nitta[174], T. Nobe[157], Y. Noguchi[71], M. Nomachi[120], I. Nomidis[31],
M.A. Nomura[27], T. Nooney[79], M. Nordberg[32], N. Norjoharuddeen[122], O. Novgorodova[47],
M. Nozaki[69], L. Nozka[117], K. Ntekas[166], E. Nurse[81], F. Nuti[91], K. O'connor[25], D.C. O'Neil[144],
A.A. O'Rourke[45], V. O'Shea[56], F.G. Oakham[31,d], H. Oberlack[103], T. Obermann[23], J. Ocariz[83],
A. Ochi[70], I. Ochoa[38], J.P. Ochoa-Ricoux[34a], S. Oda[73], S. Odaka[69], A. Oh[87], S.H. Oh[48],
C.C. Ohm[16], H. Ohman[168], H. Oide[53a,53b], H. Okawa[164], Y. Okumura[157], T. Okuyama[69],
A. Olariu[28b], L.F. Oleiro Seabra[128a], S.A. Olivares Pino[49], D. Oliveira Damazio[27],
A. Olszewski[42], J. Olszowska[42], A. Onofre[128a,128e], K. Onogi[105], P.U.E. Onyisi[11,aa],
H. Oppen[121], M.J. Oreglia[33], Y. Oren[155], D. Orestano[136a,136b], N. Orlando[62b], R.S. Orr[161],

B. Osculati[53a,53b,*], R. Ospanov[36a], G. Otero y Garzon[29], H. Otono[73], M. Ouchrif[137d],
F. Ould-Saada[121], A. Ouraou[138], K.P. Oussoren[109], Q. Ouyang[35a], M. Owen[56], R.E. Owen[19],
V.E. Ozcan[20a], N. Ozturk[8], K. Pachal[144], A. Pacheco Pages[13], L. Pacheco Rodriguez[138],
C. Padilla Aranda[13], S. Pagan Griso[16], M. Paganini[179], F. Paige[27], G. Palacino[64],
S. Palazzo[40a,40b], S. Palestini[32], M. Palka[41b], D. Pallin[37], E.St. Panagiotopoulou[10],
I. Panagoulias[10], C.E. Pandini[83], J.G. Panduro Vazquez[80], P. Pani[32], S. Panitkin[27],
D. Pantea[28b], L. Paolozzi[52], Th.D. Papadopoulou[10], K. Papageorgiou[9,s], A. Paramonov[6],
D. Paredes Hernandez[179], A.J. Parker[75], M.A. Parker[30], K.A. Parker[45], F. Parodi[53a,53b],
J.A. Parsons[38], U. Parzefall[51], V.R. Pascuzzi[161], J.M. Pasner[139], E. Pasqualucci[134a],
S. Passaggio[53a], Fr. Pastore[80], S. Pataraia[86], J.R. Pater[87], T. Pauly[32], B. Pearson[103],
S. Pedraza Lopez[170], R. Pedro[128a,128b], S.V. Peleganchuk[111,c], O. Penc[129], C. Peng[35a],
H. Peng[36a], J. Penwell[64], B.S. Peralva[26b], M.M. Perego[138], D.V. Perepelitsa[27], F. Peri[17],
L. Perini[94a,94b], H. Pernegger[32], S. Perrella[106a,106b], R. Peschke[45], V.D. Peshekhonov[68,*],
K. Peters[45], R.F.Y. Peters[87], B.A. Petersen[32], T.C. Petersen[39], E. Petit[58], A. Petridis[1],
C. Petridou[156], P. Petroff[119], E. Petrolo[134a], M. Petrov[122], F. Petrucci[136a,136b],
N.E. Pettersson[89], A. Peyaud[138], R. Pezoa[34b], F.H. Phillips[93], P.W. Phillips[133],
G. Piacquadio[150], E. Pianori[173], A. Picazio[89], E. Piccaro[79], M.A. Pickering[122], R. Piegaia[29],
J.E. Pilcher[33], A.D. Pilkington[87], A.W.J. Pin[87], M. Pinamonti[135a,135b], J.L. Pinfold[3],
H. Pirumov[45], M. Pitt[175], L. Plazak[146a], M.-A. Pleier[27], V. Pleskot[86], E. Plotnikova[68],
D. Pluth[67], P. Podberezko[111], R. Poettgen[148a,148b], R. Poggi[123a,123b], L. Poggioli[119], D. Pohl[23],
G. Polesello[123a], A. Poley[45], A. Policicchio[40a,40b], R. Polifka[32], A. Polini[22a], C.S. Pollard[56],
V. Polychronakos[27], K. Pommès[32], D. Ponomarenko[100], L. Pontecorvo[134a], G.A. Popeneciu[28d],
A. Poppleton[32], S. Pospisil[130], K. Potamianos[16], I.N. Potrap[68], C.J. Potter[30], G. Poulard[32],
T. Poulsen[84], J. Poveda[32], M.E. Pozo Astigarraga[32], P. Pralavorio[88], A. Pranko[16], S. Prell[67],
D. Price[87], M. Primavera[76a], S. Prince[90], N. Proklova[100], K. Prokofiev[62c], F. Prokoshin[34b],
S. Protopopescu[27], J. Proudfoot[6], M. Przybycien[41a], A. Puri[169], P. Puzo[119], J. Qian[92], G. Qin[56],
Y. Qin[87], A. Quadt[57], M. Queitsch-Maitland[45], D. Quilty[56], S. Raddum[121], V. Radeka[27],
V. Radescu[122], S.K. Radhakrishnan[150], P. Radloff[118], P. Rados[91], F. Ragusa[94a,94b], G. Rahal[181],
J.A. Raine[87], S. Rajagopalan[27], C. Rangel-Smith[168], T. Rashid[119], S. Raspopov[5],
M.G. Ratti[94a,94b], D.M. Rauch[45], F. Rauscher[102], S. Rave[86], I. Ravinovich[175], J.H. Rawling[87],
M. Raymond[32], A.L. Read[121], N.P. Readioff[58], M. Reale[76a,76b], D.M. Rebuzzi[123a,123b],
A. Redelbach[177], G. Redlinger[27], R. Reece[139], R.G. Reed[147c], K. Reeves[44], L. Rehnisch[17],
J. Reichert[124], A. Reiss[86], C. Rembser[32], H. Ren[35a], M. Rescigno[134a], S. Resconi[94a],
E.D. Resseguie[124], S. Rettie[171], E. Reynolds[19], O.L. Rezanova[111,c], P. Reznicek[131], R. Rezvani[97],
R. Richter[103], S. Richter[81], E. Richter-Was[41b], O. Ricken[23], M. Ridel[83], P. Rieck[103],
C.J. Riegel[178], J. Rieger[57], O. Rifki[115], M. Rijssenbeek[150], A. Rimoldi[123a,123b], M. Rimoldi[18],
L. Rinaldi[22a], G. Ripellino[149], B. Ristić[32], E. Ritsch[32], I. Riu[13], F. Rizatdinova[116], E. Rizvi[79],
C. Rizzi[13], R.T. Roberts[87], S.H. Robertson[90,o], A. Robichaud-Veronneau[90], D. Robinson[30],
J.E.M. Robinson[45], A. Robson[56], E. Rocco[86], C. Roda[126a,126b], Y. Rodina[88,an],
S. Rodriguez Bosca[170], A. Rodriguez Perez[13], D. Rodriguez Rodriguez[170], S. Roe[32],
C.S. Rogan[59], O. Røhne[121], J. Roloff[59], A. Romaniouk[100], M. Romano[22a,22b],
S.M. Romano Saez[37], E. Romero Adam[170], N. Rompotis[77], M. Ronzani[51], L. Roos[83],
S. Rosati[134a], K. Rosbach[51], P. Rose[139], N.-A. Rosien[57], E. Rossi[106a,106b], L.P. Rossi[53a],
J.H.N. Rosten[30], R. Rosten[140], M. Rotaru[28b], J. Rothberg[140], D. Rousseau[119], A. Rozanov[88],
Y. Rozen[154], X. Ruan[147c], F. Rubbo[145], F. Rühr[51], A. Ruiz-Martinez[31], Z. Rurikova[51],
N.A. Rusakovich[68], H.L. Russell[90], J.P. Rutherfoord[7], N. Ruthmann[32], Y.F. Ryabov[125],
M. Rybar[169], G. Rybkin[119], S. Ryu[6], A. Ryzhov[132], G.F. Rzehorz[57], A.F. Saavedra[152],
G. Sabato[109], S. Sacerdoti[29], H.F-W. Sadrozinski[139], R. Sadykov[68], F. Safai Tehrani[134a],

P. Saha[110], M. Sahinsoy[60a], M. Saimpert[45], M. Saito[157], T. Saito[157], H. Sakamoto[157],
Y. Sakurai[174], G. Salamanna[136a,136b], J.E. Salazar Loyola[34b], D. Salek[109],
P.H. Sales De Bruin[168], D. Salihagic[103], A. Salnikov[145], J. Salt[170], D. Salvatore[40a,40b],
F. Salvatore[151], A. Salvucci[62a,62b,62c], A. Salzburger[32], D. Sammel[51], D. Sampsonidis[156],
D. Sampsonidou[156], J. Sánchez[170], V. Sanchez Martinez[170], A. Sanchez Pineda[167a,167c],
H. Sandaker[121], R.L. Sandbach[79], C.O. Sander[45], M. Sandhoff[178], C. Sandoval[21],
D.P.C. Sankey[133], M. Sannino[53a,53b], Y. Sano[105], A. Sansoni[50], C. Santoni[37], H. Santos[128a],
I. Santoyo Castillo[151], A. Sapronov[68], J.G. Saraiva[128a,128d], B. Sarrazin[23], O. Sasaki[69],
K. Sato[164], E. Sauvan[5], G. Savage[80], P. Savard[161,d], N. Savic[103], C. Sawyer[133], L. Sawyer[82,u],
J. Saxon[33], C. Sbarra[22a], A. Sbrizzi[22a,22b], T. Scanlon[81], D.A. Scannicchio[166], M. Scarcella[152],
J. Schaarschmidt[140], P. Schacht[103], B.M. Schachtner[102], D. Schaefer[32], L. Schaefer[124],
R. Schaefer[45], J. Schaeffer[86], S. Schaepe[23], S. Schaetzel[60b], U. Schäfer[86], A.C. Schaffer[119],
D. Schaile[102], R.D. Schamberger[150], V.A. Schegelsky[125], D. Scheirich[131], M. Schernau[166],
C. Schiavi[53a,53b], S. Schier[139], L.K. Schildgen[23], C. Schillo[51], M. Schioppa[40a,40b], S. Schlenker[32],
K.R. Schmidt-Sommerfeld[103], K. Schmieden[32], C. Schmitt[86], S. Schmitt[45], S. Schmitz[86],
U. Schnoor[51], L. Schoeffel[138], A. Schoening[60b], B.D. Schoenrock[93], E. Schopf[23], M. Schott[86],
J.F.P. Schouwenberg[108], J. Schovancova[32], S. Schramm[52], N. Schuh[86], A. Schulte[86],
M.J. Schultens[23], H.-C. Schultz-Coulon[60a], H. Schulz[17], M. Schumacher[51], B.A. Schumm[139],
Ph. Schune[138], A. Schwartzman[145], T.A. Schwarz[92], H. Schweiger[87], Ph. Schwemling[138],
R. Schwienhorst[93], J. Schwindling[138], A. Sciandra[23], G. Sciolla[25], M. Scornajenghi[40a,40b],
F. Scuri[126a,126b], F. Scutti[91], J. Searcy[92], P. Seema[23], S.C. Seidel[107], A. Seiden[139],
J.M. Seixas[26a], G. Sekhniaidze[106a], K. Sekhon[92], S.J. Sekula[43], N. Semprini-Cesari[22a,22b],
S. Senkin[37], C. Serfon[121], L. Serin[119], L. Serkin[167a,167b], M. Sessa[136a,136b], R. Seuster[172],
H. Severini[115], T. Sfiligoj[78], F. Sforza[32], A. Sfyrla[52], E. Shabalina[57], N.W. Shaikh[148a,148b],
L.Y. Shan[35a], R. Shang[169], J.T. Shank[24], M. Shapiro[16], P.B. Shatalov[99], K. Shaw[167a,167b],
S.M. Shaw[87], A. Shcherbakova[148a,148b], C.Y. Shehu[151], Y. Shen[115], N. Sherafati[31],
P. Sherwood[81], L. Shi[153,ao], S. Shimizu[70], C.O. Shimmin[179], M. Shimojima[104], I.P.J. Shipsey[122],
S. Shirabe[73], M. Shiyakova[68,ap], J. Shlomi[175], A. Shmeleva[98], D. Shoaleh Saadi[97],
M.J. Shochet[33], S. Shojaii[94a], D.R. Shope[115], S. Shrestha[113], E. Shulga[100], M.A. Shupe[7],
P. Sicho[129], A.M. Sickles[169], P.E. Sidebo[149], E. Sideras Haddad[147c], O. Sidiropoulou[177],
A. Sidoti[22a,22b], F. Siegert[47], Dj. Sijacki[14], J. Silva[128a,128d], S.B. Silverstein[148a], V. Simak[130],
L. Simic[14], S. Simion[119], E. Simioni[86], B. Simmons[81], M. Simon[86], P. Sinervo[161], N.B. Sinev[118],
M. Sioli[22a,22b], G. Siragusa[177], I. Siral[92], S.Yu. Sivoklokov[101], J. Sjölin[148a,148b], M.B. Skinner[75],
P. Skubic[115], M. Slater[19], T. Slavicek[130], M. Slawinska[42], K. Sliwa[165], R. Slovak[131],
V. Smakhtin[175], B.H. Smart[5], J. Smiesko[146a], N. Smirnov[100], S.Yu. Smirnov[100], Y. Smirnov[100],
L.N. Smirnova[101,aq], O. Smirnova[84], J.W. Smith[57], M.N.K. Smith[38], R.W. Smith[38],
M. Smizanska[75], K. Smolek[130], A.A. Snesarev[98], I.M. Snyder[118], S. Snyder[27], R. Sobie[172,o],
F. Socher[47], A. Soffer[155], A. Søgaard[49], D.A. Soh[153], G. Sokhrannyi[78], C.A. Solans Sanchez[32],
M. Solar[130], E.Yu. Soldatov[100], U. Soldevila[170], A.A. Solodkov[132], A. Soloshenko[68],
O.V. Solovyanov[132], V. Solovyev[125], P. Sommer[51], H. Son[165], A. Sopczak[130], D. Sosa[60b],
C.L. Sotiropoulou[126a,126b], R. Soualah[167a,167c], A.M. Soukharev[111,c], D. South[45], B.C. Sowden[80],
S. Spagnolo[76a,76b], M. Spalla[126a,126b], M. Spangenberg[173], F. Spanò[80], D. Sperlich[17],
F. Spettel[103], T.M. Spieker[60a], R. Spighi[22a], G. Spigo[32], L.A. Spiller[91], M. Spousta[131],
R.D. St. Denis[56,*], A. Stabile[94a], R. Stamen[60a], S. Stamm[17], E. Stanecka[42], R.W. Stanek[6],
C. Stanescu[136a], M.M. Stanitzki[45], B.S. Stapf[109], S. Stapnes[121], E.A. Starchenko[132],
G.H. Stark[33], J. Stark[58], S.H Stark[39], P. Staroba[129], P. Starovoitov[60a], S. Stärz[32],
R. Staszewski[42], P. Steinberg[27], B. Stelzer[144], H.J. Stelzer[32], O. Stelzer-Chilton[163a], H. Stenzel[55],
G.A. Stewart[56], M.C. Stockton[118], M. Stoebe[90], G. Stoicea[28b], P. Stolte[57], S. Stonjek[103],

A.R. Stradling[8], A. Straessner[47], M.E. Stramaglia[18], J. Strandberg[149], S. Strandberg[148a,148b], M. Strauss[115], P. Strizenec[146b], R. Ströhmer[177], D.M. Strom[118], R. Stroynowski[43], A. Strubig[49], S.A. Stucci[27], B. Stugu[15], N.A. Styles[45], D. Su[145], J. Su[127], S. Suchek[60a], Y. Sugaya[120], M. Suk[130], V.V. Sulin[98], DMS Sultan[162a,162b], S. Sultansoy[4c], T. Sumida[71], S. Sun[59], X. Sun[3], K. Suruliz[151], C.J.E. Suster[152], M.R. Sutton[151], S. Suzuki[69], M. Svatos[129], M. Swiatlowski[33], S.P. Swift[2], I. Sykora[146a], T. Sykora[131], D. Ta[51], K. Tackmann[45], J. Taenzer[155], A. Taffard[166], R. Tafirout[163a], N. Taiblum[155], H. Takai[27], R. Takashima[72], E.H. Takasugi[103], T. Takeshita[142], Y. Takubo[69], M. Talby[88], A.A. Talyshev[111,c], J. Tanaka[157], M. Tanaka[159], R. Tanaka[119], S. Tanaka[69], R. Tanioka[70], B.B. Tannenwald[113], S. Tapia Araya[34b], S. Tapprogge[86], S. Tarem[154], G.F. Tartarelli[94a], P. Tas[131], M. Tasevsky[129], T. Tashiro[71], E. Tassi[40a,40b], A. Tavares Delgado[128a,128b], Y. Tayalati[137e], A.C. Taylor[107], G.N. Taylor[91], P.T.E. Taylor[91], W. Taylor[163b], P. Teixeira-Dias[80], D. Temple[144], H. Ten Kate[32], P.K. Teng[153], J.J. Teoh[120], F. Tepel[178], S. Terada[69], K. Terashi[157], J. Terron[85], S. Terzo[13], M. Testa[50], R.J. Teuscher[161,o], T. Theveneaux-Pelzer[88], F. Thiele[39], J.P. Thomas[19], J. Thomas-Wilsker[80], P.D. Thompson[19], A.S. Thompson[56], L.A. Thomsen[179], E. Thomson[124], M.J. Tibbetts[16], R.E. Ticse Torres[88], V.O. Tikhomirov[98,ar], Yu.A. Tikhonov[111,c], S. Timoshenko[100], P. Tipton[179], S. Tisserant[88], K. Todome[159], S. Todorova-Nova[5], S. Todt[47], J. Tojo[73], S. Tokár[146a], K. Tokushuku[69], E. Tolley[59], L. Tomlinson[87], M. Tomoto[105], L. Tompkins[145,as], K. Toms[107], B. Tong[59], P. Tornambe[51], E. Torrence[118], H. Torres[144], E. Torró Pastor[140], J. Toth[88,at], F. Touchard[88], D.R. Tovey[141], C.J. Treado[112], T. Trefzger[177], F. Tresoldi[151], A. Tricoli[27], I.M. Trigger[163a], S. Trincaz-Duvoid[83], M.F. Tripiana[13], W. Trischuk[161], B. Trocmé[58], A. Trofymov[45], C. Troncon[94a], M. Trottier-McDonald[16], M. Trovatelli[172], L. Truong[147b], M. Trzebinski[42], A. Trzupek[42], K.W. Tsang[62a], J.C-L. Tseng[122], P.V. Tsiareshka[95], G. Tsipolitis[10], N. Tsirintanis[9], S. Tsiskaridze[13], V. Tsiskaridze[51], E.G. Tskhadadze[54a], K.M. Tsui[62a], I.I. Tsukerman[99], V. Tsulaia[16], S. Tsuno[69], D. Tsybychev[150], Y. Tu[62b], A. Tudorache[28b], V. Tudorache[28b], T.T. Tulbure[28a], A.N. Tuna[59], S.A. Tupputi[22a,22b], S. Turchikhin[68], D. Turgeman[175], I. Turk Cakir[4b,au], R. Turra[94a], P.M. Tuts[38], G. Ucchielli[22a,22b], I. Ueda[69], M. Ughetto[148a,148b], F. Ukegawa[164], G. Unal[32], A. Undrus[27], G. Unel[166], F.C. Ungaro[91], Y. Unno[69], C. Unverdorben[102], J. Urban[146b], P. Urquijo[91], P. Urrejola[86], G. Usai[8], J. Usui[69], L. Vacavant[88], V. Vacek[130], B. Vachon[90], K.O.H. Vadla[121], A. Vaidya[81], C. Valderanis[102], E. Valdes Santurio[148a,148b], S. Valentinetti[22a,22b], A. Valero[170], L. Valéry[13], S. Valkar[131], A. Vallier[5], J.A. Valls Ferrer[170], W. Van Den Wollenberg[109], H. van der Graaf[109], P. van Gemmeren[6], J. Van Nieuwkoop[144], I. van Vulpen[109], M.C. van Woerden[109], M. Vanadia[135a,135b], W. Vandelli[32], A. Vaniachine[160], P. Vankov[109], G. Vardanyan[180], R. Vari[134a], E.W. Varnes[7], C. Varni[53a,53b], T. Varol[43], D. Varouchas[119], A. Vartapetian[8], K.E. Varvell[152], J.G. Vasquez[179], G.A. Vasquez[34b], F. Vazeille[37], T. Vazquez Schroeder[90], J. Veatch[57], V. Veeraraghavan[7], L.M. Veloce[161], F. Veloso[128a,128c], S. Veneziano[134a], A. Ventura[76a,76b], M. Venturi[172], N. Venturi[32], A. Venturini[25], V. Vercesi[123a], M. Verducci[136a,136b], W. Verkerke[109], A.T. Vermeulen[109], J.C. Vermeulen[109], M.C. Vetterli[144,d], N. Viaux Maira[34b], O. Viazlo[84], I. Vichou[169,*], T. Vickey[141], O.E. Vickey Boeriu[141], G.H.A. Viehhauser[122], S. Viel[16], L. Vigani[122], M. Villa[22a,22b], M. Villaplana Perez[94a,94b], E. Vilucchi[50], M.G. Vincter[31], V.B. Vinogradov[68], A. Vishwakarma[45], C. Vittori[22a,22b], I. Vivarelli[151], S. Vlachos[10], M. Vogel[178], P. Vokac[130], G. Volpi[126a,126b], H. von der Schmitt[103], E. von Toerne[23], V. Vorobel[131], K. Vorobev[100], M. Vos[170], R. Voss[32], J.H. Vossebeld[77], N. Vranjes[14], M. Vranjes Milosavljevic[14], V. Vrba[130], M. Vreeswijk[109], R. Vuillermet[32], I. Vukotic[33], P. Wagner[23], W. Wagner[178], J. Wagner-Kuhr[102], H. Wahlberg[74], S. Wahrmund[47], J. Wakabayashi[105], J. Walder[75], R. Walker[102], W. Walkowiak[143], V. Wallangen[148a,148b], C. Wang[35b], C. Wang[36b,av], F. Wang[176], H. Wang[16], H. Wang[3], J. Wang[45], J. Wang[152],

Q. Wang[115], R. Wang[6], S.M. Wang[153], T. Wang[38], W. Wang[153,aw], W. Wang[36a,ax], Z. Wang[36c], C. Wanotayaroj[118], A. Warburton[90], C.P. Ward[30], D.R. Wardrope[81], A. Washbrook[49], P.M. Watkins[19], A.T. Watson[19], M.F. Watson[19], G. Watts[140], S. Watts[87], B.M. Waugh[81], A.F. Webb[11], S. Webb[86], M.S. Weber[18], S.W. Weber[177], S.A. Weber[31], J.S. Webster[6], A.R. Weidberg[122], B. Weinert[64], J. Weingarten[57], M. Weirich[86], C. Weiser[51], H. Weits[109], P.S. Wells[32], T. Wenaus[27], T. Wengler[32], S. Wenig[32], N. Wermes[23], M.D. Werner[67], P. Werner[32], M. Wessels[60a], K. Whalen[118], N.L. Whallon[140], A.M. Wharton[75], A.S. White[92], A. White[8], M.J. White[1], R. White[34b], D. Whiteson[166], B.W. Whitmore[75], F.J. Wickens[133], W. Wiedenmann[176], M. Wielers[133], C. Wiglesworth[39], L.A.M. Wiik-Fuchs[51], A. Wildauer[103], F. Wilk[87], H.G. Wilkens[32], H.H. Williams[124], S. Williams[109], C. Willis[93], S. Willocq[89], J.A. Wilson[19], I. Wingerter-Seez[5], E. Winkels[151], F. Winklmeier[118], O.J. Winston[151], B.T. Winter[23], M. Wittgen[145], M. Wobisch[82,u], T.M.H. Wolf[109], R. Wolff[88], M.W. Wolter[42], H. Wolters[128a,128c], V.W.S. Wong[171], S.D. Worm[19], B.K. Wosiek[42], J. Wotschack[32], K.W. Wozniak[42], M. Wu[33], S.L. Wu[176], X. Wu[52], Y. Wu[92], T.R. Wyatt[87], B.M. Wynne[49], S. Xella[39], Z. Xi[92], L. Xia[35c], D. Xu[35a], L. Xu[27], T. Xu[138], B. Yabsley[152], S. Yacoob[147a], D. Yamaguchi[159], Y. Yamaguchi[120], A. Yamamoto[69], S. Yamamoto[157], T. Yamanaka[157], M. Yamatani[157], K. Yamauchi[105], Y. Yamazaki[70], Z. Yan[24], H. Yang[36c], H. Yang[16], Y. Yang[153], Z. Yang[15], W-M. Yao[16], Y.C. Yap[83], Y. Yasu[69], E. Yatsenko[5], K.H. Yau Wong[23], J. Ye[43], S. Ye[27], I. Yeletskikh[68], E. Yigitbasi[24], E. Yildirim[86], K. Yorita[174], K. Yoshihara[124], C. Young[145], C.J.S. Young[32], J. Yu[8], J. Yu[67], S.P.Y. Yuen[23], I. Yusuff[30,ay], B. Zabinski[42], G. Zacharis[10], R. Zaidan[13], A.M. Zaitsev[132,al], N. Zakharchuk[45], J. Zalieckas[15], A. Zaman[150], S. Zambito[59], D. Zanzi[91], C. Zeitnitz[178], G. Zemaityte[122], A. Zemla[41a], J.C. Zeng[169], Q. Zeng[145], O. Zenin[132], T. Ženiš[146a], D. Zerwas[119], D. Zhang[92], F. Zhang[176], G. Zhang[36a,ax], H. Zhang[35b], J. Zhang[6], L. Zhang[51], L. Zhang[36a], M. Zhang[169], P. Zhang[35b], R. Zhang[23], R. Zhang[36a,av], X. Zhang[36b], Y. Zhang[35a], Z. Zhang[119], X. Zhao[43], Y. Zhao[36b,az], Z. Zhao[36a], A. Zhemchugov[68], B. Zhou[92], C. Zhou[176], L. Zhou[43], M. Zhou[35a], M. Zhou[150], N. Zhou[35c], C.G. Zhu[36b], H. Zhu[35a], J. Zhu[92], Y. Zhu[36a], X. Zhuang[35a], K. Zhukov[98], A. Zibell[177], D. Zieminska[64], N.I. Zimine[68], C. Zimmermann[86], S. Zimmermann[51], Z. Zinonos[103], M. Zinser[86], M. Ziolkowski[143], L. Živković[14], G. Zobernig[176], A. Zoccoli[22a,22b], R. Zou[33], M. zur Nedden[17], L. Zwalinski[32]

1   *Department of Physics, University of Adelaide, Adelaide, Australia*

2   *Physics Department, SUNY Albany, Albany NY, United States of America*

3   *Department of Physics, University of Alberta, Edmonton AB, Canada*

4   *(a) Department of Physics, Ankara University, Ankara; (b) Istanbul Aydin University, Istanbul; (c) Division of Physics, TOBB University of Economics and Technology, Ankara, Turkey*

5   *LAPP, CNRS/IN2P3 and Université Savoie Mont Blanc, Annecy-le-Vieux, France*

6   *High Energy Physics Division, Argonne National Laboratory, Argonne IL, United States of America*

7   *Department of Physics, University of Arizona, Tucson AZ, United States of America*

8   *Department of Physics, The University of Texas at Arlington, Arlington TX, United States of America*

9   *Physics Department, National and Kapodistrian University of Athens, Athens, Greece*

10 *Physics Department, National Technical University of Athens, Zografou, Greece*

11 *Department of Physics, The University of Texas at Austin, Austin TX, United States of America*

12 *Institute of Physics, Azerbaijan Academy of Sciences, Baku, Azerbaijan*

13 *Institut de Física d'Altes Energies (IFAE), The Barcelona Institute of Science and Technology, Barcelona, Spain*

14 *Institute of Physics, University of Belgrade, Belgrade, Serbia*

15 *Department for Physics and Technology, University of Bergen, Bergen, Norway*

16 *Physics Division, Lawrence Berkeley National Laboratory and University of California, Berkeley CA, United States of America*

17 *Department of Physics, Humboldt University, Berlin, Germany*

18 *Albert Einstein Center for Fundamental Physics and Laboratory for High Energy Physics, University of Bern, Bern, Switzerland*

19 *School of Physics and Astronomy, University of Birmingham, Birmingham, United Kingdom*

20 [a] *Department of Physics, Bogazici University, Istanbul;* [b] *Department of Physics Engineering, Gaziantep University, Gaziantep;* [d] *Istanbul Bilgi University, Faculty of Engineering and Natural Sciences, Istanbul;* [e] *Bahcesehir University, Faculty of Engineering and Natural Sciences, Istanbul, Turkey*

21 *Centro de Investigaciones, Universidad Antonio Narino, Bogota, Colombia*

22 [a] *INFN Sezione di Bologna;* [b] *Dipartimento di Fisica e Astronomia, Università di Bologna, Bologna, Italy*

23 *Physikalisches Institut, University of Bonn, Bonn, Germany*

24 *Department of Physics, Boston University, Boston MA, United States of America*

25 *Department of Physics, Brandeis University, Waltham MA, United States of America*

26 [a] *Universidade Federal do Rio De Janeiro COPPE/EE/IF, Rio de Janeiro;* [b] *Electrical Circuits Department, Federal University of Juiz de Fora (UFJF), Juiz de Fora;* [c] *Federal University of Sao Joao del Rei (UFSJ), Sao Joao del Rei;* [d] *Instituto de Fisica, Universidade de Sao Paulo, Sao Paulo, Brazil*

27 *Physics Department, Brookhaven National Laboratory, Upton NY, United States of America*

28 [a] *Transilvania University of Brasov, Brasov;* [b] *Horia Hulubei National Institute of Physics and Nuclear Engineering, Bucharest;* [c] *Department of Physics, Alexandru Ioan Cuza University of Iasi, Iasi;* [d] *National Institute for Research and Development of Isotopic and Molecular Technologies, Physics Department, Cluj Napoca;* [e] *University Politehnica Bucharest, Bucharest;* [f] *West University in Timisoara, Timisoara, Romania*

29 *Departamento de Física, Universidad de Buenos Aires, Buenos Aires, Argentina*

30 *Cavendish Laboratory, University of Cambridge, Cambridge, United Kingdom*

31 *Department of Physics, Carleton University, Ottawa ON, Canada*

32 *CERN, Geneva, Switzerland*

33 *Enrico Fermi Institute, University of Chicago, Chicago IL, United States of America*

34 [a] *Departamento de Física, Pontificia Universidad Católica de Chile, Santiago;* [b] *Departamento de Física, Universidad Técnica Federico Santa María, Valparaíso, Chile*

35 [a] *Institute of High Energy Physics, Chinese Academy of Sciences, Beijing;* [b] *Department of Physics, Nanjing University, Jiangsu;* [c] *Physics Department, Tsinghua University, Beijing 100084, China*

36 [a] *Department of Modern Physics and State Key Laboratory of Particle Detection and Electronics, University of Science and Technology of China, Anhui;* [b] *School of Physics, Shandong University, Shandong;* [c] *Department of Physics and Astronomy, Key Laboratory for Particle Physics, Astrophysics and Cosmology, Ministry of Education; Shanghai Key Laboratory for Particle Physics and Cosmology, Shanghai Jiao Tong University, Shanghai(also at PKU-CHEP), China*

37 *Université Clermont Auvergne, CNRS/IN2P3, LPC, Clermont-Ferrand, France*

38 *Nevis Laboratory, Columbia University, Irvington NY, United States of America*

39 *Niels Bohr Institute, University of Copenhagen, Kobenhavn, Denmark*

40 [a] *INFN Gruppo Collegato di Cosenza, Laboratori Nazionali di Frascati;* [b] *Dipartimento di Fisica, Università della Calabria, Rende, Italy*

41 [a] *AGH University of Science and Technology, Faculty of Physics and Applied Computer Science, Krakow;* [b] *Marian Smoluchowski Institute of Physics, Jagiellonian University, Krakow, Poland*

42 *Institute of Nuclear Physics Polish Academy of Sciences, Krakow, Poland*

43 *Physics Department, Southern Methodist University, Dallas TX, United States of America*

44 *Physics Department, University of Texas at Dallas, Richardson TX, United States of America*

45 *DESY, Hamburg and Zeuthen, Germany*

46 *Lehrstuhl für Experimentelle Physik IV, Technische Universität Dortmund, Dortmund, Germany*

47 *Institut für Kern- und Teilchenphysik, Technische Universität Dresden, Dresden, Germany*

48 *Department of Physics, Duke University, Durham NC, United States of America*

49 *SUPA - School of Physics and Astronomy, University of Edinburgh, Edinburgh, United Kingdom*

50 *INFN e Laboratori Nazionali di Frascati, Frascati, Italy*

51 *Fakultät für Mathematik und Physik, Albert-Ludwigs-Universität, Freiburg, Germany*

52 *Departement de Physique Nucleaire et Corpusculaire, Université de Genève, Geneva, Switzerland*

53 [a] *INFN Sezione di Genova;* [b] *Dipartimento di Fisica, Università di Genova, Genova, Italy*

54 [a] *E. Andronikashvili Institute of Physics, Iv. Javakhishvili Tbilisi State University, Tbilisi;* [b] *High Energy Physics Institute, Tbilisi State University, Tbilisi, Georgia*

55 *II Physikalisches Institut, Justus-Liebig-Universität Giessen, Giessen, Germany*

56 *SUPA - School of Physics and Astronomy, University of Glasgow, Glasgow, United Kingdom*

57 *II Physikalisches Institut, Georg-August-Universität, Göttingen, Germany*

58 *Laboratoire de Physique Subatomique et de Cosmologie, Université Grenoble-Alpes, CNRS/IN2P3, Grenoble, France*

59 *Laboratory for Particle Physics and Cosmology, Harvard University, Cambridge MA, United States of America*

60 [a] *Kirchhoff-Institut für Physik, Ruprecht-Karls-Universität Heidelberg, Heidelberg;* [b] *Physikalisches Institut, Ruprecht-Karls-Universität Heidelberg, Heidelberg, Germany*

61 *Faculty of Applied Information Science, Hiroshima Institute of Technology, Hiroshima, Japan*

62 [a] *Department of Physics, The Chinese University of Hong Kong, Shatin, N.T., Hong Kong;* [b] *Department of Physics, The University of Hong Kong, Hong Kong;* [c] *Department of Physics and Institute for Advanced Study, The Hong Kong University of Science and Technology, Clear Water Bay, Kowloon, Hong Kong, China*

63 *Department of Physics, National Tsing Hua University, Taiwan, Taiwan*

64 *Department of Physics, Indiana University, Bloomington IN, United States of America*

65 *Institut für Astro- und Teilchenphysik, Leopold-Franzens-Universität, Innsbruck, Austria*

66 *University of Iowa, Iowa City IA, United States of America*

67 *Department of Physics and Astronomy, Iowa State University, Ames IA, United States of America*

68 *Joint Institute for Nuclear Research, JINR Dubna, Dubna, Russia*

69 *KEK, High Energy Accelerator Research Organization, Tsukuba, Japan*

70 *Graduate School of Science, Kobe University, Kobe, Japan*

71 *Faculty of Science, Kyoto University, Kyoto, Japan*

72 *Kyoto University of Education, Kyoto, Japan*

73 *Research Center for Advanced Particle Physics and Department of Physics, Kyushu University, Fukuoka, Japan*

74 *Instituto de Física La Plata, Universidad Nacional de La Plata and CONICET, La Plata, Argentina*

75 *Physics Department, Lancaster University, Lancaster, United Kingdom*

76 [a] *INFN Sezione di Lecce;* [b] *Dipartimento di Matematica e Fisica, Università del Salento, Lecce, Italy*

77 *Oliver Lodge Laboratory, University of Liverpool, Liverpool, United Kingdom*

78 *Department of Experimental Particle Physics, Jožef Stefan Institute and Department of Physics, University of Ljubljana, Ljubljana, Slovenia*

79 *School of Physics and Astronomy, Queen Mary University of London, London, United Kingdom*

80 *Department of Physics, Royal Holloway University of London, Surrey, United Kingdom*

81 *Department of Physics and Astronomy, University College London, London, United Kingdom*

82 *Louisiana Tech University, Ruston LA, United States of America*

83 *Laboratoire de Physique Nucléaire et de Hautes Energies, UPMC and Université Paris-Diderot and CNRS/IN2P3, Paris, France*

84 *Fysiska institutionen, Lunds universitet, Lund, Sweden*

85 *Departamento de Fisica Teorica C-15, Universidad Autonoma de Madrid, Madrid, Spain*

86 *Institut für Physik, Universität Mainz, Mainz, Germany*

87 *School of Physics and Astronomy, University of Manchester, Manchester, United Kingdom*

88 *CPPM, Aix-Marseille Université and CNRS/IN2P3, Marseille, France*

89 *Department of Physics, University of Massachusetts, Amherst MA, United States of America*

90 *Department of Physics, McGill University, Montreal QC, Canada*

91 School of Physics, University of Melbourne, Victoria, Australia

92 Department of Physics, The University of Michigan, Ann Arbor MI, United States of America

93 Department of Physics and Astronomy, Michigan State University, East Lansing MI, United States of America

94 (a) INFN Sezione di Milano; (b) Dipartimento di Fisica, Università di Milano, Milano, Italy

95 B.I. Stepanov Institute of Physics, National Academy of Sciences of Belarus, Minsk, Republic of Belarus

96 Research Institute for Nuclear Problems of Byelorussian State University, Minsk, Republic of Belarus

97 Group of Particle Physics, University of Montreal, Montreal QC, Canada

98 P.N. Lebedev Physical Institute of the Russian Academy of Sciences, Moscow, Russia

99 Institute for Theoretical and Experimental Physics (ITEP), Moscow, Russia

100 National Research Nuclear University MEPhI, Moscow, Russia

101 D.V. Skobeltsyn Institute of Nuclear Physics, M.V. Lomonosov Moscow State University, Moscow, Russia

102 Fakultät für Physik, Ludwig-Maximilians-Universität München, München, Germany

103 Max-Planck-Institut für Physik (Werner-Heisenberg-Institut), München, Germany

104 Nagasaki Institute of Applied Science, Nagasaki, Japan

105 Graduate School of Science and Kobayashi-Maskawa Institute, Nagoya University, Nagoya, Japan

106 (a) INFN Sezione di Napoli; (b) Dipartimento di Fisica, Università di Napoli, Napoli, Italy

107 Department of Physics and Astronomy, University of New Mexico, Albuquerque NM, United States of America

108 Institute for Mathematics, Astrophysics and Particle Physics, Radboud University Nijmegen/Nikhef, Nijmegen, Netherlands

109 Nikhef National Institute for Subatomic Physics and University of Amsterdam, Amsterdam, Netherlands

110 Department of Physics, Northern Illinois University, DeKalb IL, United States of America

111 Budker Institute of Nuclear Physics, SB RAS, Novosibirsk, Russia

112 Department of Physics, New York University, New York NY, United States of America

113 Ohio State University, Columbus OH, United States of America

114 Faculty of Science, Okayama University, Okayama, Japan

115 Homer L. Dodge Department of Physics and Astronomy, University of Oklahoma, Norman OK, United States of America

116 Department of Physics, Oklahoma State University, Stillwater OK, United States of America

117 Palacký University, RCPTM, Olomouc, Czech Republic

118 Center for High Energy Physics, University of Oregon, Eugene OR, United States of America

119 LAL, Univ. Paris-Sud, CNRS/IN2P3, Université Paris-Saclay, Orsay, France

120 Graduate School of Science, Osaka University, Osaka, Japan

121 Department of Physics, University of Oslo, Oslo, Norway

122 Department of Physics, Oxford University, Oxford, United Kingdom

123 (a) INFN Sezione di Pavia; (b) Dipartimento di Fisica, Università di Pavia, Pavia, Italy

124 Department of Physics, University of Pennsylvania, Philadelphia PA, United States of America

125 National Research Centre "Kurchatov Institute" B.P.Konstantinov Petersburg Nuclear Physics Institute, St. Petersburg, Russia

126 (a) INFN Sezione di Pisa; (b) Dipartimento di Fisica E. Fermi, Università di Pisa, Pisa, Italy

127 Department of Physics and Astronomy, University of Pittsburgh, Pittsburgh PA, United States of America

128 (a) Laboratório de Instrumentação e Física Experimental de Partículas - LIP, Lisboa; (b) Faculdade de Ciências, Universidade de Lisboa, Lisboa; (c) Department of Physics, University of Coimbra, Coimbra; (d) Centro de Física Nuclear da Universidade de Lisboa, Lisboa; (e) Departamento de Fisica, Universidade do Minho, Braga; (f) Departamento de Fisica Teorica y del Cosmos, Universidad de Granada, Granada; (g) Dep Fisica and CEFITEC of Faculdade de Ciencias e Tecnologia, Universidade Nova de Lisboa, Caparica, Portugal

[129] *Institute of Physics, Academy of Sciences of the Czech Republic, Praha, Czech Republic*

[130] *Czech Technical University in Prague, Praha, Czech Republic*

[131] *Charles University, Faculty of Mathematics and Physics, Prague, Czech Republic*

[132] *State Research Center Institute for High Energy Physics (Protvino), NRC KI, Russia*

[133] *Particle Physics Department, Rutherford Appleton Laboratory, Didcot, United Kingdom*

[134] [a] *INFN Sezione di Roma;* [b] *Dipartimento di Fisica, Sapienza Università di Roma, Roma, Italy*

[135] [a] *INFN Sezione di Roma Tor Vergata;* [b] *Dipartimento di Fisica, Università di Roma Tor Vergata, Roma, Italy*

[136] [a] *INFN Sezione di Roma Tre;* [b] *Dipartimento di Matematica e Fisica, Università Roma Tre, Roma, Italy*

[137] [a] *Faculté des Sciences Ain Chock, Réseau Universitaire de Physique des Hautes Energies - Université Hassan II, Casablanca;* [b] *Centre National de l'Energie des Sciences Techniques Nucleaires, Rabat;* [c] *Faculté des Sciences Semlalia, Université Cadi Ayyad, LPHEA-Marrakech;* [d] *Faculté des Sciences, Université Mohamed Premier and LPTPM, Oujda;* [e] *Faculté des sciences, Université Mohammed V, Rabat, Morocco*

[138] *DSM/IRFU (Institut de Recherches sur les Lois Fondamentales de l'Univers), CEA Saclay (Commissariat à l'Energie Atomique et aux Energies Alternatives), Gif-sur-Yvette, France*

[139] *Santa Cruz Institute for Particle Physics, University of California Santa Cruz, Santa Cruz CA, United States of America*

[140] *Department of Physics, University of Washington, Seattle WA, United States of America*

[141] *Department of Physics and Astronomy, University of Sheffield, Sheffield, United Kingdom*

[142] *Department of Physics, Shinshu University, Nagano, Japan*

[143] *Department Physik, Universität Siegen, Siegen, Germany*

[144] *Department of Physics, Simon Fraser University, Burnaby BC, Canada*

[145] *SLAC National Accelerator Laboratory, Stanford CA, United States of America*

[146] [a] *Faculty of Mathematics, Physics & Informatics, Comenius University, Bratislava;* [b] *Department of Subnuclear Physics, Institute of Experimental Physics of the Slovak Academy of Sciences, Kosice, Slovak Republic*

[147] [a] *Department of Physics, University of Cape Town, Cape Town;* [b] *Department of Physics, University of Johannesburg, Johannesburg;* [c] *School of Physics, University of the Witwatersrand, Johannesburg, South Africa*

[148] [a] *Department of Physics, Stockholm University;* [b] *The Oskar Klein Centre, Stockholm, Sweden*

[149] *Physics Department, Royal Institute of Technology, Stockholm, Sweden*

[150] *Departments of Physics & Astronomy and Chemistry, Stony Brook University, Stony Brook NY, United States of America*

[151] *Department of Physics and Astronomy, University of Sussex, Brighton, United Kingdom*

[152] *School of Physics, University of Sydney, Sydney, Australia*

[153] *Institute of Physics, Academia Sinica, Taipei, Taiwan*

[154] *Department of Physics, Technion: Israel Institute of Technology, Haifa, Israel*

[155] *Raymond and Beverly Sackler School of Physics and Astronomy, Tel Aviv University, Tel Aviv, Israel*

[156] *Department of Physics, Aristotle University of Thessaloniki, Thessaloniki, Greece*

[157] *International Center for Elementary Particle Physics and Department of Physics, The University of Tokyo, Tokyo, Japan*

[158] *Graduate School of Science and Technology, Tokyo Metropolitan University, Tokyo, Japan*

[159] *Department of Physics, Tokyo Institute of Technology, Tokyo, Japan*

[160] *Tomsk State University, Tomsk, Russia*

[161] *Department of Physics, University of Toronto, Toronto ON, Canada*

[162] [a] *INFN-TIFPA;* [b] *University of Trento, Trento, Italy*

[163] [a] *TRIUMF, Vancouver BC;* [b] *Department of Physics and Astronomy, York University, Toronto ON, Canada*

[164] *Faculty of Pure and Applied Sciences, and Center for Integrated Research in Fundamental Science and Engineering, University of Tsukuba, Tsukuba, Japan*

165 *Department of Physics and Astronomy, Tufts University, Medford MA, United States of America*
166 *Department of Physics and Astronomy, University of California Irvine, Irvine CA, United States of America*
167 ^(a) *INFN Gruppo Collegato di Udine, Sezione di Trieste, Udine;* ^(b) *ICTP, Trieste;* ^(c) *Dipartimento di Chimica, Fisica e Ambiente, Università di Udine, Udine, Italy*
168 *Department of Physics and Astronomy, University of Uppsala, Uppsala, Sweden*
169 *Department of Physics, University of Illinois, Urbana IL, United States of America*
170 *Instituto de Fisica Corpuscular (IFIC), Centro Mixto Universidad de Valencia - CSIC, Spain*
171 *Department of Physics, University of British Columbia, Vancouver BC, Canada*
172 *Department of Physics and Astronomy, University of Victoria, Victoria BC, Canada*
173 *Department of Physics, University of Warwick, Coventry, United Kingdom*
174 *Waseda University, Tokyo, Japan*
175 *Department of Particle Physics, The Weizmann Institute of Science, Rehovot, Israel*
176 *Department of Physics, University of Wisconsin, Madison WI, United States of America*
177 *Fakultät für Physik und Astronomie, Julius-Maximilians-Universität, Würzburg, Germany*
178 *Fakultät für Mathematik und Naturwissenschaften, Fachgruppe Physik, Bergische Universität Wuppertal, Wuppertal, Germany*
179 *Department of Physics, Yale University, New Haven CT, United States of America*
180 *Yerevan Physics Institute, Yerevan, Armenia*
181 *Centre de Calcul de l'Institut National de Physique Nucléaire et de Physique des Particules (IN2P3), Villeurbanne, France*
182 *Academia Sinica Grid Computing, Institute of Physics, Academia Sinica, Taipei, Taiwan*

[a] *Also at Department of Physics, King's College London, London, United Kingdom*
[b] *Also at Institute of Physics, Azerbaijan Academy of Sciences, Baku, Azerbaijan*
[c] *Also at Novosibirsk State University, Novosibirsk, Russia*
[d] *Also at TRIUMF, Vancouver BC, Canada*
[e] *Also at Department of Physics & Astronomy, University of Louisville, Louisville, KY, United States of America*
[f] *Also at Physics Department, An-Najah National University, Nablus, Palestine*
[g] *Also at Department of Physics, California State University, Fresno CA, United States of America*
[h] *Also at Department of Physics, University of Fribourg, Fribourg, Switzerland*
[i] *Also at II Physikalisches Institut, Georg-August-Universität, Göttingen, Germany*
[j] *Also at Departament de Fisica de la Universitat Autonoma de Barcelona, Barcelona, Spain*
[k] *Also at Departamento de Fisica e Astronomia, Faculdade de Ciencias, Universidade do Porto, Portugal*
[l] *Also at Tomsk State University, Tomsk, and Moscow Institute of Physics and Technology State University, Dolgoprudny, Russia*
[m] *Also at The Collaborative Innovation Center of Quantum Matter (CICQM), Beijing, China*
[n] *Also at Universita di Napoli Parthenope, Napoli, Italy*
[o] *Also at Institute of Particle Physics (IPP), Canada*
[p] *Also at Horia Hulubei National Institute of Physics and Nuclear Engineering, Bucharest, Romania*
[q] *Also at Department of Physics, St. Petersburg State Polytechnical University, St. Petersburg, Russia*
[r] *Also at Borough of Manhattan Community College, City University of New York, New York City, United States of America*
[s] *Also at Department of Financial and Management Engineering, University of the Aegean, Chios, Greece*
[t] *Also at Centre for High Performance Computing, CSIR Campus, Rosebank, Cape Town, South Africa*
[u] *Also at Louisiana Tech University, Ruston LA, United States of America*
[v] *Also at Institucio Catalana de Recerca i Estudis Avancats, ICREA, Barcelona, Spain*

^{w} Also at Department of Physics, The University of Michigan, Ann Arbor MI, United States of America

^{x} Also at Graduate School of Science, Osaka University, Osaka, Japan

^{y} Also at Fakultät für Mathematik und Physik, Albert-Ludwigs-Universität, Freiburg, Germany

^{z} Also at Institute for Mathematics, Astrophysics and Particle Physics, Radboud University Nijmegen/Nikhef, Nijmegen, Netherlands

^{aa} Also at Department of Physics, The University of Texas at Austin, Austin TX, United States of America

^{ab} Also at Institute of Theoretical Physics, Ilia State University, Tbilisi, Georgia

^{ac} Also at CERN, Geneva, Switzerland

^{ad} Also at Georgian Technical University (GTU),Tbilisi, Georgia

^{ae} Also at Ochadai Academic Production, Ochanomizu University, Tokyo, Japan

^{af} Also at Manhattan College, New York NY, United States of America

^{ag} Also at Departamento de Física, Pontificia Universidad Católica de Chile, Santiago, Chile

^{ah} Also at The City College of New York, New York NY, United States of America

^{ai} Also at School of Physics, Shandong University, Shandong, China

^{aj} Also at Departamento de Fisica Teorica y del Cosmos, Universidad de Granada, Granada, Portugal

^{ak} Also at Department of Physics, California State University, Sacramento CA, United States of America

^{al} Also at Moscow Institute of Physics and Technology State University, Dolgoprudny, Russia

^{am} Also at Departement de Physique Nucleaire et Corpusculaire, Université de Genève, Geneva, Switzerland

^{an} Also at Institut de Física d'Altes Energies (IFAE), The Barcelona Institute of Science and Technology, Barcelona, Spain

^{ao} Also at School of Physics, Sun Yat-sen University, Guangzhou, China

^{ap} Also at Institute for Nuclear Research and Nuclear Energy (INRNE) of the Bulgarian Academy of Sciences, Sofia, Bulgaria

^{aq} Also at Faculty of Physics, M.V.Lomonosov Moscow State University, Moscow, Russia

^{ar} Also at National Research Nuclear University MEPhI, Moscow, Russia

^{as} Also at Department of Physics, Stanford University, Stanford CA, United States of America

^{at} Also at Institute for Particle and Nuclear Physics, Wigner Research Centre for Physics, Budapest, Hungary

^{au} Also at Giresun University, Faculty of Engineering, Turkey

^{av} Also at CPPM, Aix-Marseille Université and CNRS/IN2P3, Marseille, France

^{aw} Also at Department of Physics, Nanjing University, Jiangsu, China

^{ax} Also at Institute of Physics, Academia Sinica, Taipei, Taiwan

^{ay} Also at University of Malaya, Department of Physics, Kuala Lumpur, Malaysia

^{az} Also at LAL, Univ. Paris-Sud, CNRS/IN2P3, Université Paris-Saclay, Orsay, France

* Deceased